Seismic Performance of Steel Shear Walls with Rectangular Openings

Nozhat Sadat Ghazi Sharyatpanahi

A Thesis in
The Department of
Building, Civil and Environmental Engineering

Presented in Partial Fulfillment of the Requirements
for the Degree of Master of Applied Science (Civil Engineering) at
Concordia University Montreal, Quebec Canada

August 2020

CONCORDIA UNIVERSITY
School of Graduate Studies

This is to certify that the thesis prepared

By: Nozhat Sadat Ghazi Sharyatpanahi

Entitled: **Seismic Performance of Steel Shear Walls with Rectangular Openings**

and submitted in partial fulfillment of the requirements for the degree of

MASc Civil Engineering

complies with the regulations of the University and meets the accepted standards with respect to originality and quality.

Signed by the final Examining Committee:

Dr. Adel Hanna	Chair
Dr. Mingyuan Chen	Examiner
Dr. Emre Erkmen	Examiner
Dr. Anjan Bhowmick	Supervisor

Approved by

Dr.Michelle Nokken , GPD Department of Building, Civil and Environmental Engineering

Dr.Mourad Debbabi, Interim Dean Gina Cody School of Engineering and Computer Science

Date

ABSTRACT

Seismic Performance of Steel Shear Walls with Rectangular Openings

Nozhat Sadat Ghazi Sharyatpanahi

Unstiffened Steel Plate Shear Wall (SPSW) has widely been accepted as an effective lateral load resisting system for resisting wind and earthquake loads. This system has significant post-buckling strength, high ductility, stable hysteretic behaviors and robust initial stiffness. Composite Plate Shear Wall (C-PSW) is also a new form of steel shear wall which has a steel plate and a layer of reinforced concrete (RC) at one or both sides of the steel plate. The steel plate and the concrete layer are connected with shear studs to have a complete composite behavior. C-PSW has some advantages over SPSW such as protection against fire and blast loading. In addition, the presence of the concrete panel can prevent buckling of the steel plate and thereby increase the stiffness, shear strength, and energy dissipation capacity of the C-PSW system in comparison to conventional SPSW system.

Often, SPSWs and C-PSWs need to accommodate large door or window size openings in the infill plates, such as when SPSWs/C-PSWs are used in the building central cores around the elevators. Current AISC design standard recommends use of horizontal and vertical local boundary elements (LBE), in the form of stiffeners, around these large rectangular openings to anchor the tension field developed in the infill plate. Research on SPSW with stiffened large openings like door and window sized openings is limited. Also research on C-PSWs with large openings is still in the initial stage and a significant amount of research is needed before it can be adopted by the Canadian steel design code. This study presents seismic performance of SPSWs and C-PSWs with door size openings in the web plate. Nonlinear FE models were developed in ABAQUS for SPSW and C-PSW with door size openings. The FE models include both material and geometric nonlinearities. The proposed FE model was validated against available experimental data. The study describes details of the validation of the finite element model. Two

multi-storey (3- and 5-storey) SPSWs and C-PSWs were designed following the capacity design concept and the guidelines of current AISC seismic design standard. The performance of selected SPSWs and C-PSWs were investigated through conducting a series of time history analysis using a suite of 8 ground motions that are developed for western Canada and are compatible with Vancouver design response spectrum. Nonlinear seismic analysis shows that both SPSWs and C-PSWs with rectangular openings exhibit excellent seismic performance with high ductility and strength when subjected to strong ground motions. Maximum contribution of various structural components (i.e., infill plate and boundary members) in resisting applied lateral loads are calculated from seismic analysis and presented in the study. The maximum interstorey drift is found to be within the code limit for both systems under all ground motions. It is observed that the designed stiffeners around the openings are very effective in limiting the in-plane and out-of-plane deformations around the rectangular openings, especially in the SPSW system and the presence of these stiffeners do not alter the recommended yielding sequence of the system. In addition, it is observed that current AISC requirement to attach horizontal and vertical LBE around rectangular opening of C-PSW is conservative and can be relaxed if the infill plate is connected with the concrete panel with adequate shear connectors.

Dedication

This thesis is dedicated to my family. A special feeling of gratitude to my loving parents, Manzar and Zia, for their endless love, support and encouragement. My brother, Behrad, who has been a constant source of support and encouragement and is very special and my husband, Arash, who always stays by my side and whose love and support sustained me throughout. I am truly thankful for having you in my life. I could not have accomplished as much as I have without their support and understanding. Words cannot describe how much I love and appreciate you.

ACKNOWLEDGEMENTS

I would like to take this opportunity to express my heartfelt gratitude to all those who contributed in some way to the work described in this thesis.

First and foremost, I would like to thank my thesis advisor, Dr. Anjan Bhowmick, for giving me the chance to reach this point, for his patient guidance, engaging me in new ideas, encouragement and advice he has provided throughout my time as his student. I have been extremely lucky to have a supervisor who cared so much about my work, and who responded to my questions and queries.

Special gratitude to my course instructors, Dr. Khaled Galal, Dr. Lucia Tirca, Dr. Amir Mofidi and Dr. Farzad Ghodoosi, for their support and direction in my graduate classes. Without their guidance and support I would not have been able to reach this stage.

I would like to express my deepest gratitude to my family for their continued love, support and encouragement.

Thanks to all my colleagues and friends for inspiring and supporting me during my graduate studies.

Finally, I would like to thank Gina Cody School of Engineering and Computer Science, Concordia University, Montreal, Canada for their support and giving me the opportunity to learn more.

Table of Contents

List of Figures

List of Tables

List of Symbols

V_{yp}	Shear Strength of SPSW
K	Elastic stiffness
D	Diameter of opening
F	Ultimate shear strength
L	Length of the plate
P_{UW}	Ultimate load of composite shear wall with opening
P_u	Ultimate load of composite shear walls without openings
$\acute{f}$	Concrete compressive strength
$\tilde{\varepsilon}_t^{pl}$	Tensile equivalent plastic strain
$\tilde{\varepsilon}_c^{pl}$	Compressive equivalent plastic strain
σ	Cauchy stress tensor
ε	Strain tensor,
d	Scalar stiffness degradation variable and depth of specimen
ε^{pl}	Plastic strain
D_0^{el}	Initial (undamaged) elastic stiffness of the material
D^{el}	Degraded elastic stiffness tensor

$\bar{\sigma}$	Effective stress tensor
$\dot{\varepsilon}^{pl}$	Plastic flow
$\dot{\lambda}$	Plastic consistency parameter
G	Flow potential
β	Dilation angle
f_t	Uniaxial tensile strength of concrete
f_c	Uniaxial compressive strengths of concrete
m	Eccentricity of the plastic potential surface
$\bar{p}$	Effective hydrostatic stress
$\bar{q}$	Mises equivalent effective stress
S	Deviatoric part of the effective stress tensor $\bar{\sigma}$
α	Uniaxial compressive strength, Angle of tension field
f_{b0}	Compressive strength under biaxial loading of concrete
$\bar{\sigma}_{max}$	Maximum effective principal stress
$\bar{\sigma}_t$	Effective tensile cohesion stress
$\bar{\sigma}_c$	Effective Compressive cohesion stress

γ	Shape of loading surface in the deviatoric plane
f_c	Compressive strength of concrete
K_c	Distances between the hydrostatic axis of compression meridian and the tension Meridian in the deviatoric cross section
f_{b0}	Compressive strength under biaxial loading
f_{c0}	Compressive strength under uniaxial loading
ψ	Dilation angle
β_1	Dilation angle
μ	Viscosity parameter
t	Time step, thickness of steel plate
$\dot{\varepsilon}_1 p$	Axial plastic strain
$\dot{\varepsilon}_v p$	Volumetric plastic strain
σ_{c0}	Failure stress of concrete under uniaxial compression
σ_{t0}	Failure stress of concrete under uniaxial tension
σ_{cu}	Ultimate stress of concrete under uniaxial compression
$\tilde{\varepsilon}_t^{ck}$	Concrete cracking strain in uniaxial tension
$\tilde{\varepsilon}_c^{in}$	Concrete crushing strain in uniaxial compression

$\tilde{\varepsilon}_c^{in}$	Concrete inelastic strain in uniaxial compression
ε_{0c}^{el}	Elastic strain corresponding to undamaged concrete material
ε_c	Total concrete compressive strain
σ_c	Concrete compressive stress
E_0	Initial elastic stiffness
d_c	Concrete damage parameter in compression
ε_0	Peak strain at maximum strength
E_c	Initial young's modulus of concrete in compression
E_t	Initial young's modulus of concrete in tension
σ_t	Concrete tensile stress
d_t	Concrete damage parameter in tension
ε_t	Total concrete tensile strain
f_{cr}	Peak concrete tensile stress
ε_{cr}	Concrete strain at the peak tensile stress
V	Design base shear
V_{min}	Minimum allowable design base shear

V_{max}	Maximum allowable design base shear
$S(T_a)$	Design spectral acceleration
T_a	Fundamental period of the structure
h_n	Total building height
M_v	Amplification factor to account higher mode effect
I_E	Importance factor for earthquake loads and effects
W	Seismic weight of the building
R_d	Ductility related force modification factor
R_o	Over strength factor
F_x	Distributed shear of each storey
F_t	Extra concentrated load at the top of the structure
h_i	Height above the ground to i^{th} storey
V_r	Factored shear resistance of the infill steel plate
F_y	Yield stress
t_w	Thickness of the infill steel plate
L	Distance between vertical member of shear wall center line

h	Distance between horizontal member of shear wall center-lines
A_b	Average cross-sectional area of the horizontal boundary elements around the steel plate
A_c	Average cross-sectional area of the vertical boundary elements around the steel plate
I_c	Average moment of inertia of the vertical members bounding the steel panel
$V_{ns(exp)}$	Expected shear strength of the stiffened steel plate
A_{sp}	Horizontal area of the stiffened steel plate
w_{xci}	Horizontal distributed force applicable to the columns
w_{yci}	Vertical distributed load applicable to the beams
F_{yp}	Yield strength of the steel plate
w_{xbi}	Horizontal distributed load applicable to the beams
w_{yci}	Vertical distributed load applicable to the beams
h_s	Storey height
I_{tb}	Moment of inertia of the HBE above the steel plate
I_{bb}	Moment of inertia of the HBE located on the bottom of the steel plate
τ_{cr}	Critical shear buckling stress of a plate subjected to pure shear
K_{sl}	Critical stress coefficient

ν	Poisson ratio
b	Steel plate width.
φ	Aspect ratio of two sides of the panel
c	Center to center distances of shear studs
K_{sg}	Global buckling factor
D_x	Flexural stiffness for bending about x axis
D_y	Flexural stiffness for bending about y
I_x	Moment of inertia about the x axis
I_y	Moment of inertia about the y axis
c_x	Center to center distances of shear studs in x direction
c_y	Center to center distances of shear studs in y directions
h	Concrete panel thickness
D	Shear stud diameter
t_1	Thickness of the steel plate above the opening
t_2	Thickness of steel plate at the level of opening
L_{cf}	Clear distance between the VBE flanges

L_1	Width of steel plates on left side of the opening
L_3	Width of steel plates on right side of the opening
N_u	Axial force of the LBE
A	Peak ground acceleration
V	Peak ground velocity
T_1	Fundamental period

Chapter One

1. Introduction

1.1 General

Steel Plate Shear Wall (SPSW) is a relatively new structural system that turned to a practical and acceptable lateral load resisting system especially for the seismic applications. The system has been used in different types of buildings and in different countries like Japan, North America, and China. SPSW system has been accepted in North American steel design standard.

The conventional steel plate shear wall system consists of stiffened/thick infill plate or unstiffened steel plate. The unstiffened SPSW is composed of an infill steel plate connected to boundary beams and columns called Horizontal Boundary Elements(HBE) and Vertical Boundary Elements(VBE), respectively. Stiffened steel plate shear wall consists of an infill steel plate connected to the boundary steel frame and is stiffened by vertical and horizontal stiffeners.

Nowadays, steel plate shear wall with thin unstiffened steel plates is preferred. Research on SPSWs showed that the thin infill plate tends to buckle under small applied lateral load. After the infill plate is buckled, tension field develops in the infill plate. Thus, in addition to the bending stiffness provided by the boundary frame, lateral stiffness and strength are provided by the diagonal tension field generated in the infill plate.

A significant amount of studies showed that SPSW system has many advantages including of high ductility, large level of energy absorption, initial stiffness, strength, lower interstorey drift and drift robustness under cyclic loading (Thorburn et al. 1983; Timler nad Kulak 1983; Tromposch and Kulak 1987; Caccese et al 1993; Driver et al. 1998; Elgaaly an Lui 1997; Rezai 1999; Lubell et al. 2000; Berman and Bruneau 2005; Qu et al. 2008 and Bhowmick 2009, 2010).This system also offers a light-weight structure, decreases foundation cost, increases floor area, and provides better quality control when compared to a conventional reinforced concrete shear wall. Despite its advantages, the system suffers from some shortcomings. The major drawback affecting the cost efficiency of the system is that always large column sections are required in capacity design process. Because post-buckling of the steel plate due to tension field creates large lateral forces on the boundary columns and the moment and additional axial forces are large in the columns of the SPSW. Also, in addition to the need for fire protection like

other steel structural systems, SPSW has a very low out of plane stiffness which is a problem in the case of impact loading (Ghosh 2010) and the overall buckling of steel plate has negative impact on the shear strength, stiffness, and energy dissipation capacity of the system (Zhao 2004). Furthermore, large inelastic deformations of the steel plate can cause the connections of its boundary elements undergo large cyclic rotations and interstorey drifts (Allen 1980).

In order to overcome the shortcomings of the SPSWs the concrete layer was introduced to SPSW to act as a composite system. This system is called Composite Plate Shear Wall (C-PSW). C-PSW system is identical with stiffened steel plate in terms of replacing the steel stiffeners with concrete panel. In this system, a layer of in-situ or pre-cast reinforce concrete is added to one or both side of the steel plate. To ascertain the complete composite behavior in the system, the steel plate and the concrete cover are connected by means of bolts or shear studs. The main role of concrete layer is to prevent steel plate from early shear buckling. This new system offers advantages in comparison to reinforced concrete shear walls (RC Walls) and SPSWs. A C-PSW has smaller thickness and less weight in comparison to RC walls with the same shear capacity which is very beneficial as it provides more usable floor space, smaller foundation and smaller seismic forces. In construction of C-PSW with pre-cast or cast in place walls, the reinforced concrete walls can be attached to steel plate at any convenient time during construction.

Addition of concrete panel will prevent the early local and global buckling of the steel plate therefore the shear yielding of the steel plate will occur (Astaneh-Asl 2002). Moreover, the concrete panel increases lateral strength and stiffness of the overall system, provides more ductile behavior in comparison with the SPSW (Zhao 2004) and acts as fire/explosion protection and sound and temperature insulation (Astaneh-Asl 2002).

Post-earthquake damage of the C-PSW is limited to shear yielding of steel plates so the building can continue its complete functionality with a little or without any repair after the earthquake event (Astaneh-Asl 2002).

While a significant amount of experimental and numerical studies was done on SPSWs, research on C-PSWs is limited. One important issue with both SPSW and C-PSW is that they often have to accommodate large openings due to passing utilities or architectural demands like doors and windows. While few studies are available on circular perforation in SPSW, research

on door and window sized rectangular openings is very limited and to the best of the author's knowledge, no study has been done to investigate the behavior of SPSW and C-PSW with large rectangular openings under real seismic loadings. It is evident that this field of study needs more research in order to identify the behavior and key parameters for seismic design.

1.2 Objective and Scope

Location and size of openings in steel shear walls can significantly influence stiffness and strength of the lateral load resisting systems. Current code only provides shear strength equation for regularly spaced circular perforations in the infill plate of SPSW. Thus, it is important to investigate the behavior of SPSWs and C-PSWs with large stiffened or unstiffened rectangular openings in the web of the lateral load resisting systems. Seismic performance of SPSWs and C-PSWS with large rectangular openings is yet to be investigated. Thus, one of the objectives of this study is to evaluate seismic performance of SPSW and C-PSW with large openings like doors. In order to do so, first finite element models with material and geometrical nonlinearities were developed and validated against experimental studies. The validated FE model is then used to evaluate seismic performance of SPSW and C-PSW systems with large rectangular openings by conducting a series of time history analysis. Maximum contributions of various structural components (i.e., infill plate and boundary members) in resisting applied lateral loads were obtained. The variation of maximum interstorey drifts in all stories was assessed to be within the code limits for these systems.

Another objective of this research is to determine the effectiveness of the designed stiffeners to limit in-plane and out-of-plane deformations around the rectangular openings and whether presence of opening and stiffeners around the opening alter the yielding sequence of the systems.

Current AISC recommends the rectangular openings be sufficiently stiffened with horizontal and vertical local elements having full width and height of the shear wall panel. A significant amount of stiffeners may need to be welded to meet this requirement and this often makes the shear wall system quite expensive and less popular to the construction industry. One of the objectives of this research is to investigate whether we can somewhat relax the requirement of stiffeners around openings.

1.3 Overview and Organization of Thesis

To achieve the above-mentioned research objectives, a detailed numerical study is carried out to develop and evaluate the behavior and seismic performance of SPSWs and C-PSWs with rectangular openings.

In this chapter, an introduction to SPSW and its advantages and drawbacks, an introduction to C-PSW, why this system is required and how it can solve the drawbacks of the current SPSW system and its benefits for being used as a lateral load resisting system are presented. Also the need for the current research and its objectives are described.

To better understand the knowledge gap and gather useful information for the research objectives, a review of relevant literature is presented in Chapter 2. In chapter 2, extensive review of experimental and numerical studies conducted on SPSWs is summarized, followed by studies conducted on C-PSWs. Then, the studies done on SPSWs and C-PSWs with openings are described.

Chapter 3 presents the FE model developments for SPSW and C-PSW in detail. FE model validation is also described in this chapter by comparing the results with two experimental studies of quasi-static cyclic analysis.

Chapter 4 illustrates the design of 3-storey and 5-storey SPSWs and C-PSWs with door opening. The design approach was based on capacity design approach and AISC Design guide 20. The description of the selected buildings, SPSW and C-PSW design procedure, FE modeling of these systems, selection and scaling of ground motion records used later for seismic analysis are also described in this chapter.

Chapter 5 investigates the seismic performance of the selected 3- and 5- storey SPSWs by conducting a series of time history analysis using a suite of 8 ground motions compatible with the design response spectrum of Vancouver, Canada. Maximum contributions of structural components in resisting applied lateral loads are obtained from seismic analysis. Effectiveness of the designed stiffeners to limit both in-plane and out-of-plane deformations around the rectangular openings is examined from seismic analysis. Also, whether the use of the local boundary elements (stiffeners) around the rectangular openings alters the recommended yielding sequence of the SPSW system is investigated in the chapter.

Chapter 6 describes the performance of selected C-PSWs with door size openings with and without LBEs around the opening. The performance of selected C-PSWs are further investigated through conducting a series of time history analysis using a suite of 8 ground motions that are selected in Chapter 4. Maximum contributions of various structural components (i.e., infill plate and boundary members) in resisting applied lateral loads are calculated from seismic analysis. The variation of maximum inter-storey drift in all stories for both multi-storey C-PSWs is obtained. In addition, the stiffness requirements for the stiffeners around the door sized openings of C-PSW system are evaluated from nonlinear seismic analysis.

Finally, Chapter 7 summarizes the findings of this thesis and presents the topics and areas for future research.

Chapter Two

2. Literature review

2.1 Introduction

Steel Plate Shear Wall (SPSW) is a relatively new structural system that turned to a practical and acceptable lateral load resisting system especially for the seismic applications. SPSW can be thought of as a girder in which the VBEs are assumed as the girder flanges, infill steel plate as the girder web and HBEs as stiffeners for the girder web. This system has many advantages consisting possession of high ductility, large level of energy absorption, initial stiffness, strength, lower interstorey drift and drift robustness under cyclic loading (Thorburn et al. 1983, Timler and Kulak 1983, Tromposch and Kulak 1987, Caccese et al. 1993, Driver et al. 1998, Elgaaly and Lui 997, Rezai 1999, Lubell et al. 2000, Berman and Bruneau 2005, Qu et al. 2008, Bhowmick 2009). This system also offers a light-weight structure, speed and simplicity of construction, decreases foundation cost, increases floor area, and better quality control when compared to a conventional reinforced concrete shear wall.

C-PSW is composed of the elements of SPSW and reinforced concrete panel. This system was introduced to overcome the shortcomings of the SPSWs such as the overall buckling of steel plate.

Several related experimental and numerical studies on SPSW, SPSW with opening, C-PSW and C-PSW with opening are described in this chapter.

2.2 Selected Studies on Steel Plate Shear Wall (SPSW)

In the early years, the design of SPSW was based on the concept of preventing shear buckling in the infill plate. So the common applications of the steel plate shear wall system was with relatively thick plates or closely spaced stiffeners in order to prevent infill plate buckling until shear yielding capacity of the steel plate.

At that time, stiffeners were favored because high-energy dissipation capacity and ductility of the system was assured. Takahashi et al. (1973) investigated both steel plate shear wall and concrete shear wall and concluded that although incorporating stiffeners resulted in

higher shear strength, stiffness, ductility, and energy-dissipation capacity of the system, the addition of the stiffeners is a relatively labor-intensive, time-consuming, and costly fabrication process. Later, by conducting more studies on SPSWs, researchers presented the idea of using the post-buckling strength of steel plate. Canadian researchers at the University of Alberta for the first time introduced unstiffened SPSWs with thin infill plate as an acceptable system by investigating the post-buckling capacity from the diagonal tension field of the infill plates. Afterwards, and particularly in North America, many researches focused on the post-buckling behavior of the unstiffened thin steel infill walls. Thorburn et al. (1983), Timler and Kulak (1983), and Tromposch and Kulak (1987) studied the post-buckling strength of steel plate shear walls by testing several single and multi-storey steel shear wall specimens without stiffeners under quasi-static cyclic load. Thorburn et al. (1983) proposed the strip model and an equation for tension field action which is later modified by Timler and Kulak (1983). Tromposch and Kulak (1987) conducted parametric studies and depicted that frames with fixed beam-to-column connections could dissipate as much as three times more energy as that dissipated by frames with simple beam-to-column connections.

Kulak (1991) and Driver et al. (1998) performed monotonic and cyclic loadings tests on unstiffened steel shear walls and concluded that this system has good ductility, high lateral strength and that the absorbed energy increases with deflection. The strip model proposed by Thorburn et al. (1983) was later improved by some other researchers like Chen (1991), Caccese et al. (1993), Lubell (1997); Driver et al. (1998a), Elgaaly (1998). Many other researchers such as Behbahanifard et al. (2003), Berman and Bruneau (2003), Sabouri-Ghomi et al. (2005), Bhowmick (2009, 2010, 2014), Kharrazi et al. (2010a, 2010b) made significant contributions in SPSW research.

Berman and Bruneau (2008) introduced a capacity design approach for design of vertical boundary elements(VBEs) in SPSWs and verified that their proposed approach is more accurate than other pre-existing approaches (Indirect Capacity Design (ICD) approach and the Combined Linear Elastic Computer Programs and Capacity Design Concept (LE+CD)). They showed that their proposed approach predicts the axial loads and moment of VBEs closer to the results of non-linear static pushover analysis.

2.3 Selected Studies on Steel Plate Shear Wall (SPSW) with opening

Roberts and Sabouri-Ghomi (1991) conducted the first study on unstiffened steel plate shear panel with and without a central circular opening. They conducted tests on series of specimens and concluded that strength and stiffness of the specimens with a central circular opening are decreased by increasing the opening diameter. They also proposed that this reduction can be conservatively estimated by applying a linear reduction factor to the strength and stiffness of a similar solid panel.

The proposed strength and stiffness reduction factor for a perforated panel is as follows:

$$\frac{V_{yp.pref}}{V_{yp}} = \frac{K_{pref}}{K_{panel}} = [1 - \frac{D}{d}] \qquad 2.1$$

where $V_{yp.perf}$ /V_{yp} and K_{perf} /K_{panel} are the ratios of strength and elastic stiffness, respectively, of a perforated panel specimen to an identical solid panel specimen, D is the diameter of the central circular opening and d is the panel depth. Schematic of the test specimen is depicted in Figure 2.1.

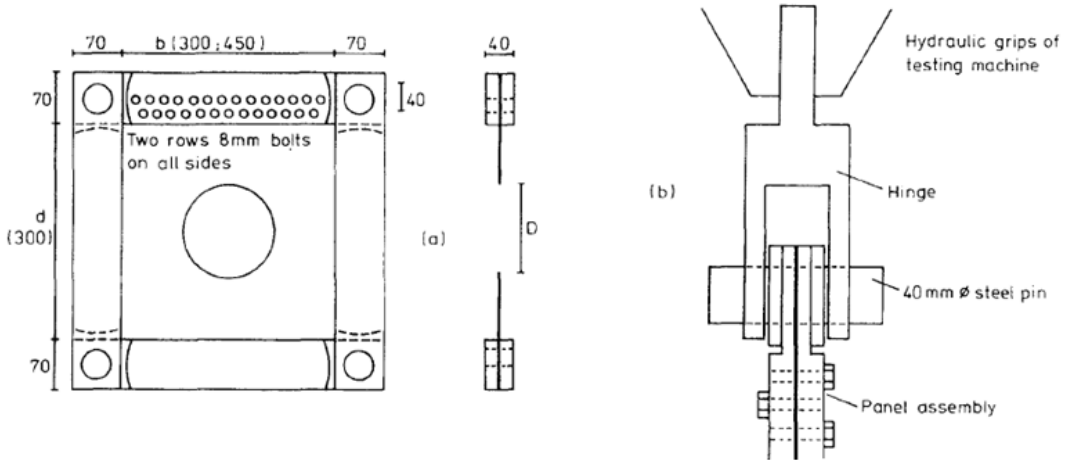

Figure 2.1: Detail of panel with center circular opening tested by Roberts and Sabouri-Ghomi (1991); a) Perforated panel; b) Hinge

Deylami and Daftari (2000) studied the behavior of steel shear wall with large rectangular opening by analysis of more than 50 models with large rectangular opening in the center of the panel with finite element method. The opening had only two stiffeners with limited length on its vertical edges which were not continued across the height of the panel. They came

to this conclusion that introduction of even a relatively small percentage of opening caused an important reduction in shear capacity. Typical specimen is shown in Figure 2.2.

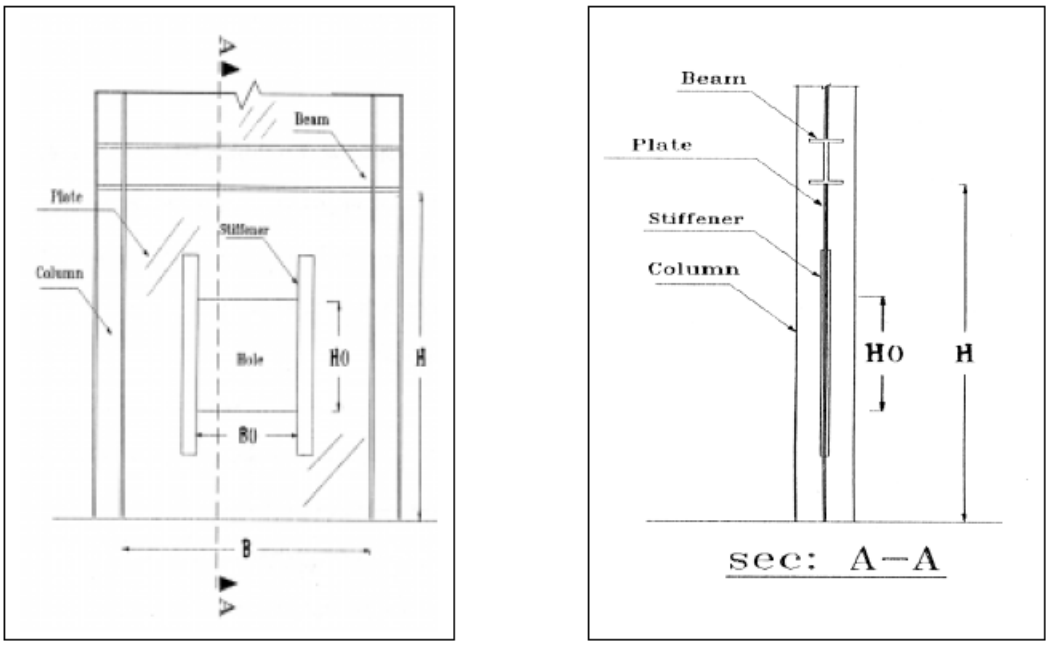

Figure 2.2: Typical steel plate shear wall computed by Deylami and Daftari (2000)

Vian and Bruneau, (2004, 2005) analytically and experimentally studied the pattern of multiple regularly spaced circular perforations in the infill plate and reinforced quarter-circle cut-outs in the upper corners of the infill plate. They conducted tests on three specimens of steel panel shear wall under cyclic quasi-static loading. One specimen had a solid panel and the other two had openings, one with 20 openings of diameters 200 mm and the other with quarter circle cutouts in the panel corners. The specimens are shown in Figure 2.3. In order to make sure yielding occurs at optimum locations in beam and infill plate, Vian and Bruneau (2004) used reduced beam sections for beams at the ends and low yield strength steel infill panels. The results showed that thin panel with small yield strength reduces the strength though energy dissipation will start earlier by the panel. Also presence of openings in the panels decreases the stiffness and strength. Therefore, they concluded that steel plate shear walls with low yield strengths are a practical choice for resistance against lateral loads during earthquakes and in the circumstances where steel plates with small yield strength are not available, panels with openings can be used.

Figure 2.3: Vian and Bruneau (2004) test Specimens with solid panel (right), panel with 20 holes (center) and panel with cutout on the top corners (left)

Later, Purba and Bruneau (2009) conducted more numerical analysis on the previous experimental results of Vian and Brneau (2004) and proposed an equation to determine the shear strength of a perforated infill plate with the specific perforation pattern. They proposed a more precise reduction factor than what was proposed by Roberts and Sabouri-Ghomi (2000) for calculating the strength of a perforated panel. The proposed reduction factor is:

$$\frac{V_{yp.pref}}{V_{yp}} = 1 - \alpha \frac{D}{S_{diag}} \qquad 2.2$$

where α is the correction factor, equal to 0.70, D is the diameter of perforations with equally spaced of diagonal width S_{diag}.

According to the researches done by Alinia et al. (2007, 2008) presence of discontinuity in steel plate tension zones have considerable influence on buckling and post-buckling behavior of panels. Pellegrino et al. (2009) also investigated the linear and nonlinear behavior of steel plates with circular and rectangular holes under shear loading and showed that the shear buckling coefficient is noticeably affected by dimensions of the holes.

Valizadeh et al. (2012) studied cyclic behavior of perforated steel plate shear walls with a circular opening at the center of the panel, experimentally. Their results showed that the presence of opening significantly reduces the energy absorption of the system and decreases the initial stiffness and strength.

Hosseinzadeh and Tehranizadeh (2012) studied the nonlinear behavior of SPSWs with stiffened large rectangular openings used as windows or doors in buildings. They numerically analyzed a number of SPSWs with rectangular openings and horizontal and vertical local

boundary elements (LBE) around the opening and concluded that the behavior of the system was not affected much by the location, type (window or door) and geometry of the openings. In addition, creation of opening in SPSWs increased the ultimate strength and stiffness, while it slightly decreased the ductility ratio.

Bhowmick (2014) examined the seismic behavior of unstiffened thin steel plate shear walls with circular perforations placed at the center of the infill plates and proposed shear strength equation for SPSWs with circular perforations at the center based on the finite element results.

Barkhordari et al. (2014) studied the behavior of SPSWs with rectangular openings stiffened with LBEs along the full height of the opening. The results showed that introduction of stiffened openings always decreases the strength of the infill plate, initial stiffness and ductility of SPSW, while it somewhat increases the frame strength. In addition, they came to the conclusion that unlike Hosseinzadeh (2012) for the partial-height openings with horizontal and vertical LBEs, the behavior of SPSWs with stiffened full height openings is affected by the location and length of the openings.

Sabouri-Ghomi and Mamazizi (2015) evaluated the influence of two openings on the structural behavior of SPSWs. The spacing of the opening affected the lateral bearing capacity, stiffness, and energy absorption slightly. Moreover, the presence of opening reduced the values of these parameters. Figure 2.4 shows the deformed state of specimens for experimental and numerical models.

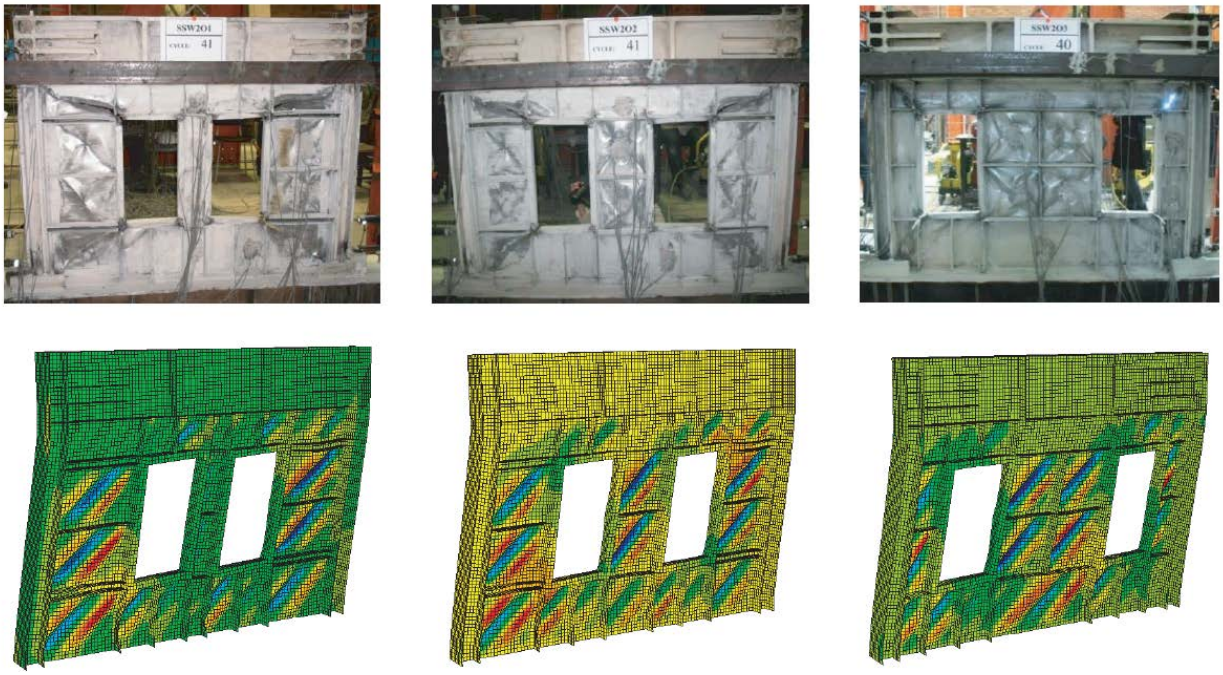

Figure 2.4: Experimental and numerical specimens at the end of the test (Sabouri-Ghomi and Mamazizi 2015)

Bahrebar et al. (2016) investigated the hysteretic performance of corrugated and perforated-web SPSWs by finite element analysis. Their results showed that introduction of web opening can lower the load-bearing capacity of the infill plate and if not detailed properly, it adversely affects the cyclic performance and energy absorption capability of the system. Introduction and increasing of the size of the web opening reduces energy dissipation capacity of the system and the contribution of the infill plate in performance. Therefore, it increases the overall system demand on the boundary frame members.

Afshari and Gholhaki (2018) evaluated the shear strength of steel plate shear wall with openings in different locations by finite element method and proposed empirical equation for calculating the amount of reduction in the shear strength of the wall with arbitrary opening position in any zone of the plate.

2.4 Selected Studies on Composite Steel Plate Shear Wall (C-PSW)

Several numerical and experimental researches conducted on composite steel shear walls are reviewed, followed by a review of research done on C-PSWs containing openings.

In the years of 1998 to 2001 Astaneh-Asl (1998; 2001) analytically and experimentally investigated the behavior of steel plate shear wall and composite shear wall under cyclic loads. Results showed that introducing a concrete layer to steel plate causes better stress distribution in the steel plate and tension field lines occur in a wider region.

Later, Astaneh-Asl et al. (2002) and Zhao and Astaneh-Asl (2004) further studied composite shear walls and proposed two types of composite shear walls, which are called "traditional" and "innovative" C-PSWs. The innovative wall had a gap between the reinforced concrete panel and the boundary frame while in the traditional wall the reinforced concrete panel is attached to the boundary frame. The study composed of tests on two specimens of ½-scale, three stories shear wall under cyclic loads. Typical test specimen of the tests is shown in Figure 2.5 and with more detail in Figure 2.6.

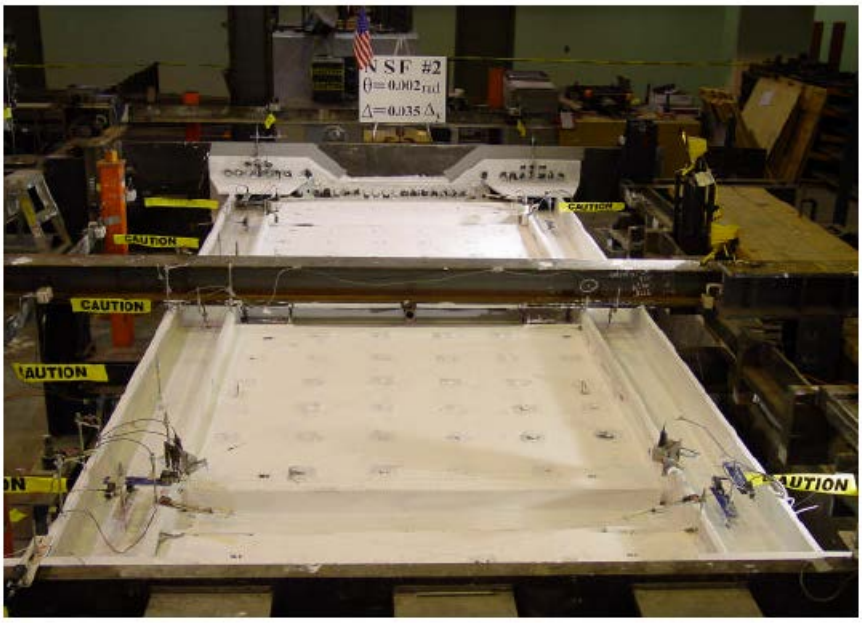

Figure 2.5: Composite Plate Shear wall specimen (Zhao and Astaneh-Asl 2004)

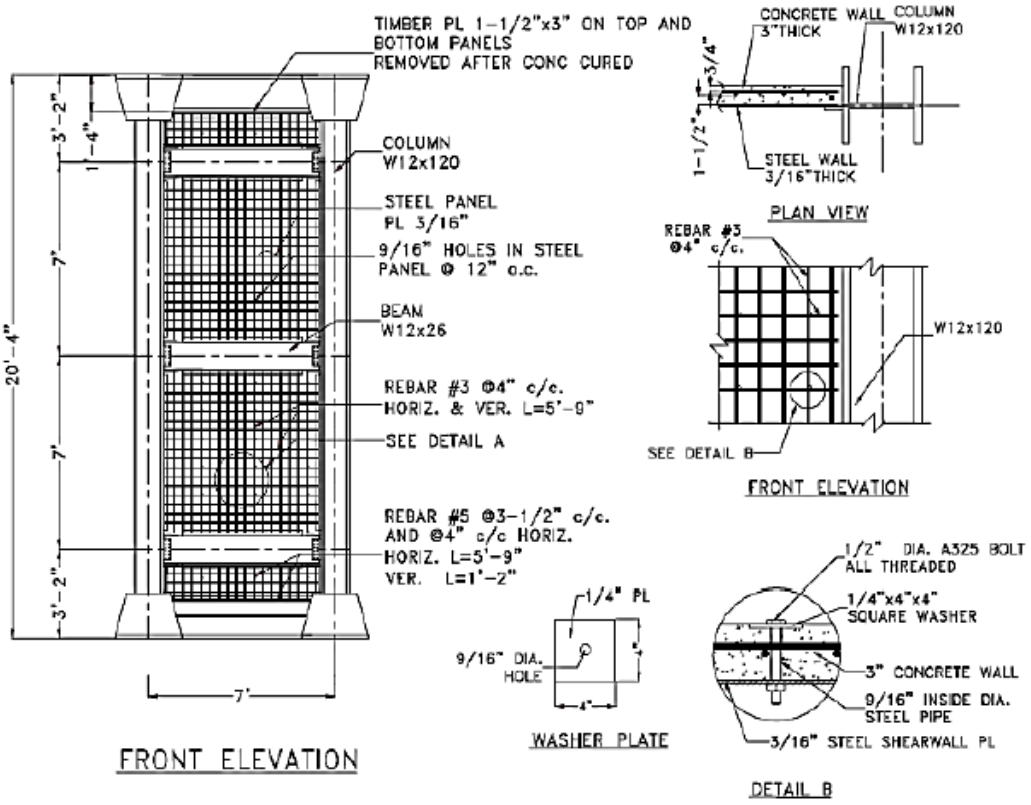

Figure 2.6: Composite Plate Shear wall specimen and the details of used elements (Zhao and Astaneh-Asl 2004)

The test results showed that in the innovative system, concrete damage under relatively large cycles was less in comparison with the traditional system. Both specimens behaved in ductile manner until the drift angle of 0.05. In 2009, Rahaei and Hatami studied the effects of bolt spacing on the behavior of the composite steel plate shear wall (C-PSW). Their investigation consists of analytical and experimental portions. They came to this conclusion that increasing the distance between bolts up to a certain distance increases ductility and energy absorption capacity of the system while decreases the out of plane displacement of steel, the maximum normal stress of the studs and the slope of the load–displacement curve.

Arabzadeh et al. (2011) investigated the behavior of composite steel plate shear walls by performing experiments on the following parameters: the direction of reinforcement in the concrete panel, the gap between reinforced concrete and the boundary frame, number of bolts, thickness of the steel plate and specimen length to width ratio.

Their tests results showed that by increasing the number of bolts, buckling load of C-PSW increases and by decreasing bolt spacing, ductility reduces whereas steel plate capacity increases. If the reinforced concrete panels were used at both sides of the steel plate, strength and energy dissipation of the system will be enhanced but ductility will be reduced.

Gou et al. (2011) worked on the behavior of steel plate and composite plate walls and found that not only the majority of the shear is resisted by the steel plate but also framing members play a great role in carrying the storey shear. They also illustrated that reinforced concrete panel restrains the overall buckling of the steel plate and so, the energy absorption capacity and ductility of the composite shear wall are higher than the identical SPSW.

From the most recent studies, Shafaei et al. (2016) have done analytical study on the C-PSW with concrete panel on one side with gap between concrete panel and the boundary elements. The aim was to understand the effects of the concrete panel thickness on the behavior of the C-PSW. They concluded that the concrete panel prevents the steel plate from buckling and the infill steel plate will resist lateral load by pure shear yield. Moreover, the shear capacity and the ultimate shear strength enhances by increasing the concrete panel thickness up to a specific value and exceeding that value will not have any effects on these parameters.

Zhen and Yingshu (2015) experimentally investigated failure mode, shear resistance, lateral stiffness, and buckling mode of composite shear wall by conducting tests on six specimens. They used a precast concrete slab to prevent steel plate buckling. They came to the following conclusions: a) the concrete layer enhances the lateral stiffness and increases the buckling strength or shear resistance of steel plate so that earthquake-resistant behavior of the system will be enhanced b) the width-thickness ratio of the steel plate affects the shear-carrying capacity and failure mode, and c) to prevent boundary failure in the case of low width-thickness ratio of steel plate adequate bonding is required.

Dey and Bhowmick (2016) conducted nonlinear finite element analysis on a 4-storey and 6-storey composite plate shear wall (C-PSW) and showed that the boundary members and the reinforced concrete panel carries more shear than what is considered for design of C-PSW in AISC 341-10. They also indicated that designing the boundary columns according to capacity design concepts gives similar axial forces and moments as the nonlinear seismic analyses. Also, they presented a formula for estimating the fundamental period of C-PSW.

2.5 Studies on Composite Plate Shear Wall (C-PSW) with opening

In this part, the few studies that were conducted so far on C-PSWs with openings are reviewed. Shafaei et al. (2017) conducted a study on composite steel plate shear walls with an unstiffened opening. They numerically investigated the effect of opening with different locations and different sizes on the behavior of C-PSW. To conduct this study, first they verified their FE model by comparing the results of their ABAQUS model with the results of previously experimented C-PSWs and SPSWs including the SPSW specimen (SPSW2) tested by Lubell et al. (2000) and three C-PSW specimens (a three-storey C-PSW specimen tested by Zhao et al. (2004) a single-storey C-PSW specimen tested by Arabzedeh et al. (2011), and a single-storey C-PSW specimen tested by Ayazi et al. (2015). In this study, nonlinear finite element "push-over" analyses of various single storey C-PSWs and their corresponding SPSWs were conducted. Abaqus Dynamic/ Explicit solver and displacement-controlled loading procedure were chosen for push over analysis. Their selection of elements for FE modelling is as following. The infill steel plate was modeled with shell elements (SR4) and boundary elements were modeled with solid elements (C3D8R). For C-PSW, they used solid elements (C3D8R) for simulating the concrete panel. Bolts were modeled with three-dimensional beam elements (B31) and rebar with 2-node three-dimensional truss elements (T3D2). Boundary conditions were selected in a way to simulate the real conditions in the buildings. For modeling the fixed base, the bottom nodes of columns (webs and flanges) were fixed and the out of plane displacements of upper beam web was restrained for simulating the effect of slab.

For investigating the behavior of C-PSW with openings, Shafaei et al. (2017) primarily compared "Shear load vs. storey drift" and "Tangent stiffness vs storey drift" of the C-PSW, its corresponding SPSW and the steel frame all without opening. Figure 2.7 depicts the comparison.

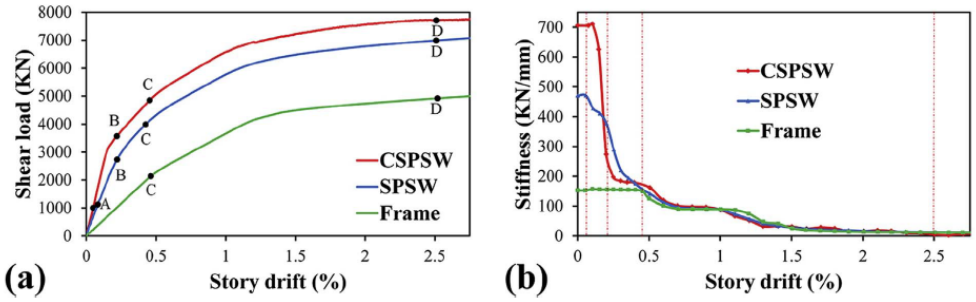

Figure 2.7: Comparison of C-PSW, SPSW and steel frame (Shafaei et al. 2017)

Then, Shear load vs. storey drift of the C-PSW, infill composite wall, SPSW and steel plate all with and without openings were compared as shown in Figure 2.8.

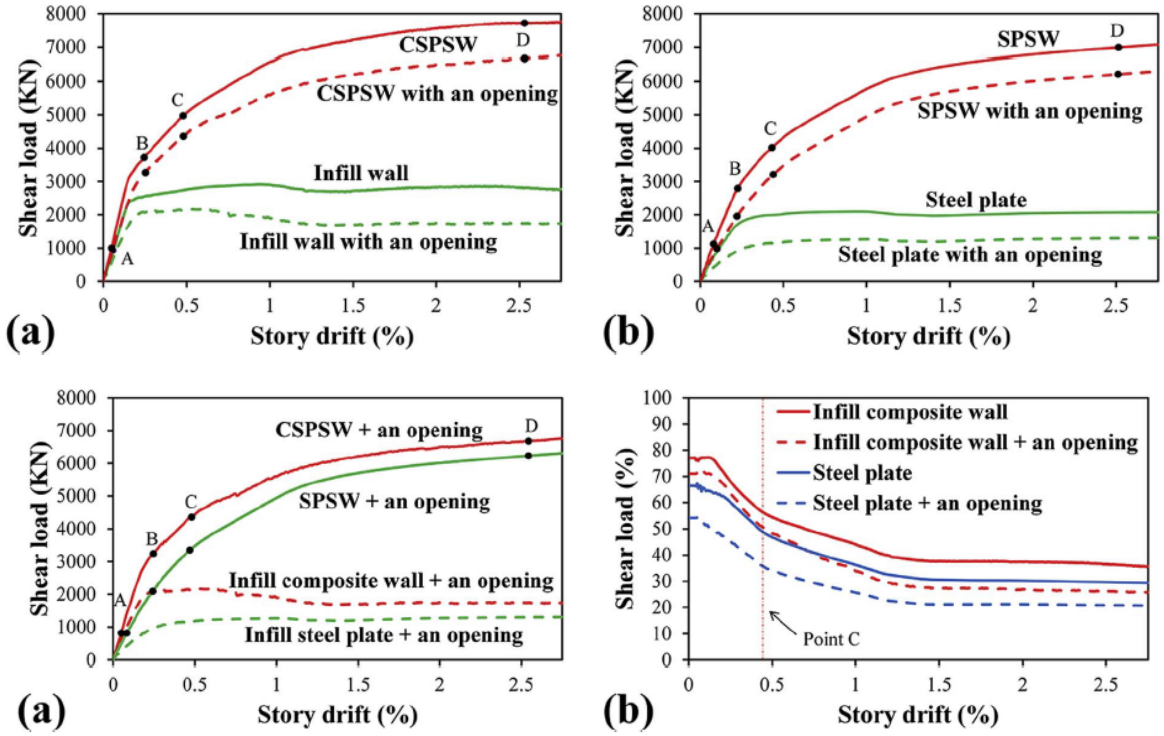

Figure 2.8: Curves of comparison between C-PSW and SPSW with and without opening (Shafaei et al. 2017)

In order to study the effect of opening location on the behavior of C-PSWs and its corresponding SPSWs, four square openings with sides (as shown with ‘a` in Figure 2.9) of 500, 1000, 1500, and 2000 mm were selected. Figure 2.9 shows the geometry for FE model of Shafaei et al. (2017)). It was assumed that while the size of square opening is constant, their locations are varied; the pattern was repeated with a new square size but with different opening locations, which are depicted in Figure 2.10. Finally, the initial elastic stiffness, ultimate shear strength, ductility ratio and energy absorption of these models were compared with each other.

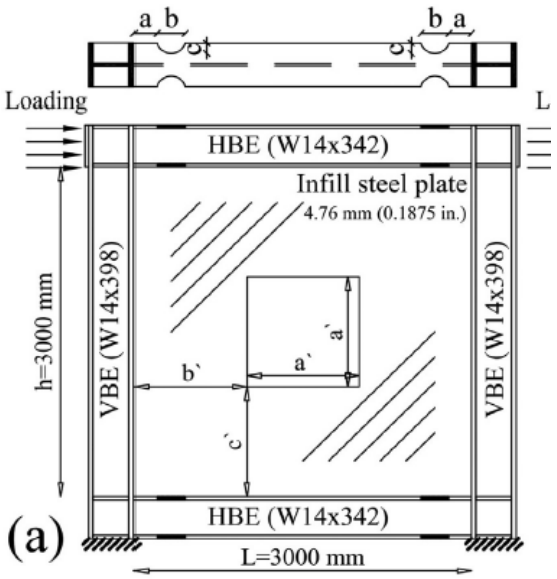

Figure 2.9: FE model details (Shafaei et al. 2017)

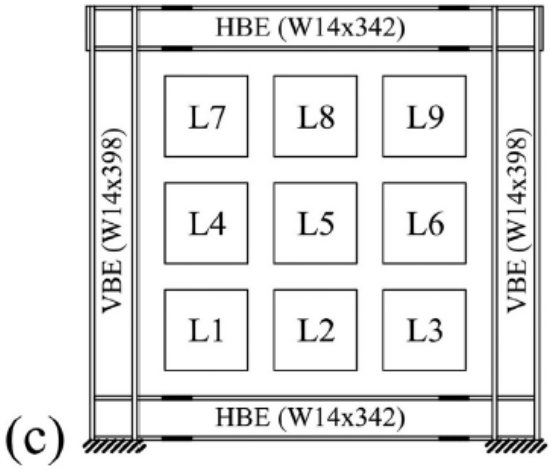

Figure 2.10: Various opening locations (Shafaei et al. 2017)

For evaluating the influence of the opening size on the behavior of C-PSWs and SPSWs, circular opening with 12 different diameters was introduced at the center of C-PSWs and its corresponding SPSWs. Figure 2.11 show the typical model. The initial stiffness, ultimate shear strength, ductility ratio, and energy absorption of these FE models were compared and formulas for initial stiffness and the ultimate shear strength of the infill composite wall with a centrally located opening were presented.

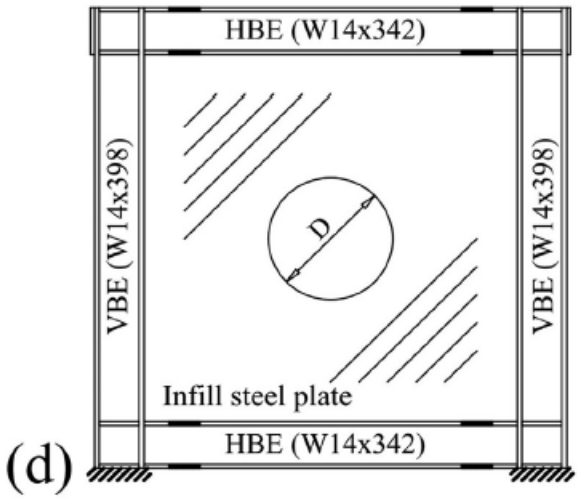

Figure 2.11: Centrally located opening (Shafaei et al. 2017)

Using the explained procedure, Shafaei et al. (2017) concluded that C-PSW and SPSW, with and without an opening, have a completely different behavior. The reinforced concrete panel in C-PSW with the solid wall and in C-PSW with a square opening prevents global and local elastic buckling and the first yield in the infill steel plate starts from outside. But in the SPSW with opening local and global buckling occurs and partial tension fields developed. The use of reinforced concrete panel in C-PSW makes inelastic out-of-plane deformation of the infill steel plate considerably lower than its corresponding SPSW.

In C-PSW the location of the opening does not affect the initial stiffness, ductility ratio and energy absorption of the system, while in SPSW theses parameter are affected by the location of the opening and if the opening is located on the tension field, the initial stiffness will have its most decline.

The results from assessing the size of opening are summarized in the following table (Table 1).

Table 1: Results from investigation of centrally located circular opening with different diameter size

Assessed parameters	C-PSW	SPSW
Initial elastic stiffness	-Linearly reduced as the opening ratio increased -Presented relation: $\boldsymbol{K_{opening} = K_{solid}(1 - 0.85\,\frac{D}{L})}$ (*)	-Decreased as the opening size increased
Ultimate shear strength	-Linearly decreased as the opening ratio increased - Presented relation: $F_{u_{opening}} = F_{u_{solid}}(1 - \frac{D}{L})$ (*)	-Decreased as the opening size increased
Ductility ratio	-Constant up to the opening ratio (D/L) of 35%, and after that it begins to decline as the opening ratio increased -As the opening ratio increased the slope of ductility ratio reduction line of C-PSWs is steeper than its corresponding SPSWs	-Immediate reduction as the opening ratio increased
energy absorption	-Severely reduced as the opening ratio increased -The reduction is noticeably higher than the corresponding SPSWs	-Severely reduced by increasing the opening ratio

(*) where "K" is the initial elastic stiffness, "F" is ultimate shear strength, "D" is the diameter of the circular opening and "L" is the length of the plate

Arabzadeh et al. (2017) numerically and experimentally investigated the effects of opening used as windows or doors in buildings on the Composite Steel Shear Wall (CSSW) behaviour. The study started with designing CSSWs of a 10- storey building according to AISC Seismic Provisions (AISC 2005). Then, for numerical investigation ABAQUS/Standard with implicit approach was used to conduct Eigenvalue and incremental nonlinear pushover analyses. In order to model the infill plates and boundary frame members, general-purpose four-node doubly-curved shell element with reduced integration (ABAQUS element S4R) was used. Also,

eight-node brick element with reduced integration (ABAQUS element C3D8R) was utilized for modeling the concrete panel. To simulate the existing situation, the bottom layer of numerical specimens was fixed in all directions as well as the out of plane direction for beam webs. ATC-24 protocol was used for cyclic loading. Loads were applied along the upper beam. Arabzadeh et al. (2017) validated their modeling procedure by comparing their pushover analysis with Park et al. (2007) and cyclic analysis with Sabouri-Ghomi et al. (2012).

In order to assess the effect of opening on shear wall parameters, 4 finite element models of steel and composite shear wall were built and compared. The models are depicted in Figure 2.12. The Shear force-displacement curves of the models were obtained.

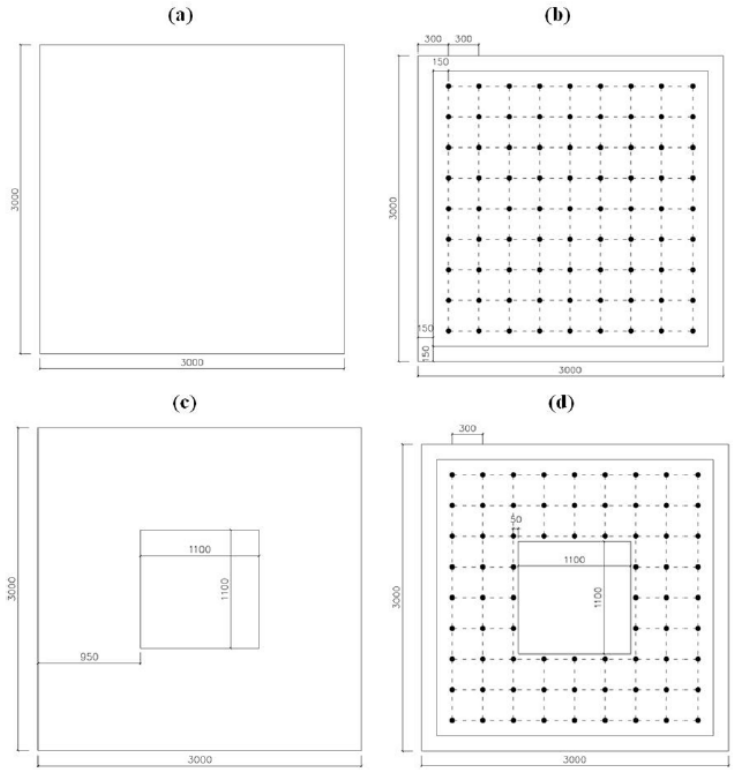

Figure 2.12: FE model details: a) steel shear wall without opening, b) Composite shear wall without opening, c) steel shear wall containing opining, d) Composite shear wall containing opening (Arabzadeh et al. 2017)

Evaluating the behavior of composite shear wall due to location of opening was done by comparison of pushover curves of 7 finite element models. Figure 2.13 demonstrates the opening positions of the 7 models.

As per their design, all the FE model specimens had a steel plate thickness of 3mm and concrete thickness of 100mm just on one side of the plate.

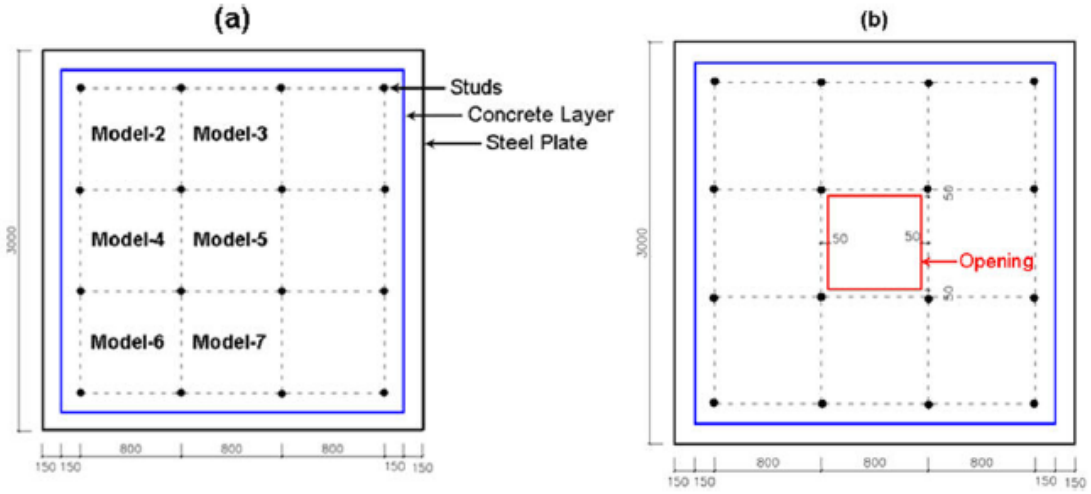

Figure 2.13: a) Location of openings in 7 FE composite shear wall models b) location of opening in model number 5 (Arabzadeh et al. 2017)

Experimental investigation was done by applying load with a hydraulic jack at the most upper part of the three constructed specimens. The specimens were a one bay, one storey composite shear wall with window opening at the center, a one bay, three-storey composite shear wall with window opening at the top right corner and a one bay, three-storey composite shear wall with door opening at the bottom right corner. All the specimens were constructed in 1:3 scale. Beam to column connections were rigid and the concrete layer was cast on one side of the steel plates. Also, Arabzadeh et al. (2017) used a gap between the concrete panel and the boundary frames to prevent interaction between them. Figure 2.14 shows the specimens.

In conducting the experimental study, Arabzadeh et al. (2017) restrained out-of-plane displacement by using lateral supports at the level of top storey. The top horizontal displacement of the specimens was recorded by a number of linear variable displacement transducers (LVDTs) and used as the displacement control parameter.

Figure 2.14: Specimens used for the experimental study (Arabzadeh et al. 2017)

Experimental and numerical studies of Arabzadeh et al. (2017) showed good agreement with each other and therefore, the FE models were demonstrating the real behavior of the structures. They also concluded that the steel plate shows a better behavior when stiffened by the concrete panel. Resistance reduction by creating opening in the steel plate shear wall is more than creating opening in composite shear wall (CSSW) and the CSSW has higher maximum shear strength and stiffness in comparison to steel shear wall. Their study also showed that CSSW with and without opening shows equal resistance when placing the studs close together.

Based on the curves obtained from CSSW numerical models with different opening locations, Arabzadeh et al. (2017) indicated that introducing the opening will decrease the resistance of composite shear wall but different opening positions do not affect the CSSW's initial stiffness. The percentage of resistance reduction in CSSW with opening in comparison with the same CSSW without opening was 11% when the opening was at the corner and 2% when it was at the center. Therefore, locating the opening at the sides and corners will cause more resistance reduction. This is on the contrary with the behavior of steel shear wall Sabouri-Ghomi et al. (2012) previously presented. Their results showed that steel shear wall resistance reduction due to opening is more when opening is located at the center.

Meghdadaian and Ghalehnovi (2019) conducted research on the effects of openings on the seismic performance of composite steel plate shear wall (C-PSW) and present methods for improving its behavior. The study included both numerical and experimental investigations. In order to verify the experimental procedure, they compared their result to that of obtained by Arabzadeh et al. (2011).

In order to evaluate the effect of opening and proposing an appropriate method for improving the negative effect due to opening, two series of C-PSWs with a 2×1.5m rectangular opening were constructed. The first specimen was a composite shear wall with opening, the second was composite shear wall with opening and 45-degree rebar at the corners of the opening, the third was composite shear wall with opening and a steel plate frame around the opening and the last one was a composite shear wall with opening and both the 45-degree rebar at the corners and a steel plate frame around the opening. The specimens were named CSWO1, CSWO2, CSWO3 and CSWO4, respectively, as illustrated in Figure 2.15.

The constructed specimens were laterally loaded according to ATC 24 loading protocol.

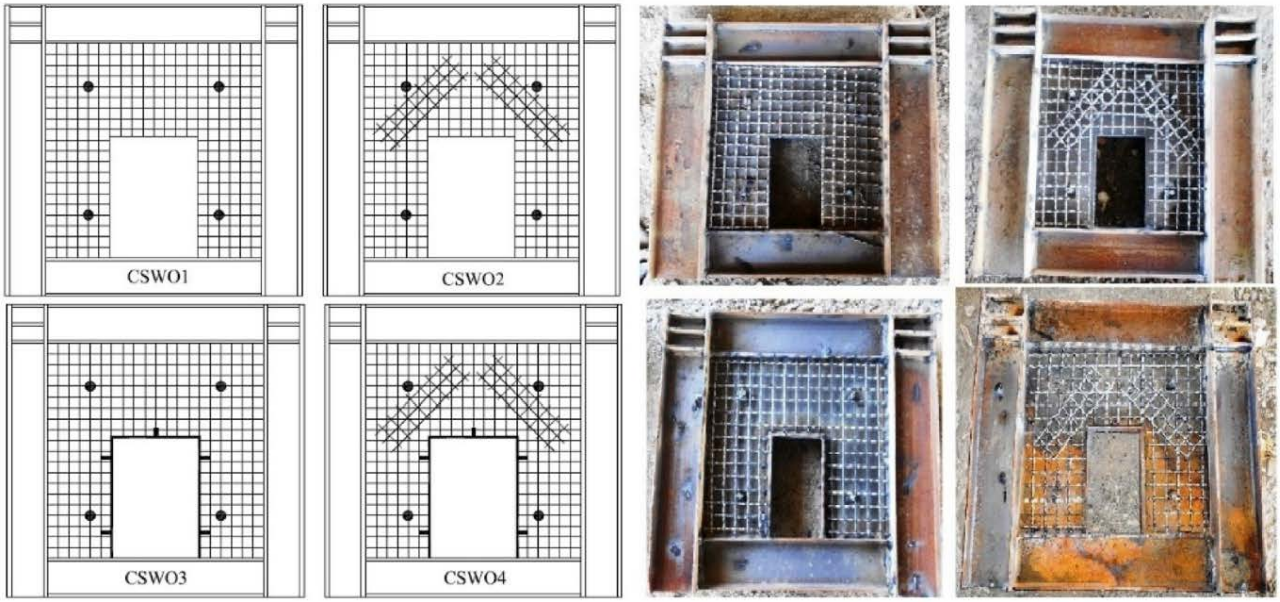

Figure 2.15: Specimens used for experimental investigation (Meghdadaian and Ghalehnovi 2019)

For numerical assessment the same specimens used in the tests were developed in ABAQUS. Modeling was verified by comparing the results of FE models with that of obtained

from tests. In modeling the C-PSWs with ABAQUS software, beam, column and concrete cover were modeled by solid elements (C3D8R), steel plate with shell element (S4R) and bolts with beam element (B31). The degrees of freedom of the lowest beam were fixed in all directions to consider the base restrains.

During the study they also investigated the variation of the drift ratio versus the variation of strengthening steel plate around the opening. The resulted curves are demonstrated in Figure 2.16. Figure 2.16 shows that the drift of the system could be reduced by thickening the infill plate and strengthening plate up to certain values but beyond those values they do not noticeably affect the drift ratio.

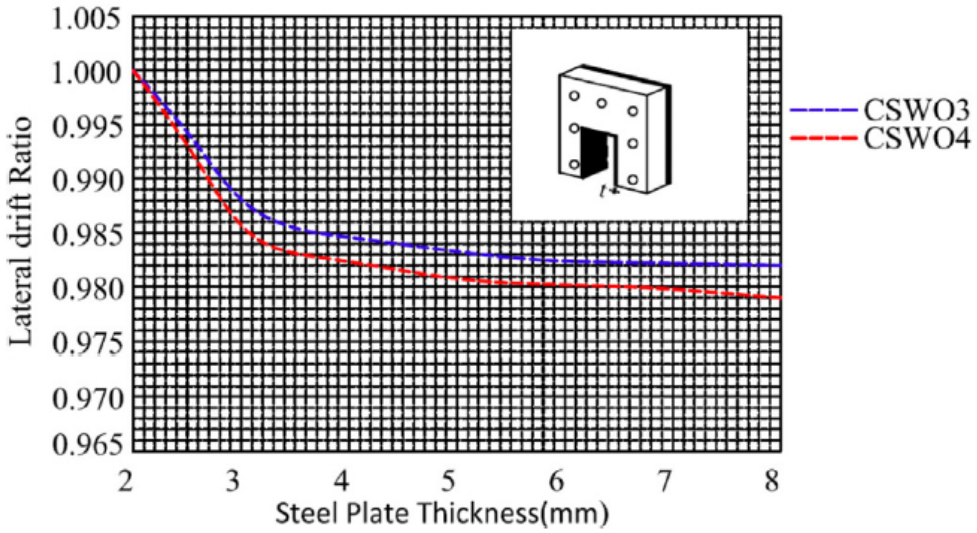

Figure 2.16: Drift ratio vs. steel plate thickness obtained by Meghdadian and Ghalehnovi (2019)

By conducting nonlinear regression on the results of their ABAQUS models, Meghdadaian and Ghalehnovi (2019) proposed the following empirical relation for the ultimate strength of C-PSW.

$$\boldsymbol{P_{UW} = P_u\left(\frac{\alpha^a \beta^b}{dc^\lambda}\right)} \qquad 2.3$$

In this formula" P_{UW}"is the ultimate load of composite shear wall with opening, "P_u" is the ultimate load of composite shear walls without openings. "a", "b", "c" and "d" are unknown coefficients and powers that were calculated in a way that the average error of each model is minimized. α, β and λ are wall and opening dimensions as depicted in Figure 2.17.

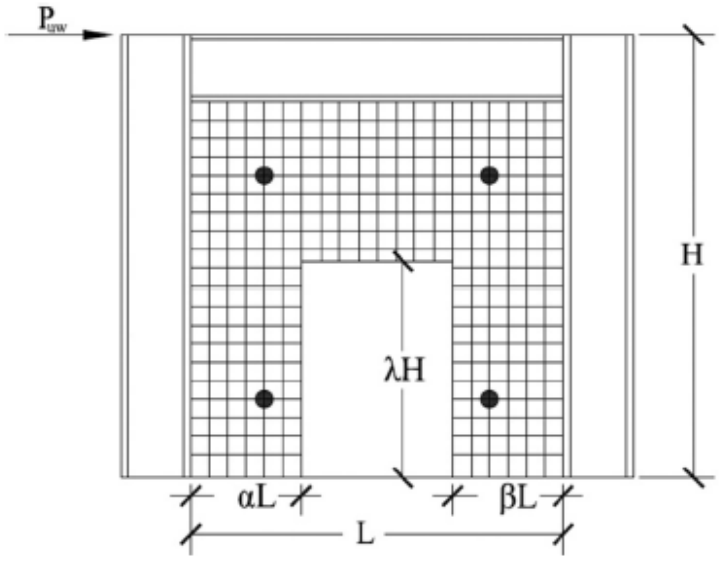

Figure 2.17: α, β and λ definition (Meghdadaian and Ghalehnovi 2019)

Meghdadaian and Ghalehnovi (2019) concluded that presence of opening in C-PSW decreased the energy absorption and stiffness of the system as well as increasing the displacement. Using steel frame around the opening and rebar in 45 degrees at the corners of opening decreased the negative effects by recovering some of the overall stiffness loss and preventing the concrete from cracking, respectively. It was mentioned that between these two methods utilizing steel plate around the opening is more effective.

Based on the method used for improving the negative effect of opening, the amounts of change in stiffness, energy absorption and displacement varied. When no improvement method was used, presence of opening increased lateral displacement by 45%. When the metal frame was located around the opening, lateral displacement increased up to 25%. Also, energy absorption capacity reduced 50% when no improving method was used and it decreased 20% when the metal frame was used.

The fourth model (combination of 45-degree rebar and steel frame) was found to be the best method for compensating the negative effect of opening.

2.6 Summary

Several experimental and numerical research studies were conducted on SPSWs with openings and limited number on C-PSWs with openings. Results showed that location and size of openings in theses shear walls can significantly influence stiffness and strength of these lateral load resisting systems. Often, SPSWs and C-PSWs need to accommodate large door or window sized openings in the infill plates, such as when SPSWs/C-PSWs are used in the building central cores around the elevators. Research on SPSWs and C-PSWs with large openings is still in the initial stage and no study has been done to investigate the behavior of SPSW and C-PSW with large rectangular openings under real seismic loadings. This research will study seismic performance of code designed SPSWs and C-PSWs with large rectangular (door sized) openings.

Chapter Three

3. Finite Element Analysis of Composite Steel Plate Shear Walls with opening

3.1 Introduction

In this chapter the development of finite element model including selection of analysis type, element type and material properties are discussed. The boundary condition and initial considerations are also explained. In modeling the SPSW and C-PSW non-linear properties of material and geometry nonlinearity were considered and are described in this chapter.

In order to ascertain the accuracy of obtained results from FE models, the results were verified with the results of Arabzadeh et al. (2017) and Zhao (2004).

3.2 Selection of Finite Element Analysis Technique

The commercially available finite element software ABAQUS (2018) was used to study the behavior of steel plate and composite steel plate shear walls. ABAQUS is a powerful FE analysis software that is able to solve extensive range of problems from simple linear analyses to most challenging nonlinear simulations. The concrete damaged plasticity model exists in this software is suitable for modeling concrete material (used in C-PSWs) and its nonlinear behavior.

The modeling and analysis technique should be selected carefully in order to minimize convergence problem and be analytically less expensive. ABAQUS uses implicit or explicit approach for dynamic integration. Selection between implicit or explicit procedures requires understanding the characteristics of each procedure. ABAQUS/standard uses an implicit approach while ABAQUS/explicit uses an explicit formulation for analyzing the simulation. Implicit and explicit approaches use different methods for solving the nonlinear problems. ABAQUS/Standard utilizes Newton-Raphson method and combining incremental and iterative procedures for solving nonlinear problems. In this approach several load increments are made and approximate equilibrium configuration at the end of each load increment is found. In other words, calculation of the current time step is based on the results of the previous time step. The

iterations continue until convergence. This process is based on the equilibrium of the externally applied loads and the internal structural forces. This method is unconditionally stable and can be used for large time steps.

Unlike implicit approach ABAQUS/Explicit determines the solution without iterating and by explicitly using the kinematic conditions at one increment to calculate the kinematic conditions at the next increment. This means that at the end of each increment the stiffness matrix is updated and the increment displacement is obtained. With this approach quasi-static analysis could be performed by proper control of the kinetic energy. In this approach no convergence and iteration checking is required. The time increment should be small enough in order to lie on the curve.

In situations that ABAQUS/Explicit can be used to analyze the problem, it is more attractive because for the same problem it uses much less disk space and memory compared to ABAQUS/Standard. ABAQUS/Explicit has the capability to analyze the following types of problems:

- High-speed (short duration) dynamics
- Large, nonlinear, quasi-static analyses
- Highly discontinuous post buckling and collapse simulations
- Coupled temperature-displacement(dynamic)
- Structural acoustic

It should be mentioned that convergence problems can occur in the implicit approach. As an example, Behbahanifard et al. (2003) experienced convergence problem in their analyses of SPSW models under quasi-static loading. So they utilized the explicit formulation for their analysis instead.

Based on the described characteristics of explicit and implicit approaches, the explicit method was selected for model validation and for nonlinear pushover analyses. But in seismic analysis, when the full structural system and damping are considered, explicit approach requires a significant amount of time for analysis, so implicit approach was used instead. Also, for push-over analysis the displacement-controlled procedure was utilized in this research.

3.3 Characteristics of the Finite Element Model

3.3.1 Geometry and Initial Conditions

FE model of C-PSW was developed and validated with the experimental studies. Also, the FE model was used to study the seismic behavior and investigate key seismic parameters of C-PSW and SPSW with openings. The C-PSW model for validation was developed in a way to make it as close as to the experimental specimen of Arabzadeh et al. (2017) and Zhao (2004). All geometrical dimensions of the FE models are the same as the conducted tests.

First, C-PSW without opening was modeled and verified. The specimen was the experimental model of Zhao et al. (2004), as shown in Figure 2.6. Then, another C-PSW specimen with a square opening at the center tested by Arabzadeh et al. (2017) was modeled and verified. The C-PSW specimen was named “S1” in their study.

Both of the specimens used for FE validation had gap between the concrete panel and the boundary elements. Beam to column connections were fixed and lateral bracing on the beam level were provided. In the modeling procedure, the bottom nodes of both columns flanges and webs were prevented from all displacement to simulate the fix support condition. Also, the out-of-plane displacement of beam webs were restrained, same as what was done in the conducted tests to replicate the effects of the concrete slab in each storey.

According to Driver et al. (1997), neglecting the fish plate in FE modeling does not affect the overall behavior of steel plate shear walls. Thus, in the modeling procedure fish plates were not modeled and the infill steel plate was considered directly connected to the boundary elements. Also, instead of modeling the shear studs, the concrete panel and the steel plate were connected together using ABAQUS beam connector. The reinforcement with appropriate reinforcement ratio was applied as a smeared layer in the concrete shell. In the SPSW, the initial imperfection was considered for infill steel plates to initiate buckling in the plates and develop tension fields.

In C-PSW, the contact between the concrete panel and steel plate was just by means of shear studs and frictionless contact was considered between the steel plate and the concrete

panel. Other researchers like Rahai and Hatami (2009), Ayazi et al. (2012), Shafaei et al. (2017) also neglected the friction between the steel infill and the RC panel in their C-PSWs models.

3.3.2 Element Selection

ABAQUS software allows modelling of most engineering materials. Selection of elements is based on the expected behavior and analysis purposes. The behavior of C-PSW under lateral loads is yielding of the steel plate in shear and development of tension cracks in concrete panel.

In this study, shell element type was used for modeling the infill plates, boundary elements and the concrete panels. The web and flanges of beams and columns, infill plate and concrete panel were modeled using general-purpose four node doubly-curved shell element with reduced integration (ABAQUS element S4R). General-purpose elements are free to deform with transverse shear. If the shell thickness increases, these elements will use thick shell theory. S4R is a 4-node, quadrilateral, stress/displacement shell element with reduced integration, which has a large strain formulation and is suitable for finite membrane strains and large rotations. S4R element forms the element internal force vector just at one integration point which is located at mid-surface. This element also provides three translations and three rotational degrees of freedom for every node. Utilizing S4R element is also a good match with the concrete damaged plasticity model. If the elements are not distorted or loaded in in-plane bending, using reduced integration method gives reasonably accurate results while reducing the running time noticeably (ABAQUS manual documentation).

3.3.3 Materials Properties

SPSW is composed of steel material and the C-PSW is composed of steel and concrete material for which the material properties should be defined in the software.

3.3.3.1 Steel material properties

In order to define steel material, the density, Young's Modulus, Poisson's ratio, Yield stress, plastic strain and hardening type should be introduced into the software. In the validation process, the quantities of these parameters were defined similar to the values identified by researchers. In seismic analysis for the selected C-PSWs and SPSWs of this research, the stress-

strain curves of the conventional structural steel standards ASTM-A36 is used for infill plate and ASTM-572 for boundary members. In these analyses, the Von-Mises yield criterion and combined hardening model was adopted. Raleigh proportional damping with a damping ratio of 5% was considered for the seismic analysis.

3.3.3.2 Concrete material properties

Performance of C-PSW highly depends on its reinforced concrete panel. In C-PSW, diagonal cracks develop in the concrete panel under lateral forces. Therefore, to obtain the accurate behavior of concrete in C-PSW under dynamic loads, selection of a suitable concrete constitutive model is required.

Different methods (concrete smeared cracking, cracking model for concrete and concrete damaged plasticity) exist in ABAQUS for simulating the behavior of concrete material. The concrete smeared cracking is appropriate for modeling concrete behavior under monotonic loadings with fairly low confining pressures. The cracking model for concrete can be utilized when the behavior is dominated by tensile cracking. It models discontinuous brittle behavior in concrete. The concrete damage plasticity (CDP) which is used herein is an appropriate method for taking both main two failure mechanisms of concrete into account. The two failure mechanisms in concrete are tensile cracking and compressive crushing. CDP model is a continuum, plasticity-based damaged model for concrete. It is able to simulate elastic and plastic behavior of concrete in tension and compression, irreversible damage when fracture occurs and stiffness recovery under reverse dynamic loads.

In the validation process, concrete compressive strength ($\acute{f_c}$) of 25 MPa and 28 MPa (same values as utilized in the experimental studies) are defined for modeling the specimen of Arabzadeh et. al (2017) and Zhao et al. (2004), respectively. In models used for seismic investigations, concrete with compressive strength of 28 MPa is selected. In this study, the strain-stress curve is calculated based on the proposed method by Hsu and Hsu (1994), which is described later.

3.3.4 ABAQUS Concrete damaged plasticity model

One of the strength hypotheses is the Drucker– Prager hypothesis (1952). This hypothesis has a cone shape failure surface. Drucker– Prager yield criterion is often used for concrete where both normal and shear stresses can determine failure.

Concrete Damaged Plasticity model (CDP) is the modified form of the Drucker–Prager strength hypothesis. According to the modifications done by Lubliner (1989), Lee and Fenves (1998) the shape of failure surface is not necessarily a circle and can be changed by the effect of another parameter named K_c which is described later in the chapter.

The ABAQUS CDP model assumes that the main failure mechanisms of concrete are crushing in compression and cracking in tension. Two hardening variables namely; tensile equivalent plastic strain ($\tilde{\varepsilon}_t^{pl}$) and compressive equivalent plastic strain ($\tilde{\varepsilon}_c^{pl}$), controls the evolution of the failure surface. The stiffness degradation in CDP model is initially isotropic and defined by degradation variable d_t in tension region and d_c in compression region.

The states of damage are independently characterized using hardening variables $\tilde{\varepsilon}_t^{pl}$ and $\tilde{\varepsilon}_c^{pl}$ for tension and compression. $\tilde{\varepsilon}_t^{pl}$ is equivalent plastic strains in tension and $\tilde{\varepsilon}_c^{pl}$ is equivalent plastic strains in compression.

Increase in the amount of hardening variables is representative of crushing or cracking in concrete. The reduction of inelastic stiffness and formation of yield surface is controlled by these parameters.

3.3.5 Defining Concrete Damage Plasticity parameters in ABAQUS

In order to model the concrete material using CDP model, dialation angle, K_c, $\frac{f_{b0}}{f_c}$, eccentricity, complete mathematical relationships of stress-strain curves in tension and compression along with their damage curve parameters should be defined in ABAQUS.

3.3.5.1 K_c Parameter:

This parameter defines the ratio of the distances between the hydrostatic axis of compression meridian and the tension meridian in the deviatoric cross section. A value of 2/3 is suggested for K_c parameter in the CDP model

3.3.5.2 Eccentricity Parameter:

Eccentricity parameter in CDP model is representative of the plastic potential eccentricity and is used for adjusting the shape of plastic potential surface. This parameter indicates the rate of approach of the plastic potential hyperbola to its asymptote and has a small positive value. The value of this parameter can be calculated as a ratio of tensile strength to compressive strength, as suggested by Jankowiak et al. (2005). If the Eccentricity Parameter is equal to 0, the surface in the meridional plane is straight line which was the classic Drucker-Prager hypothesis. CDP model suggests 0.1 as an appropriate value for this parameter.

3.3.5.3 f_{b0}/f_{c0}:

Next parameter that should be defined to the software for modeling the concrete material is the ratio of f_{b0}/f_{c0}. With this parameter, the state at which the concrete undergoes failure under biaxial compression is defined. f_{b0} (σ_{b0}) is the biaxial strength and f_{c0}(σ_{c0}) is the uniaxial strength. ABAQUS manual suggests 1.16 as a default value for this parameter.

3.3.5.4 Dilation Angle:

In general, Dilatancy is the volume change observed in granular materials when they are subjected to shear deformations. The value of dialation angle depends on both the type of material and its application.

For concrete this parameter can be obtained from concrete tri-axial compressive test and calculated as the ratio of the plastic volume change over plastic shear strain (Vemeer and de Borst 1984). In concrete the value of this parameter can take any amounts between zero and its friction angle.

In ABAQUS manual, the value of $15°$ and $36.31°$ is recommended for this parameter. Other researchers suggest various amounts for this value. Lubliner et al. (1989) recommended $8° - 15°$and Lee and Fenves (1998) recommended $34.6°$ for this value. Also

earlier an equation was presented by Vemeer and de Borst (1984) for calculation of dilation angle as follows:

$$\sin \beta_1 = \frac{\dot{\varepsilon}_v p}{-2\dot{\varepsilon}_1 p + \dot{\varepsilon}_v p} \qquad 3.1$$

where β_1 is the dilation angle, "$\dot{\varepsilon}_1 p$" is the axial plastic strain increment and "$\dot{\varepsilon}_v p$" is the volumetric increment. Their experimental investigations showed that the dilation angle of concrete is at least $20°$ less than its friction angle which will be around $37°$.

Later, Syed (2012) validated the proposed equation of Vemeer et al.(1984) and presented the values of dilations angle as $25° - 35°$ for concrete with normal weight. Also, they mentioned that the value of shear strength is affected by dilation angle but at the material level the values of compressive/tensile strength and strain hardening/softening regions are not dependent to dilation angle when the dilation angle is between $20° - 55°$. In this research, the dilation angle of $31°$ was selected in validation, pushover and seismic analysis process.

3.3.5.5 Viscosity parameter

In ABAQUS software, convergence difficulties may happen due to softening behavior of material models and stiffness degradation. To solve this problem, the viscosity parameter (μ) should be defined. In another words, μ is the smallest positive number that can improve the analysis convergence. In this study, the value of 0.001 is selected for viscosity.

Tension/Compression recovery factor is also required to be defined in the CDP model. According to Syed (2012)'s investigations, the size and orientation of the loop of the stress-strain curves are dependent on Tension/Compression recovery factor. Also, the type of material is reported to be the nature of variation in the loop. But the grade of concrete does not affect the loop.

Therefore, the default values recommended by ABAQUS (compressive stiffness recovery factor equal to 1 and tensile stiffness recovery factor equal to 0) are selected for these parameters. These value are interpreted as full compressive stiffness recovery upon crack closure when loading changes from tension to compression, and no tension stiffness recovery for the case of changing loads from compression to tension (when concrete crushing appears).

3.3.6 Concrete response under uniaxial tension and compression:

The main features of concrete response under tension and compression are described in this section. Concrete has an elastic linear stress-strain relationship under uniaxial tension until the stress reaches the failure stress (σ_{t0}) which is the state of initiation of micro cracking in concrete. Exceeding this stress macroscopic micro-cracks start to form with a softening stress-strain response and induces strain localization in the concrete structure. This trend continues until the stresses reaches to near zero where the concrete failed.

The response of concrete under uniaxial compression is also linear to the point of initial yield (σ_{c0}). Above the ultimate stress (σ_{cu}), the concrete shows hardening followed by strain softening. In ABAQUS, uniaxial stress-strain curve is converted to stress versus plastic-strain curve.

The relation between stress and cracking strain ($\tilde{\varepsilon}_t^{ck}$) in uniaxial tension, and stress and crushing strain ($\tilde{\varepsilon}_c^{in}$) in uniaxial compression can be determined using uniaxial tension/compression stress-strain curves.

3.3.6.1 Stress-Strain curve for uniaxial compression

The most accurate method for determining the stress-strain relation for a specific concrete is to conduct uniaxial compression tests. Figure 3.1 shows stress-strain relation in compression for CDP model. In CDP model, inelastic strain ($\tilde{\varepsilon}_c^{in}$) should be given as an input data. In order to determine the inelastic strain values, the elastic part (corresponding to the undamaged material) is deducted from the total strains of the uniaxial compression test:

$$\tilde{\boldsymbol{\varepsilon}}_{\mathbf{c}}^{\mathbf{in}} = \boldsymbol{\varepsilon}_{\boldsymbol{c}} - \boldsymbol{\varepsilon}_{\mathbf{0}\boldsymbol{c}}^{\boldsymbol{el}} \qquad 3.2$$

where "$\tilde{\varepsilon}_c^{in}$" is the inelastic strain, "ε_{0c}^{el}" is the elastic strain corresponding to the undamaged concrete material: $\varepsilon_{0c}^{el} = \frac{\sigma_c}{E_0}$, "$\varepsilon_c$" is the total concrete compressive strain, , "σ_c" is the concrete compressive stress and "E_0" is the young modulus.

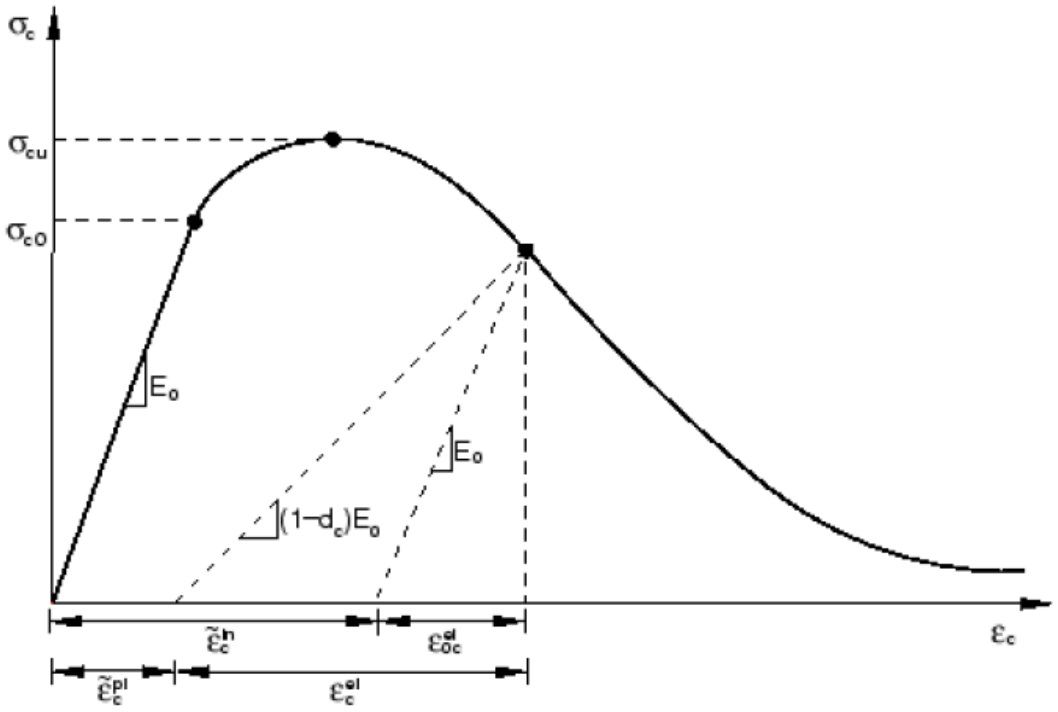

Figure 3.1 : stress-strain relation in compression for CDP model, crushing strain ($\tilde{\varepsilon}_c^{\text{in}}$) definition in compression hardening model (ABAQUS user's manual)

In order to introduce unloading data to ABAQUS CDP model, compressive damage curves ($d_c - \tilde{\varepsilon}_c^{in}$) should be provided. Then inelastic strain values were converted to plastic strain values automatically. The equation used for converting the inelastic strain to plastic strain is as follows:

$$\tilde{\varepsilon}_c^{\text{pl}} = \tilde{\varepsilon}_c^{in} - \frac{d_c}{(1-d_c)} \frac{\sigma_c}{E_0} \qquad 3.3$$

where d_c is the damage parameter and is calculated as the ratio of the degraded strength to the peak strength.

When the calculated plastic strain values are negative and/or decreasing with increasing inelastic strain ABAQUS gives an error. This situation is most probable when the compressive damage curves are incorrect. Also in the case of not defining compressive damage ABAQUS assumes $\tilde{\varepsilon}_c^{\text{pl}} = \tilde{\varepsilon}_c^{in}$ and the model behaves as a plasticity model.

3.3.6.2 Concrete constitutive model in compression

As described earlier, concrete response is defined by stress-strain curves. In FE modeling, for defining nonlinear part of the concrete response mathematical equation is required. Several equations have been provided by researches such as Hognestad (1951), Smith et al. (1955), Saenz (1955), Popovics (1973), Yip (1998) and constitutive models of Chang and Mander (1994), Belarbi and Hsu (1994) and Hsu and Hsu (1994).

In this research the constitutive model presented by Hsu and Hsu (1994) was used to define the complete concrete stress-strain curve under compression. As reported by Hsu and Hsu (1994), the formulations can be used to calculate the stress-strain relation for concrete with compressive strength of up to 62 MPa and above this value some modifications should be done. The reason for selecting this model was its capability to estimate concrete strains and stresses up to the complete failure and that the entire relationship could be found with just concrete compressive strength ($\acute{f}_c$) value. The stress-strain curve has a linear relation up to the point equal to 0.5 times of ultimate compressive strength and for the rest of the curve the following formula is used:

$$\sigma_c = \left(\frac{\beta\left(\frac{\varepsilon_c}{\varepsilon_0}\right)}{\beta - 1 + \left(\frac{\varepsilon_c}{\varepsilon_0}\right)^{\beta}}\right)\acute{f}_c \quad (3.4)$$

$$\text{where } \beta = \frac{1}{1 - \left[\frac{\acute{f}_c}{\varepsilon_0 E_c}\right]} \quad (3.5)$$

$$\varepsilon_0 = 8.9 \times 10^{-5}\acute{f}_c + 2.114 \times 10^{-3} \quad (3.6)$$

$$E_c = 1.2431 \times 10^{2}\acute{f}_c + 3.28312 \times 10^{3} \quad (3.7)$$

In the above equations, "σ_c" demonstrates the concrete average compressive stress, "$\acute{f}_c$" is the peak compressive stress of the concrete, "ε_0" is the peak strain at maximum strength, "ε_c"

is the average compressive strain and "E_c" is the initial elastic modulus of concrete in compression and should be inserted in the equation with the unit of Ksi.

The value of concrete compressive strength used for specimen of Arabzadeh et al. (2017) and Zhao et al. (2004) was 25 MPa and 28 MPa, respectively. These values were used in the validation process. And for the models used for seismic analysis, concrete with compressive strength of 28 MPa was selected. The compression hardening and the progressive damage relations were calculated as expressed in section 3.3.6.1.

Figure 3.2 to Figure 3.5 show the concrete compression hardening and damage parameter curves calculated based on Hsu and Hsu (1994) constitutive model.

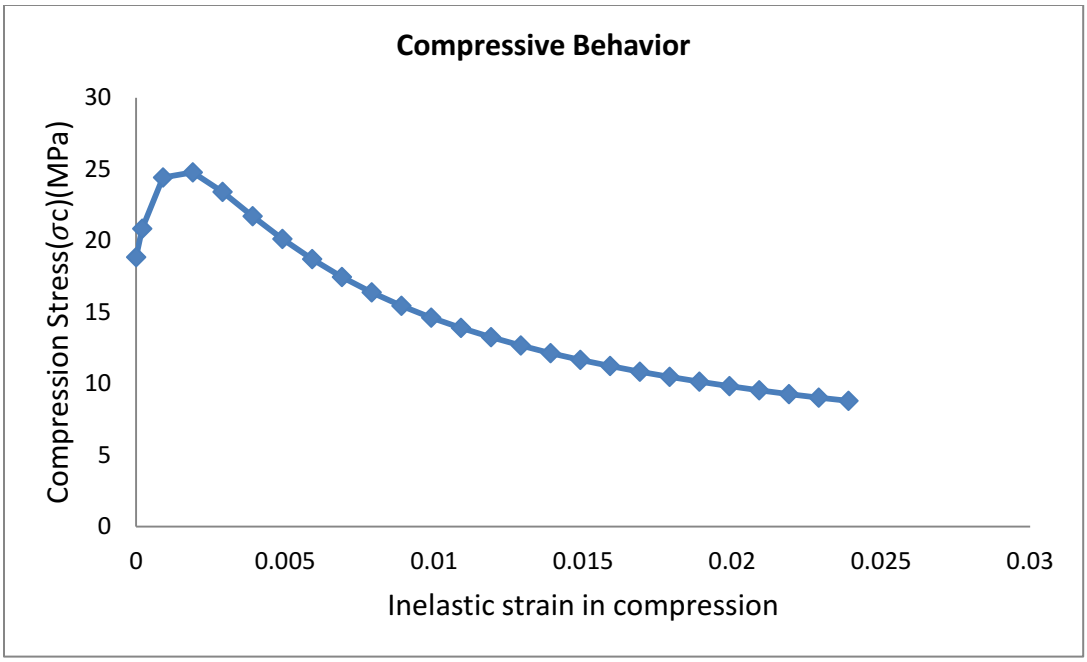

Figure 3.2 : Concrete compression hardening curve for concrete with compressive strength 25 MPa

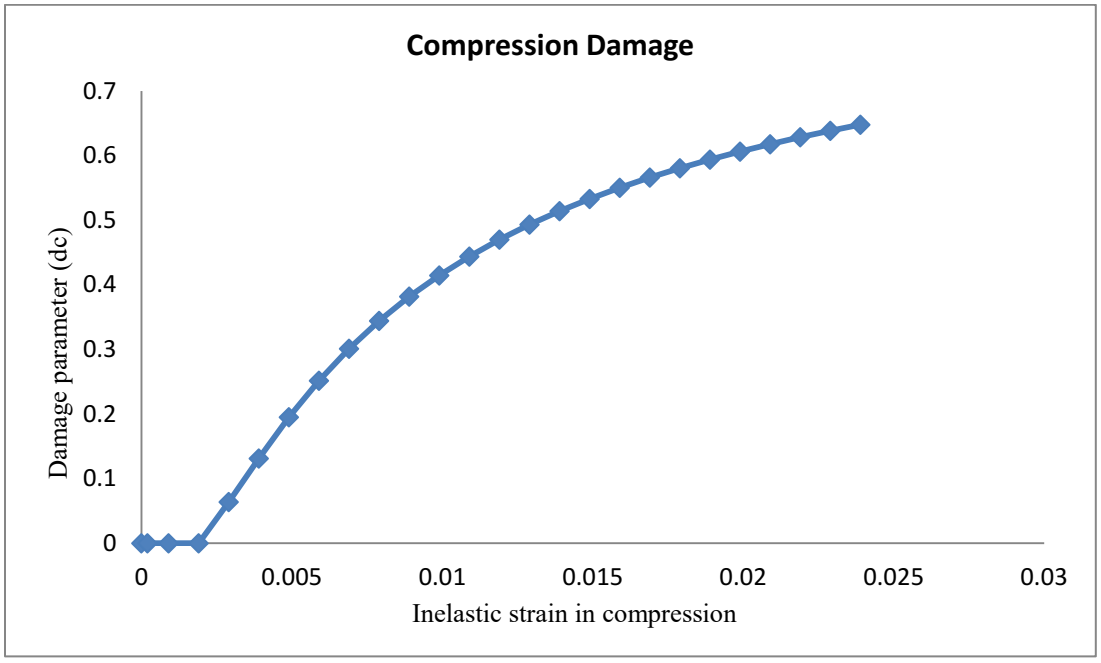

Figure 3.3: Concrete damage parameter values for concrete with compressive strength 25 MPa

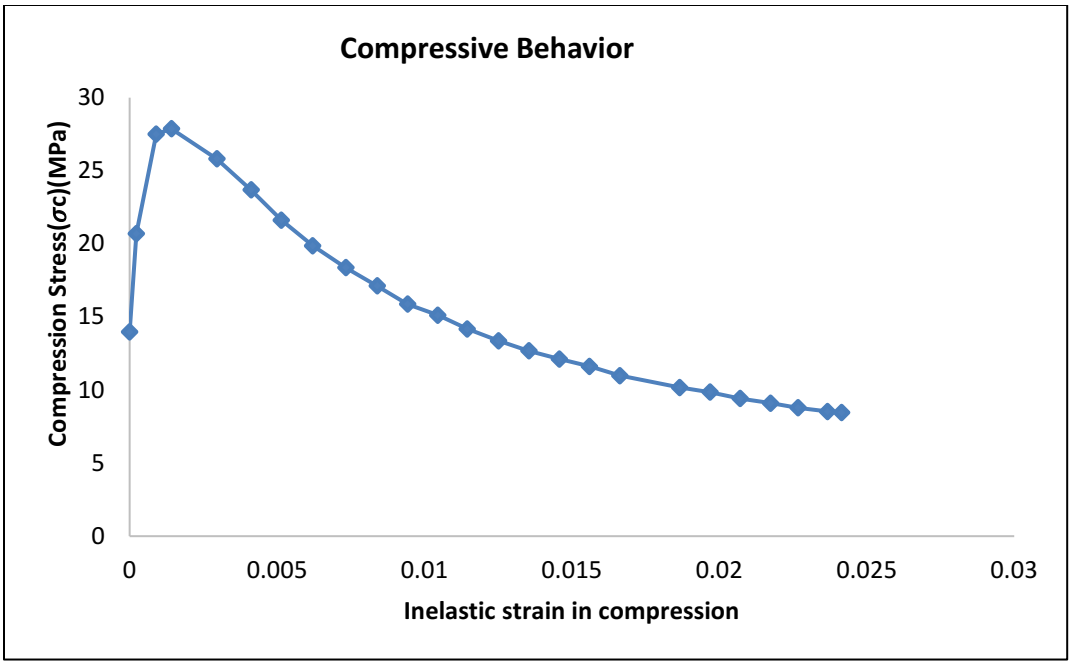

Figure 3.4: Concrete compression hardening curve for concrete with compressive strength 28 MPa

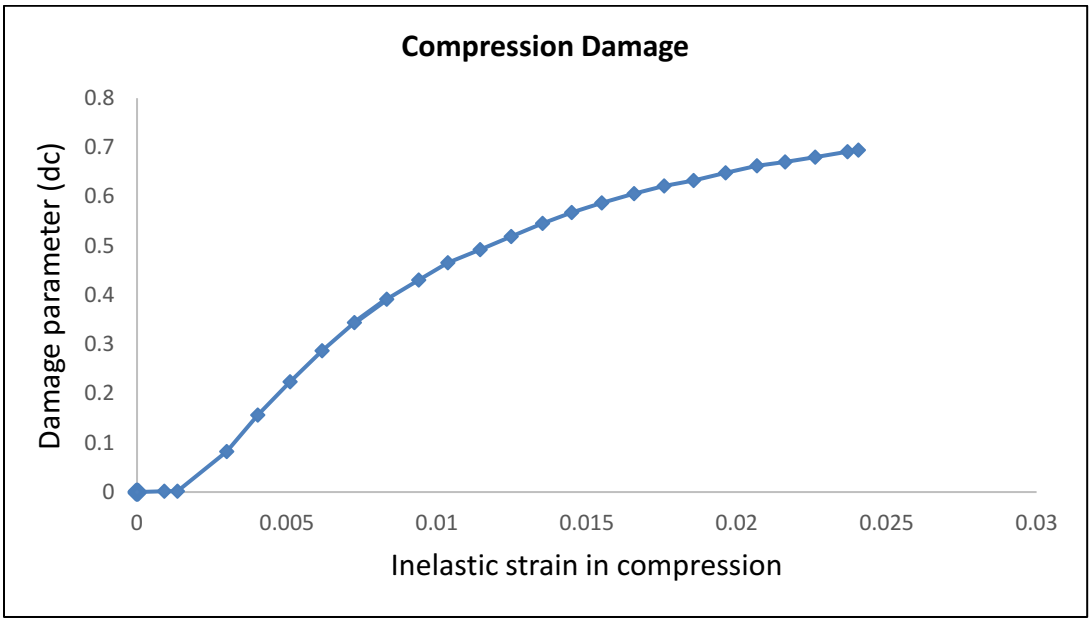

Figure 3.5: Concrete damage parameter values for concrete with compressive strength 28 MPa

3.3.6.3 Stress-Strain curve for uniaxial tension

The cracking strain $\tilde{\varepsilon}_t^{ck}$ in the CDP model is used to take into account the tension stiffening phenomenon .Tension Stiffening in reinforced concrete is the increase in stiffness of a

cracked member due to the development of tensile stresses in the concrete between the cracks. Therefore, the phenomenon such as aggregate interlocking in a crack and concrete-to-steel adhesion between cracks should be taken into account. In the tension zone, the tensile stress in concrete gradually decreases as cracking develops. The strain after cracking is measured as subtraction of the elastic strain of undamaged material from the total strain.

Figure 3.6 shows the stress-strain relation in tension for CDP model. The parameters that should be provided to the software to simulate the tensile behavior of reinforced concrete are young's modulus (E_t), tensile stresses and their corresponding cracking strains ($\sigma_t - \tilde{\varepsilon}_t^{ck}$) and tensile damage curves ($d_t - \tilde{\varepsilon}_t^{ck}$) calculated using concrete constitutive model for the selected concrete grade. $\tilde{\varepsilon}_t^{ck}$ is defined as follows:

$$\tilde{\varepsilon}_t^{ck} = \varepsilon_t - \varepsilon_{0t}^{el} \tag{3.8}$$

$$\varepsilon_{0t}^{el} = \frac{\sigma_t}{E_t} \tag{3.9}$$

where '$\tilde{\varepsilon}_t^{ck}$' is the cracking strain, 'ε_t' is the total concrete tensile strain, 'ε_{0t}^{el}' is the elastic strain corresponding to undamaged concrete material and 'σ_t' is the concrete tensile stress.

ABAQUS necessitates choosing $\sigma_t \geq \frac{\sigma_{t0}}{100}$ so that the numerical problems are prevented.

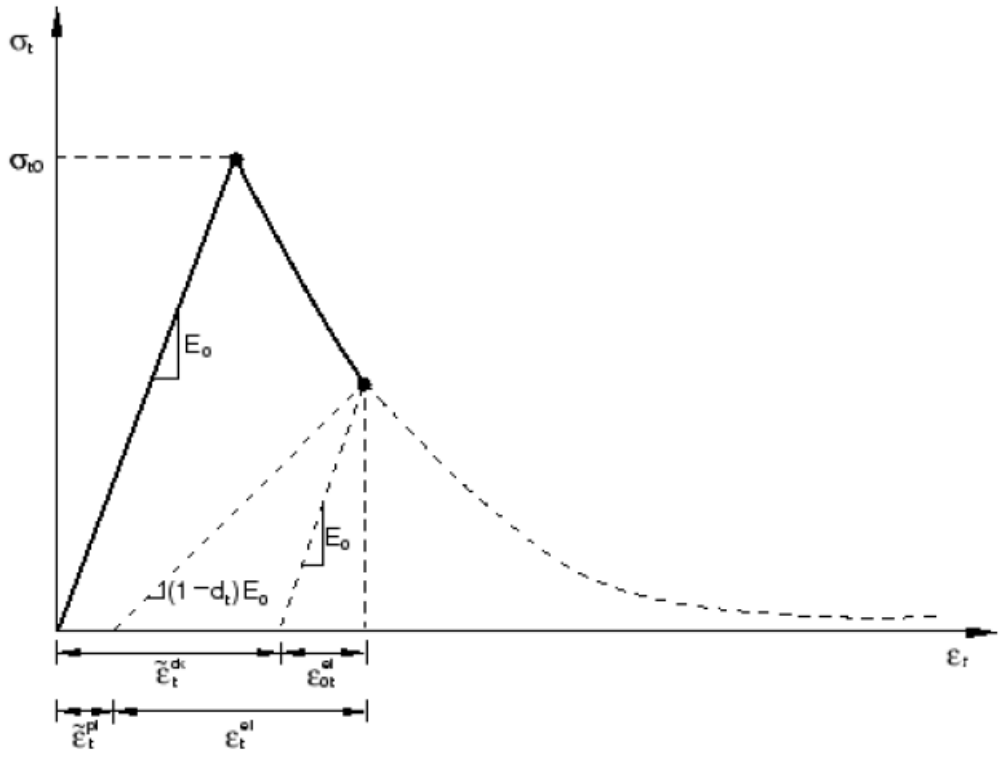

Figure 3.6 : Stress-strain relation in tension for CDP model, cracking strain ($\tilde{\boldsymbol{\varepsilon}}_{\mathbf{t}}^{\mathbf{ck}}$) definition in tension stiffening model (ABAQUS user's manual)

For simulating the unloading, damage parameters (d_t) along with their corresponding cracking strains($\tilde{\varepsilon}_t^{ck}$) should be defined in the software. Using these parameters ABAQUS calculates plastic strain values with the following equation:

$$\tilde{\boldsymbol{\varepsilon}}_{\mathbf{t}}^{\mathbf{pl}} = \tilde{\boldsymbol{\varepsilon}}_{\mathbf{t}}^{\mathbf{ck}} - \frac{\mathbf{d_t}}{\mathbf{1-d_t}}\frac{\boldsymbol{\sigma}_{\mathbf{t}}}{\mathbf{E_0}} \qquad 3.10$$

The damage parameter (d_t) is calculated as the ratio of degraded strength to the peak strength ($1 - \frac{\sigma_t}{f_{cr}}$). Where "$f_{cr}$" is the peak concrete tensile stress.

All the required parameter mentioned above for taking into account tension stiffening, strain-softening and interaction of reinforcement with concrete were provided to the software using the selected concrete constitutive model which is described in the next section.

3.3.6.4 Concrete constitutive model in tension

In order to provide the tensile stress-strain curve, similar to Figure 3.6, the concrete constitutive model of Belarbi and Hsu (1994) was selected. They presented constitutive models for average tensile stress strain relation for the reinforced concrete by conducting experiments on reinforced concrete panels subjected to normal stresses. Their proposed model was also validated later by other researchers like Pang and Hsu (1995), Hsu and Zhang (1996), Mansour, Lee and Hsu, (2001), Hsu and Zhu (2002). The proposed method is described below.

For $\varepsilon_c \leq \varepsilon_{cr}$ $\sigma_t = E_t \varepsilon_c$ 3.1

For $\varepsilon_c \geq \varepsilon_{cr}$ $\sigma_t = f_{cr}(\frac{\varepsilon_{cr}}{\varepsilon_c})^{0.4}$ 3.2

Where:

$E_t = 3875\sqrt{\acute{f}_c}\ (Mpa)$ 3.3

$f_{cr} = 0.31\sqrt{\acute{f}_c}$ 3.4

$\varepsilon_{cr} = 0.00008$

where "ε_c" is the concrete strain, "ε_{cr}" is concrete strain at the peak tensile stress," σ_t" is the average concrete tensile stress,"E_t" is the initial young's modulus for the average stress-strain relation, "f_{cr}" is the peak concrete tensile stress and "$\acute{f}_c$" is the concrete compressive strength.

The stress-strain curve obtained using these expressions increases linearly until the peak tensile stress where is the onset of micro cracking and after that point it has a reduction with the power of 0.4. As it was mentioned earlier, concrete with compressive strengths of 25 and 28 MPa are selected in this study. Then, the cracking strains, tensile stresses vs. cracking strain curve and tensile damage curve were calculated, as described in the current and previous sections (3.3.6.2). The tension stiffening and damage curve are shown in Figure 3.7 to Figure 3.10.

ABAQUS suggests that the total value of concrete tensile strain for the zero tensile stress be equal 0.001. The Belarbi and Hsu (1994) concrete constitutive model does not provide strain

value for zero tensile stress. On the other hand, according to Chang and Mander (1994) concrete constitutive model, zero tensile stress can be assumed for concrete when the tensile strain becomes equal to cracking strain. Therefore, in this study the value of 0.001 was selected as the concrete strain for tensile failure.

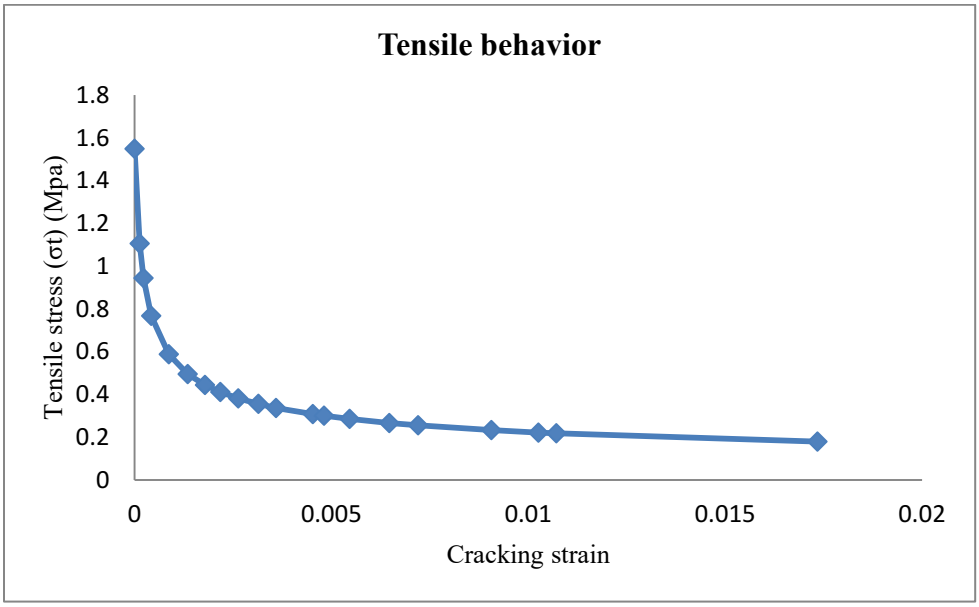

Figure 3.7: Concrete tension stiffening curve for concrete with compressive strength 25 MPa

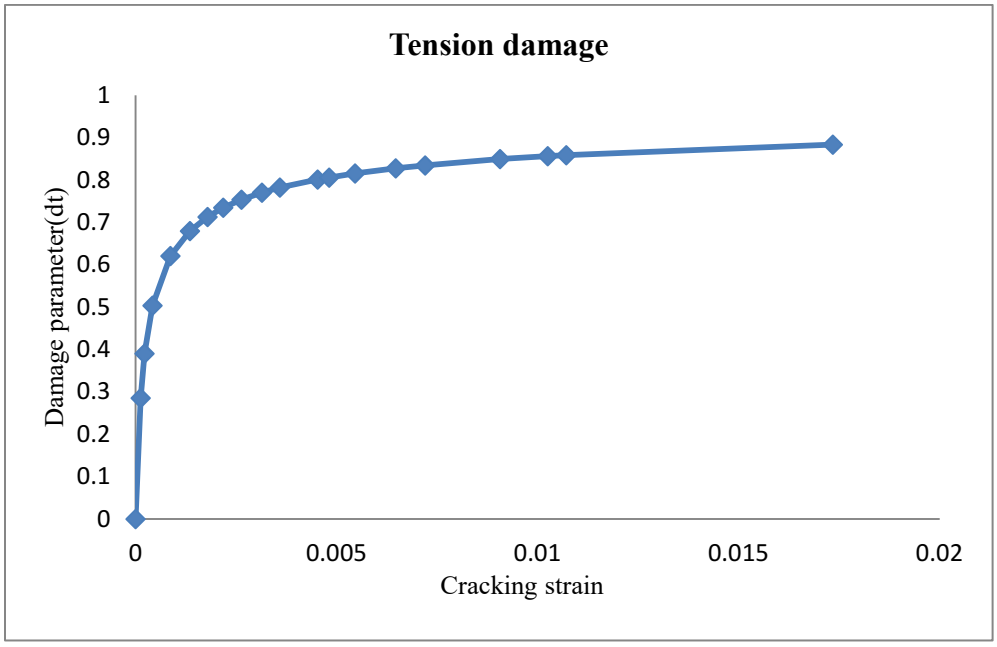

Figure 3.8: Concrete damage parameter values for concrete with tension strength 25 MPa

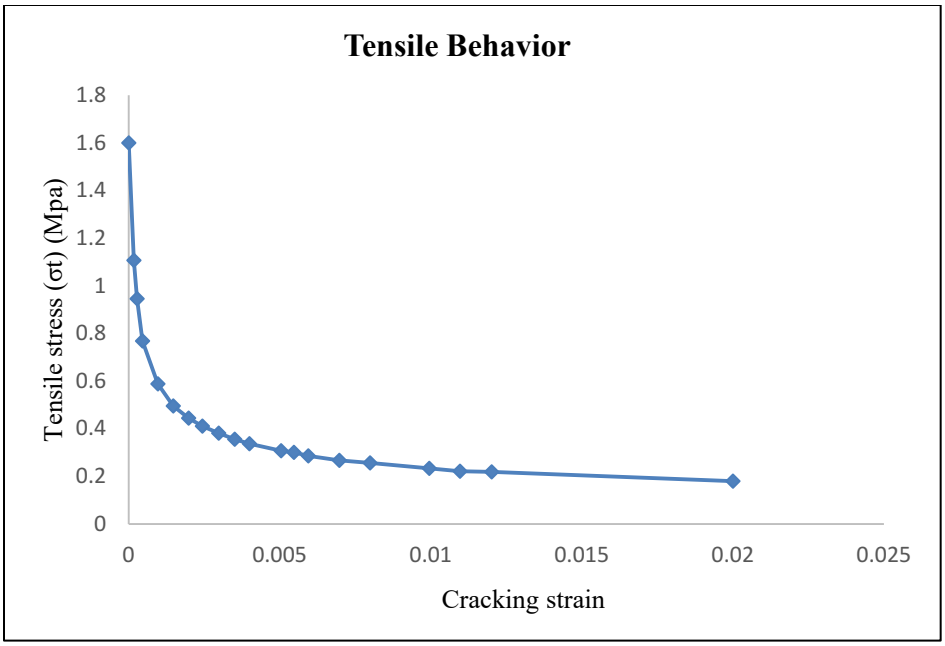

Figure 3.9: Concrete tension stiffening curve for concrete with compressive strength 28 MPa

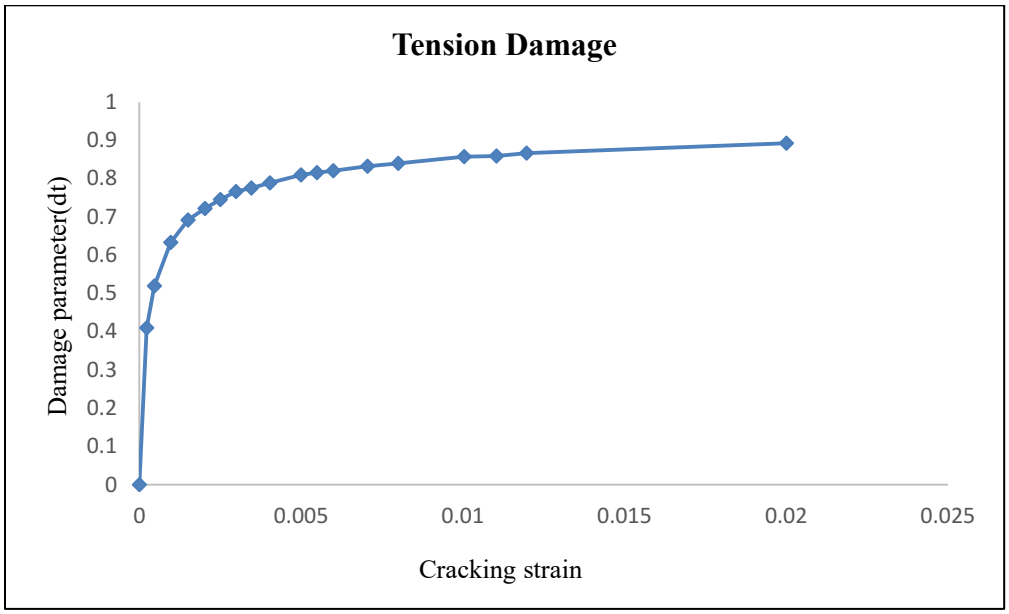

Figure 3.10: Concrete damage parameter values for concrete with tension strength 28 MPa

3.4 Validation of the finite element model

First, finite element model of C-PSW without opening was developed in ABAQUS and validated. The selected specimen was the "specimen one" tested by Zhao et al. (2004). Then, experimental C-PSW specimen of Arabzadeh et al. (2017) which had opening in the plate was developed and validated. Validation was done by obtaining the pushover curves of these models and comparing the results with the conducted tests.

3.4.1 Validation for Zhao et al. (2004) Specimen

Zhao et al. (2004) conducted cyclic tests on two half scale specimens. The specimens have steel plates with yield stress of 305 MPa and steel boundary frames with yield stress of 370 MPa. The concrete has compressive strength of 28 MPa. The concrete panel was used on one side of the specimens and connected to the steel plate with bolts. The steel plates were first bolted to the fish plates and then shop-welded to the surrounding boundary frame. The moment connections were used for connecting beams and columns. The boundary condition was provided in the test in a way that simulates the real condition of C-PSW in the building. The cyclic load was applied at the top of the specimen. Local and global displacements were recorded using a number of Linear Variable Displacement Transducers (LVDT). The selected specimen for validation is the specimen one which has a 32 mm gap between reinforced concrete panel and the steel boundary frames, as shown in Figure 2.6.

The developed FE model had the same material properties, dimensions and boundary conditions as the conducted test. In order to obtain the pushover curve, the FE model was pushed up to the same drift value as was applied in the test. The selected elements and other criteria used in the FE modeling are explained before.

Figure 3.11 and Figure 3.12 show the FE model and comparison of the results. Finite element analysis (FEA) showed a very good agreement with the test results. The figure indicates that the finite element model predicts the initial stiffness and the ultimate capacity of the specimen very well. The small difference between the FE analysis and the test may be due to the difference in the way of application of displacement in the experiment and in the FE model. This also can be the result of the small differences in the actual experimental specimen with its associated set up

and that of the FE model like shear studs used in the actual experiment for connecting the concrete panel with steel plate that was modeled with bolt connectors in the FE model or the fish plates that were ignored in the FE model.

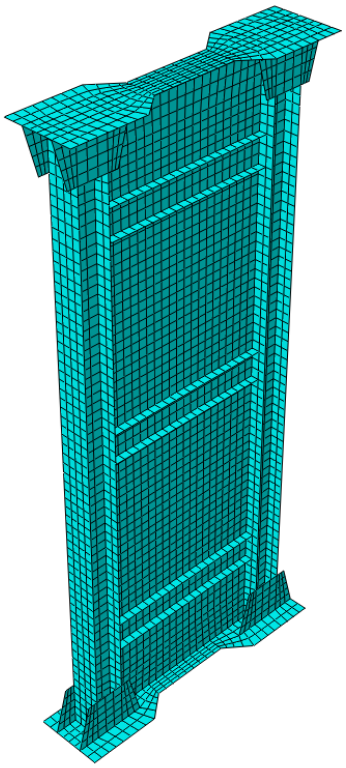

Figure 3.11: Developed FE model of Zhao et al (2004)

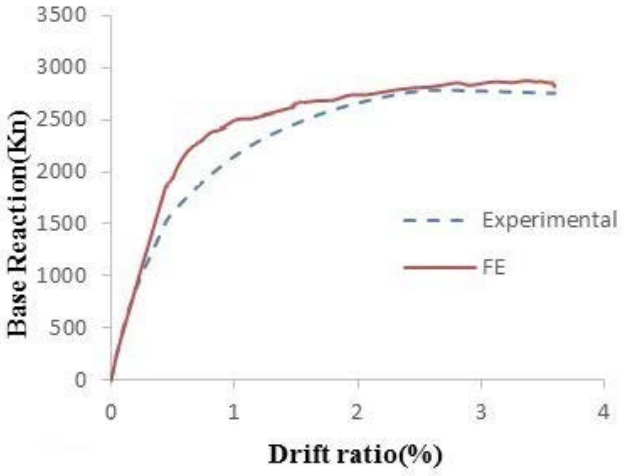

Figure 3.12: Validation of FE model; comparison of pushover analysis with test result of Zhao et al. (2004)

3.4.2 Validation for Arabzadeh et al. (2017) Specimen

Arabzadeh et al (2017) conducted a one storey C-PSW specimen with a rectangular window opening at the center. Fixed beam to column connections were provided by groove welding. Also, the connection of steel plate to the boundary frame was with fish plates. The steel plate was welded to the fish plate and the fish plate to the boundary frame. The specimen had reinforced concrete layer at one side of the steel plate and bolts were used for connecting the concrete panel to the steel plate. A gap of 50mm was present between the concrete panel and the boundary frames. Concrete with compressive strength of 25 MPa was used in the test.

Lateral bracings were provided on the beam level to prevent out of plane displacement. Yield strength for the columns and beams flanges, columns and beams webs were 280.2 and 339.18 MPa, respectively. Also yield strength of the steel plate was 237.08 MPa. The one storey specimen named specimen "S1" was used for FE validation. The schematic of specimen is illustrated in Figure 3.13.

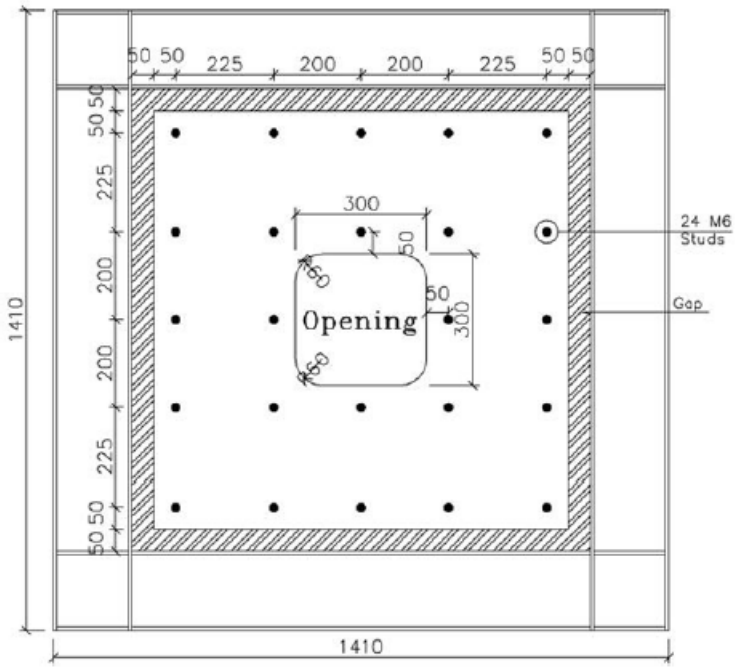

Figure 3.13: Specimen S1 used by Arabzadeh et al. (2017)

The FE model was developed with same dimensions, material properties and boundary conditions as it was reported in the tests. The FE model is depicted inFigure 3.14. A nonlinear push over and cyclic analysis was conducted on the FE model. In order to obtain the push over

curve, similar to the displacement loading applied to the top beam in the test, the FE model was pushed up to the maximum displacement occurred in the test. The base reaction was then read. Finally, the base reaction-top displacement curve was compared with the envelope of the hysteresis curves obtained from the physical test, which is shown in Figure 3.15. Also, cyclic analysis was conducted and compared with the results of physical test. Finite element analysis (FEA) showed an excellent agreement in initial stiffness and the peak capacity of the test specimen was overestimated by about 6.5%.

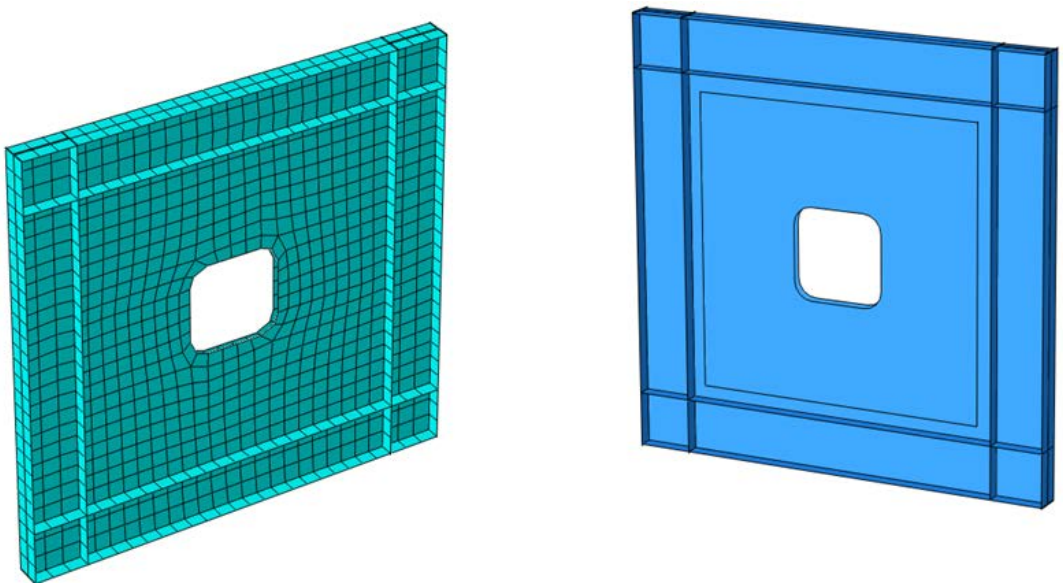

Figure 3.14: Developed FE model of Arabzadeh et al.(2017); Meshed geometry (left), schematic view (right)

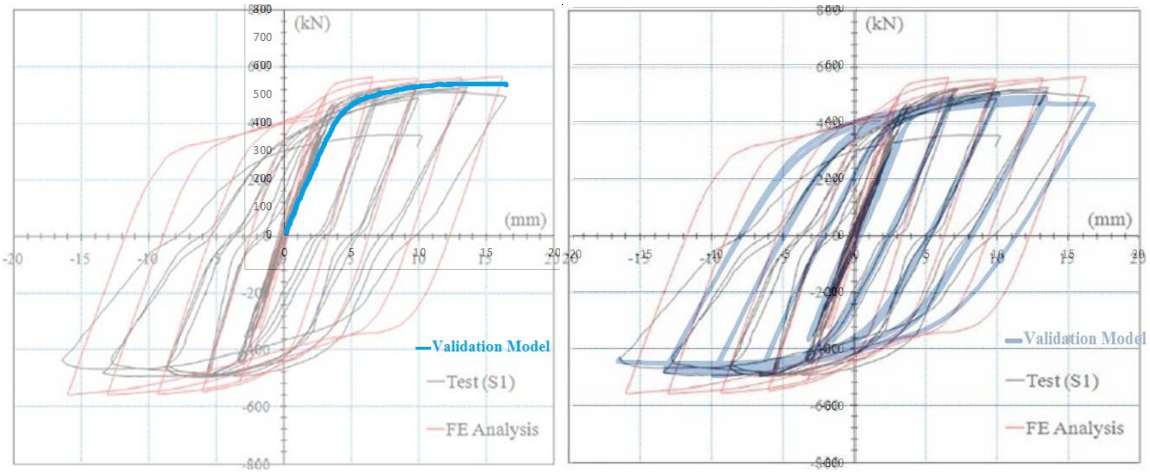

Figure 3.15: Validation of FE model; comparison of pushover analysis (right) and hysteresis curves (left) with test result of Arabzadeh et al. (2017)

Chapter Four

4. Selection and Seismic Design of SPSWs and C-PSWs

4.1 Introduction

In this chapter 3- storey and 5- storey SPSWs and C-PSWs are selected and designed based on the Capacity design concept. The description of the selected buildings, SPSW and C-PSW design procedure, FE modeling of these systems, selection and scaling of ground motion records used later for seismic analysis are also described in this chapter.

4.2 Description of the selected Building

Two identical hypothetical buildings one with C-PSWs and one with SPSWs were designed. The C-PSWs and SPSWs were modeled to evaluate the performance of these systems. The buildings were located in Vancouver and have identical plans. The plan view of the buildings containing beams, columns and SPSWs or C-PSWs are illustrated in Figure 4.1. The total area of the building was 2160(m^2). The buildings were located in very dense soil and have site class "C" according to NBC 2015. As shown in Figure 4.1 the building is symmetrical and has four identical SPSWs/C-PSWs in each direction. So each SPSW/C-PSW was assumed to resist one-fourth of the design seismic loads in each direction. The selected SPSWs/C-PSWs had a span length of 5 meter and a storey height of 4 meter. Therefore, the SPSW/C-PSW has an aspect ratio of 1.25. The 3-storey building has a total height of 12 m and the 5-storey building has a total height of 20m. The elevation view of the selected SPSW/C-PSW is shown in Figure 4.2. The buildings had dead load of 4.5 (kPa) for each floor and 2.5 (kPa) for the roof and the live load of 2.4 (kPa) for each floor and snow load for the roof. Live load reduction factors were considered for column design. Beams, columns and local boundary elements of SPSW/C-PSW had the yield strength of 370 MPa and the infill steel plates had the yield strength of 305 MPa. The modulus of elasticity and Poisson ratio were taken as 200 GPa and 0.3 for all steel members, respectively. Horizontal boundary elements (HBEs), Vertical Boundary Elements (VBEs) and local boundary elements (LBEs) used around the opening of SPSWs/C-PSWs were connected using moment resisting connections and the VBE were connected to the adjacent

beams with pin connections. The base of the building was pinned to the ground. In the building with C-PSWs, the concrete panel was attached to the steel plate with 13 mm diameter A325 bolts. According to NBC 2015, the load combination of 1.0D+0.5L+1.0E was considered for each floor and 1.0D+0.25S+1.0E for the roof (where D is the dead load, L is the live load, E is the earthquake load and S is the snow load).

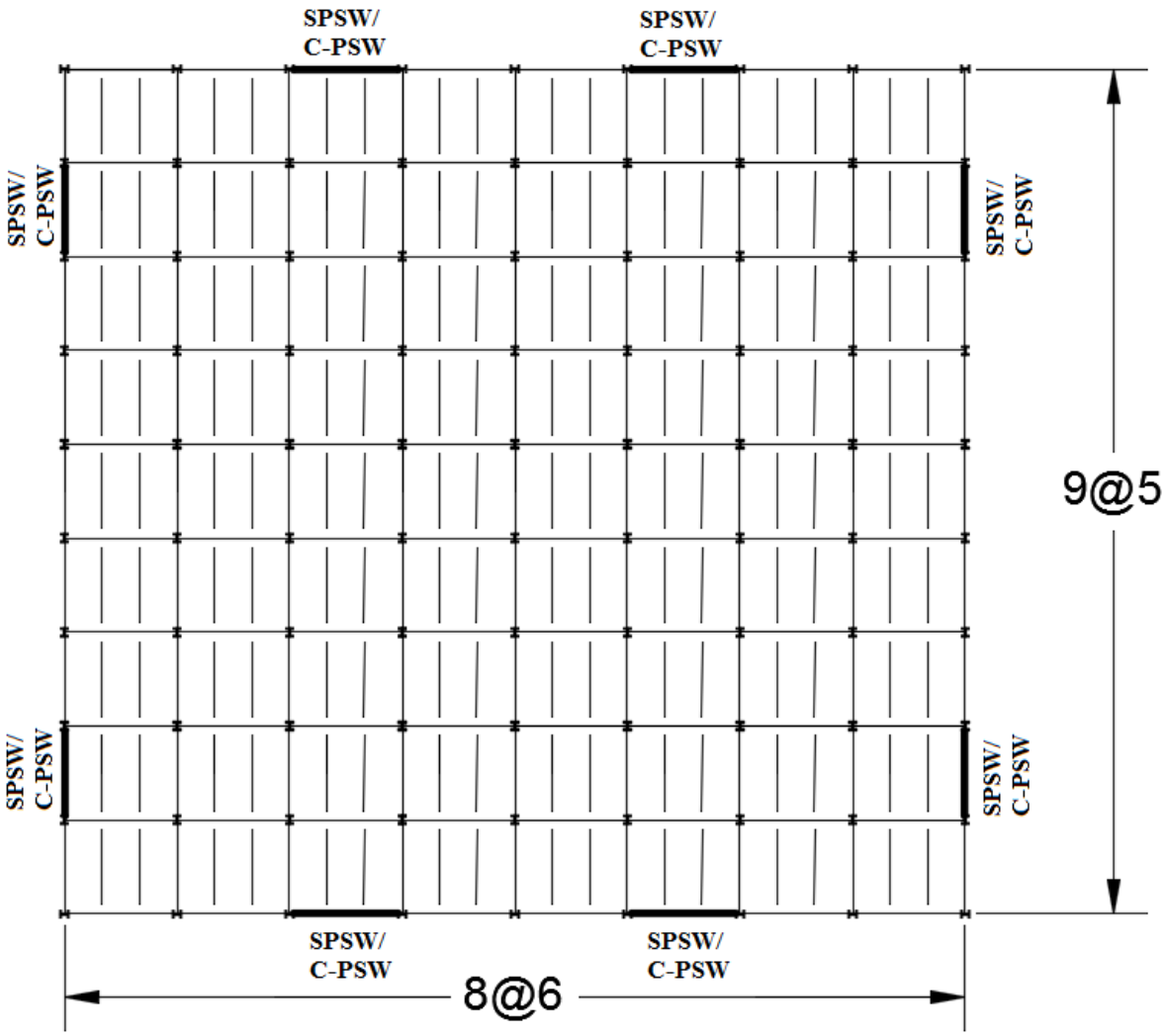

Figure 4.1: Plan view of the selected building

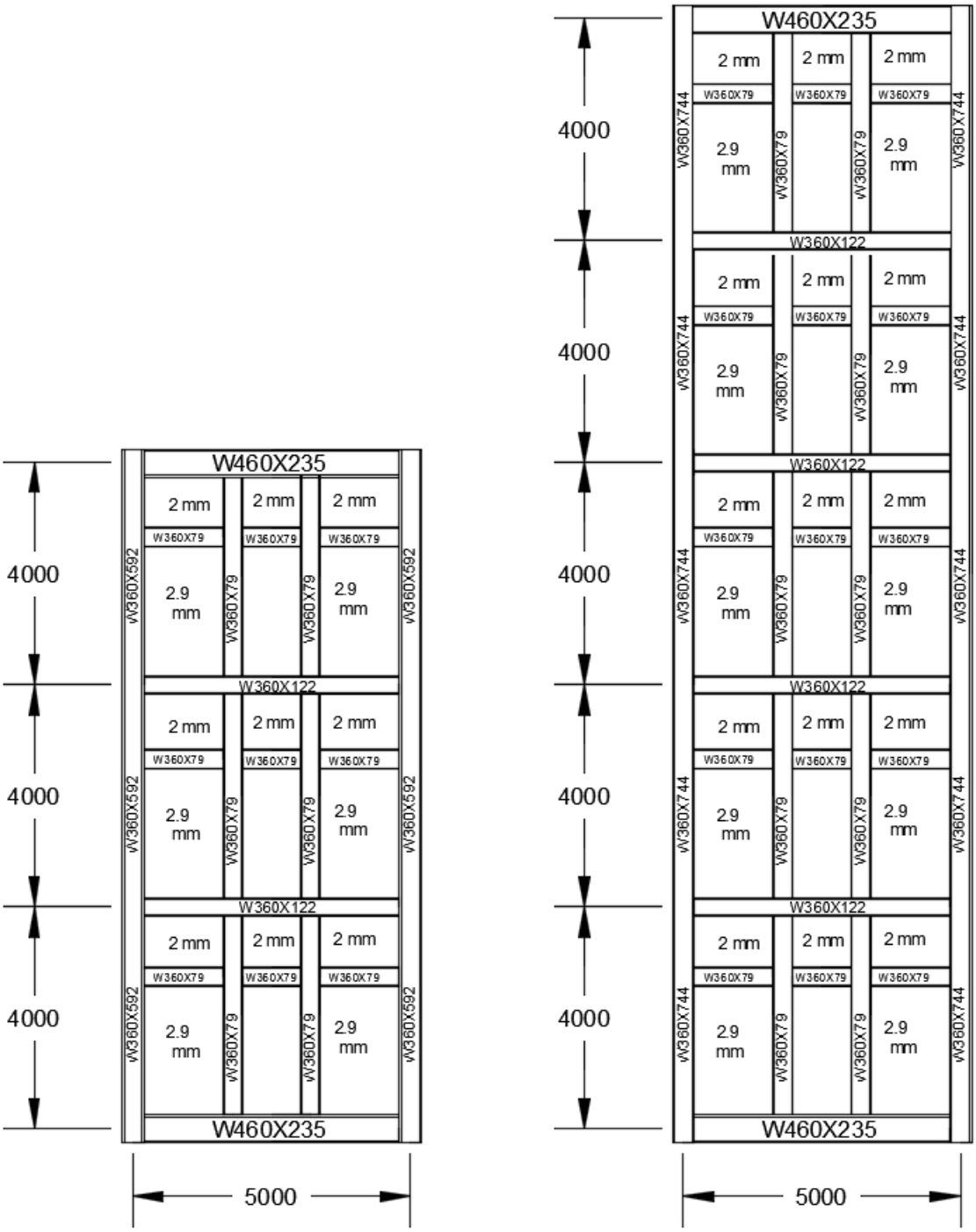

Figure 4.2: Elevation view of the selected shear walls

4.3 Seismic design of SPSW/C-PSW

In order to design the SPSW/C-PSW, first the amount of lateral forces applied to the building at each storey should be defined. Therefore, base shear calculation and distribution at each storey was done using the equivalent static force method according to NBC 2015. The design base shear was calculated as follows (NBCC 2015):

$$V = \frac{S(T_a)M_v I_E W}{R_d R_o} \quad 4.1$$

$$V_{min} = \frac{S(2.0)M_v I_E W}{R_d R_o} \quad 4.2$$

$$\mathrm{V_{max}} = \mathrm{Max}\begin{cases} \frac{2}{3}\frac{\mathrm{S(0.2)I_E W}}{\mathrm{R_d R_o}} \\ \frac{\mathrm{S(0.5)I_E W}}{\mathrm{R_d R_o}} \end{cases} \text{and} \quad 4.3$$

where $\mathrm{S(T_a)}$ is the design spectral acceleration, $\mathrm{T_a}$ is the fundamental period of the structure and is equal to $0.05(h_n)^{3/4}$ for shear walls, where h_n is the height of the shear wall , $\mathrm{M_v}$ is an amplification factor for consideration of higher mode effects on the base shear, $\mathrm{I_E}$ is the importance factor for earthquake loads and effects, W is the seismic weight of the building and according to NBC 2015, 100% dead load, 25% snow load , 60% of storage and 100% of contents of any tanks should be considered for seismic weight calculations, R_d is ductility related force modification factor which in this case was equal to 5.0. R_o is the over strength factor and was equal to 1.6.

The distribution of base shear in each level is as follows:

$$F_x = (V - F_t)\frac{W_x h_x}{\sum_1^n W_i h_i} \quad 4.4$$

where $\mathrm{F_t}$ is extra concentrated load at the top of the structure and if $\mathrm{T_a} > 0.7(\mathrm{sec})$ then $\mathrm{F_t} = 0.07\mathrm{T_a V} < 0.25\mathrm{V}$; otherwise, $\mathrm{T_a} = 0$. $\mathrm{W_x}, \mathrm{W_i}$ are the portion of "W" which are located at the level x or i and $\mathrm{h_x}, \mathrm{h_i}$ are the heights above the base to the level x or i.

SPSWs were designed according to capacity design concept. The capacity design concept indicates that the boundary elements are designed in a way that the steel plate can reach its full

capacity. Also in the design procedure it is assumed that all the shear in going to be resisted by the steel plate. The factored shear resistance of the infill steel plate "V_r" is given as:

$$V_r = 0.42\,\varphi F_y t_w L \sin 2\alpha \qquad 4.5$$

where F_y is the steel plate yield strength, t_w is the thickness of the infill steel plate, L is the distance between vertical member centerline, α is the angle of tension field calculated as follows:

$$\tan^4 \alpha = \frac{1+\frac{t_w L}{2A_c}}{1+t_w h[\frac{1}{A_b}+\frac{h^3}{360 I_c L}]} \qquad 4.6$$

where "h" is the distance between horizontal member center-lines, A_b and A_c are average cross-sectional area of the horizontal and vertical boundary elements around the steel plate, respectively, I_c is the average moment of inertia of the vertical members bounding the panel.

In the case of having opening, the web plate shear strength above the opening is given by:

$$V_n = \varphi 0.42 F_y t_1 [L_1 \sin(2\alpha_1) + L_2 \sin(2\alpha_2) + L_3 \sin(2\alpha_3)] \qquad 4.7$$

And the web plate shear strength at the level of opening is:

$$V_n = \varphi 0.42 F_y t_2 [L_1 \sin(2\alpha_4) + L_3 \sin(2\alpha_5)] \qquad 4.8$$

where $\varphi = 0.9$ in LRFD design; α is the tension field angle for each panel, t_1 and t_2 are the thickness of infill steel plate above and at the level of the opening, respectively. All other parameters are shown in Figure 4.3.

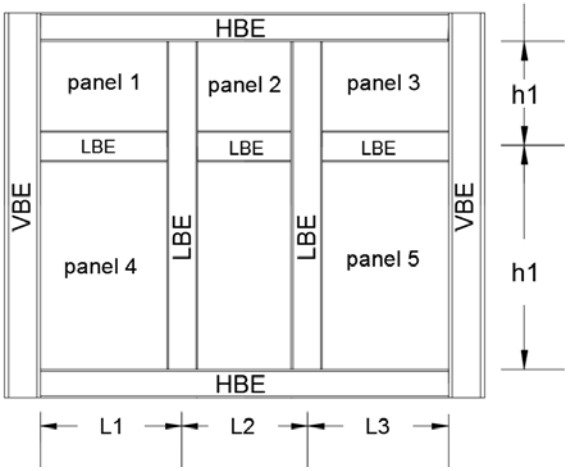

Figure 4.3: Definition of parameters of equation 4.7 and 4.8

The concept behind C-PSW system is that the concrete panel provides enough lateral stiffness for the steel plate to reach its shear yield strength. According to this concept and AISC341-16, the shear strength of concrete was not considered for design and all the shear was assumed to be resisted by the steel plates.

In this study and in the absence of proper design guidelines for C-PSWs in the Canadian design standard, the SPSW was designed according to capacity design concept and the concrete panels were designed according to AISC 341-16. The capacity design concept requires that the boundary elements be designed in a way that the steel plate can reach its full capacity.

According to AISC 341-16, the concrete panel thickness should be a minimum of 100 mm on each side when concrete is provided on both sides of the steel plate and a minimum of 200 mm when concrete is provided on one side of the steel plate. The reinforcement ratio in both directions should not be less than 0.0025 and maximum bar spacing should not exceed 450 mm. Therefore, according to calculations and AISC recommendations, the concrete thickness of 200mm and reinforcement ratio not less than of 0.0025 with spacing within the allowable range was selected. The C-PSW was selected to have a 45 mm gap between the concrete panels and the boundary elements. The system was the "innovative C-PSW" introduced as the better C-PSW system by Astaneh Asl (2002). This system was selected so that the boundary elements do not impose additional forces on the concrete panels and the degree of damage to the concrete panels remains limited.

In a C-PSW, as the concrete panel stiffens the steel plate it is desired that the steel plate resists the storey shears by yielding in shear. So, the expected strength of the stiffened steel plate in shear is given as:

$$V_{ns(exp)} = 0.6R_yF_yA_{sp} \tag{4.9}$$

where R_y is the ratio of the expected yield stress to the specified minimum yield stress, F_y is the steel yield strength and A_{sp} is horizontal area of the stiffened steel plate ($t_w * L$).

The factored design shear strength of the infill steel plate is:

$$V = \varphi V_n = \varphi 0.6R_yF_yA_{sp} \tag{4.10}$$

where φ is equal to 0.9 for LRFD design.

The infill plate should resist the storey shear calculated by NBC 2015. So, the thickness of the steel plate can be calculated using equation (4.10)

In the case opening in the web, the web plate shear strength above the opening is given by:

$$V_n = \varphi 0.6 F_y t_1 [L_1 \sin(2\alpha_1) + L_2 \sin(2\alpha_2) + L_3 \sin(2\alpha_3)] \quad 4.11$$

And the web plate shear strength at the level of opening is:

$$V_n = \varphi 0.6 F_y t_2 [L_1 \sin(2\alpha_4) + L_3 \sin(2\alpha_5)] \quad 4.12$$

All the parameters were defined earlier.

The horizontal boundary elements (HBEs) and vertical boundary elements (VBEs) should be designed to remain essentially elastic under the maximum forces that can be generated by the fully yielded steel webs. Based on this philosophy and according to Berman and Bruneau (2008) and CSA S16-14, boundary elements were designed to develop the full capacity of the infill plates.

In the SPSWs and C-PSWs, lateral forces are resisted and transferred through steel plate tension field action and tension and compression in columns. When shear force applies on steel plate, tension fields with a specific angle occur. The uniform distributed forces from steel plate tension field action on boundary elements are as follows:

$$w_{xci} = F_{yp} t_{wi} (\sin\alpha)^2 \quad 4.13$$

$$w_{yci} = 0.5\, F_{yp} t_{wi} \sin(2\alpha) \quad 4.14$$

$$w_{xbi} = 0.5\, F_{yp} t_{wi} \sin(2\alpha) \quad 4.15$$

$$w_{yci} = F_{yp} t_{wi} (\cos\alpha)^2 \quad 4.16$$

where w_{xci} is the horizontal and w_{yci} is the vertical distributed forces on the column due to tension field action of the steel plate, $F_{yp}$is the yield strength of the steel plate, t_{wi} is the steel plate thickness, α is the angle of tension field, $w_{xbi}$and $w_{yci}$are horizontal and vertical distributed forces on the boundary beams due to tension in the steel plate, respectively.

HBEs and HVEs were designed based on these distributed forces and the free body force analysis shown in Figure 4.4 and Figure 4.5.

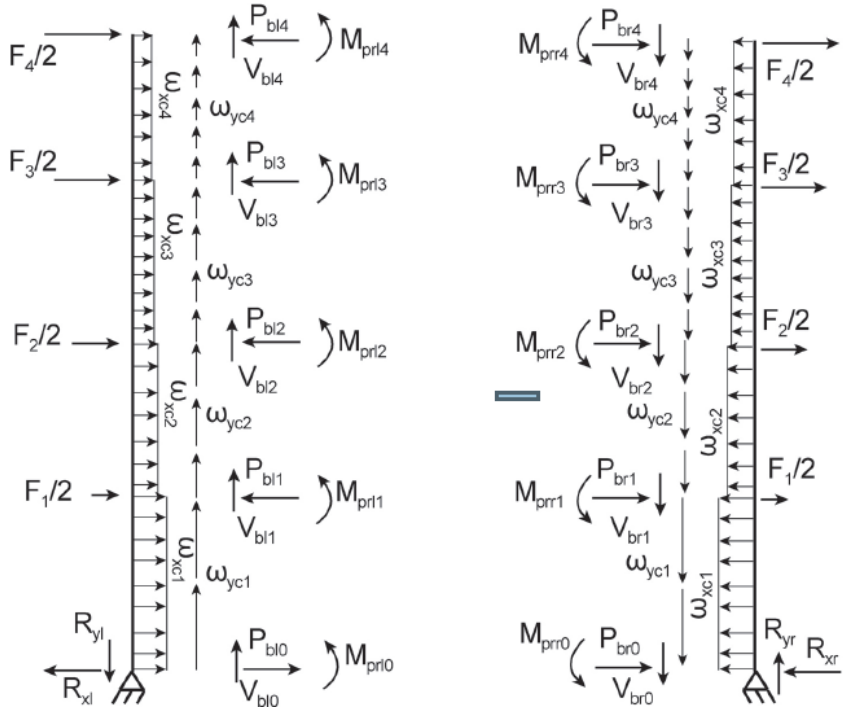

Figure 4.4: Free body diagram of VBE members (Berman and Bruneau 2008)

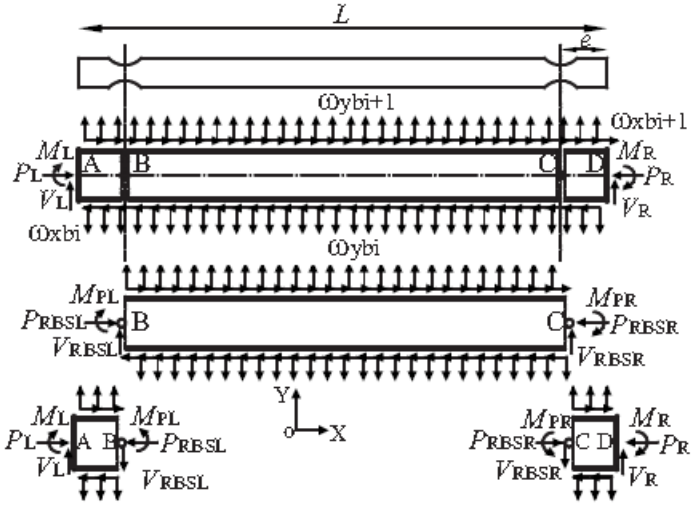

Figure 4.5: Free body diagram of intermediate HBE members (Qu and Bruneau 2010)

To ensure that the boundary beams and columns have adequate stiffness to provide uniform tension field in the infill steel, CAN/CSA S16-14 recommends that the HBES and VBEs satisfy the following equations:

$$I_c \geq \frac{0.0031 t_w h_s^4}{L} \quad 4.17$$

$$I_{tb} \geq \frac{t_w L^4}{650L - (\frac{t_w h_s^4}{I_c})} \quad 4.18$$

$$I_{bb} \geq \frac{t_w L^4}{267L - (\frac{t_w h_s^4}{I_c})} \quad 4.19$$

where I_c is the moment of inertia of the column cross-section, t_w is the infill steel plate thickness, $h_s$is the storey height, L is the bay width, I_{tb} is the moment of inertia of the HBE above the steel plate and I_{bb} is the moment of inertia of the HBE located on the bottom of the steel plate.

For determining the shear stud spacing, the C-PSW can be considered as stiffened steel plate where the concrete has the role of stiffeners along the vertical and horizontal shear stud lines. The role of the concrete, same as stiffeners, was to prevent the steel plate from global buckling and let the steel plate to yield before buckling.

The critical shear buckling stress of a plate subjected to pure shear is calculated by the following equation:

$$\tau_{cr} = \frac{K_{sl} \pi^2 E}{12(1-\nu^2)} (\frac{t_w}{b})^2 \quad 4.20$$

where K_{sl} is the critical stress coefficient, E is the modulus of elasticity for steel plate, ν is the Poisson ratio of steel plate, t_w is the steel plate thickness and b is the steel plate width.

K_{sl} is calculated according to Alinia et al. (2009) by the following equation:

$$\mathrm{K_{sl}} = 5.34 + \frac{4}{\varphi^2} \quad 4.21$$

where φ is the aspect ratio of two sides of the panel whichever is greater.

According to AISC341-16, the concrete-steel composite panel should be stiff enough to avoid overall buckling. Therefore, the concrete thickness should be enough to provide stiffness for the steel plate to yield before buckling. In order to satisfy this criterion, the concrete panel can be transformed to horizontal and vertical equivalent steel stiffeners and the required shear stud spacing and concrete thickness can be calculated according to the elastic buckling theory of orthotropic plates. Thus, the shear stud spacing is calculated as follows:

$$\tau_{cr} \geq \tau_y \tag{4.22}$$

where τ_{cr} and τ_y are:

$$\tau_{cr} = \frac{K_{sl}\pi^2 E}{12(1-\nu^2)}\left(\frac{t_w}{c}\right)^2 \tag{4.23}$$

$$\tau_y = \frac{F_y}{\sqrt{3}} \tag{4.24}$$

where "c" is the shear stud spacing in each direction. Other parameters were described earlier.

For the selected C-PSWs with steel plate thickness 2mm , $F_y = 305\ \text{MPa}$ and transforming the concrete to the equivalent steel stiffeners with same spacing in both horizontal and vertical directions the shear stud spacing of 180mm was selected.

Adequate concrete thickness can be calculated with the exact solutions obtained by Seydel (1933) for long orthotropic simply supported plates in shear. The shear stress for closely spaced stiffeners is as following:

$$\tau_{crg} = \frac{K_{sg}\pi^2}{d^2 t}(D_x)^{3/4}(D_y)^{1/4} \tag{4.25}$$

where K_{sg} is the global buckling factor and has the minimum value of 3.64 for pinned connection of plate to frame and 6.9 for the rigid connection of plate to frame, D_x and D_y are the flexural stiffness for bending about x and y axis, respectively and are calculated as:

$$D_x = \frac{EI_x}{c_x} + \frac{Et^3}{12(1-\nu^2)} \tag{4.26}$$

$$D_y = \frac{EI_y}{c_y} + \frac{Et^3}{12(1-\nu^2)} \quad 4.27$$

I_x and I_y are the moment of inertia about the x and y axis, $c_x$and c_y are center to center distances of shear studs in the x and y directions, respectively.

To avoid global buckling before local buckling, τ_{crg} should be greater that τ_{cr}. Thus, by considering that the stiffeners are equally spaced and have the same moment of inertia in both directions, $\nu = 0.3$ and $n = \frac{E_s}{E_c}$ the minimum required concrete panel thickness will be:

$$h > 0.65 t_w \left(\frac{K_{sl} h^2 n}{K_{sg} cD} - \frac{cn}{D}\right)^{1/3} \quad 4.28$$

where h is the minimum required concrete panel thickness, D is the shear stud diameter and other parameters are defined earlier.

For the selected C-PSWs in this study, a value of 3.64 was conservatively used for $K_{sg}$and shear studs of A325 with diameter 13mm were used. Finally, with the calculations and according to limitation of AISC 314-16 for concrete thickness, the concrete panel with thickness of 200mm was selected.

4.3.1 Design of Local Boundary Elements (LBEs)

According to AISC341-16, boundary members shall be provided around openings in steel plate and composite steel plate shear wall webs with openings to anchor the web plate tension unless tests justified the use of unreinforced openings. The design of these local boundary elements (LBEs) were done according to AISC Design Guide 20. The web plate located on either sides of the opening must be selected thicker to provide the stiffness and strength equal to solid panel without opening. As the same total area of web plate will produce similar stiffness and strength, the thickness of the web plate on either side of opening is calculated as:

$$t_2 = t_1\left(\frac{L_{cf}}{L_1 + L_3}\right) \quad 4.29$$

where t_2 is the thickness of steel plate on either side of opening, t_1 is the thickness of the steel plate without an opening, $L_{cf}$is the clear distance between the VBE flanges, $L_1$and L_3 are the width of steel plate on either side of the opening, as shown in Figure 4.6.

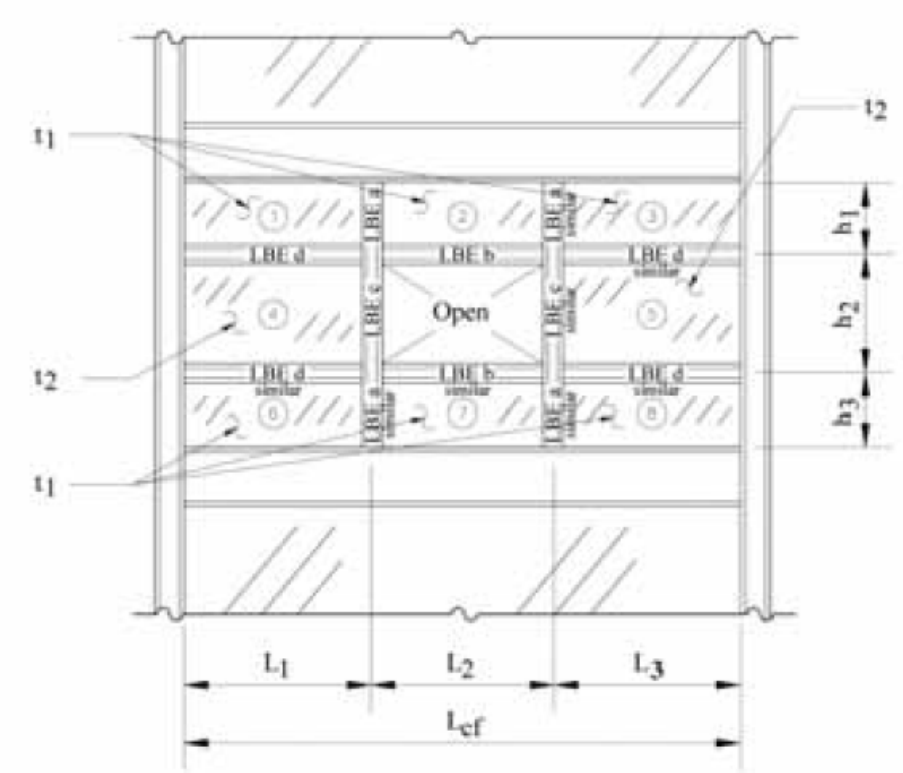

Figure 4.6: Definition of parameters in Equation 4.29 (AISC Design Guide 20)

The LBEs were designed based on the required strength. The horizontal LBEs were designed individually and were supported by vertical LBEs in out of plane direction. The vertical LBEs were designed with an unbraced length equal to storey height. The vertical LBEs should provide adequate bracing for compression forces in HBEs so "nodal bracing" conditions should be satisfied for these elements according to AISC 360.

According to AISC Design guide 20, reaction forces of vertical LBEs will add to the shear of HBEs. The HBE sections should be checked to be able to resist this additional shear. Figure 4.7 shows the forces from LBE acting on HBE for the top floor.

VBE sections should be checked for the forces applied on VBEs due to steel plate tension field action and reactions from LBEs, as shown in Figure 4.8.

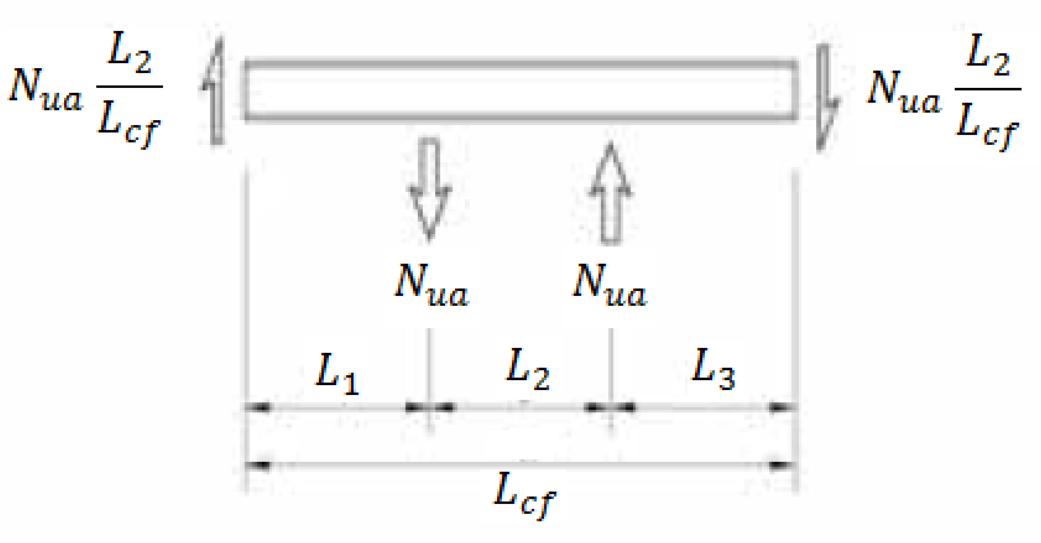

Figure 4.7: Forces from LBEs on HBE above opening (AISC design guide 20)

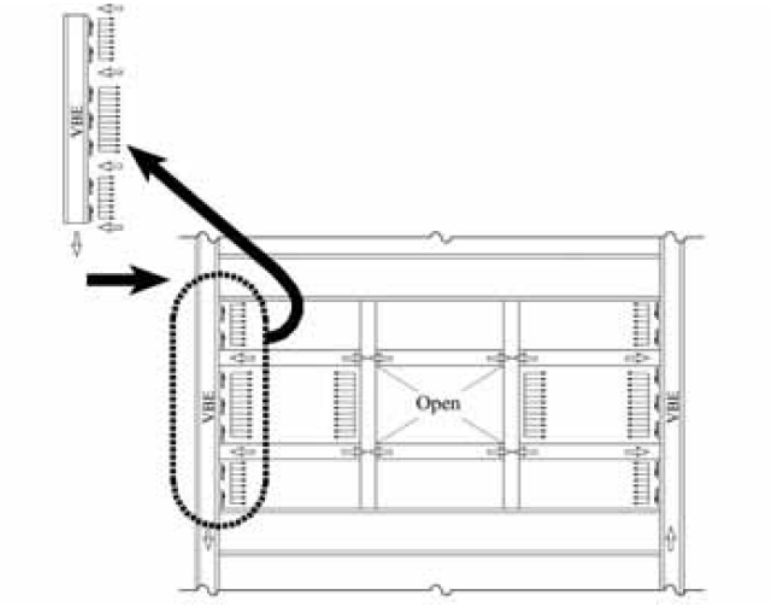

Figure 4.8: Forces on the VBEs (AISC design guide 20)

4.4 Selection of SPSWs and C-PSWs

Based on NBC 2015, the equivalent static lateral forces were determined for the described 3-storey and 5-storey buildings. Table 4.1 shows the estimated equivalent lateral forces for the two buildings. A 2 mm infill plate was selected as a minimum practical thickness for welding and handling for both 3-storey and 5-storey buildings above the level of opening and 2.9

mm at the level of opening. However, by calculation smaller thickness was also sufficient for these structures. As mentioned before, boundary beams and columns were designed according to the Canadian steel design standard CAN/CSA S16-14, Berman and Bruneau (2008) and Qu and Bruneau (2010). As the HBEs had axial forces, reduced plastic moment was used in HBE design and also columns were designed to take the reduced plastic moments from beams. All the HBEs and VBEs were designed as beam-column members. Consistent column sections from bottom to the top of the buildings were selected. W360X592 was used for the VBEs of the 3-storey building and W360X744 was chosen for VBEs of the 5-storey building. The top and bottom HBEs had larger sections due to uniform distributed yield forces from infill plates on one side; however, the intermediate HBEs had smaller sections as yield forces from the infill plate of two adjacent stories would cancel out each other. Sections used for all the members and elevation view of the buildings with door and windows opening are illustrated in Figure 4.2.

Table 4.1: Equivalent lateral forces according to NBC 2015 for 3- and 5- storey buildings

3-storey		5-storey	
Storey	Lateral forces (kN)	Storey	Lateral forces (kN)
3	948.4	5	1036
2	977.7	4	1281.6
1	488.8	3	961.2
		2	640.8
		1	320.4

4.5 Finite element model of selected C-PSWs and SPSWs with openings

The finite element models of the selected C-PSWs and SPSWs with openings were developed with the same modeling techniques and analysis procedure used for validation, which was explained in section 3.3. Optimal mesh sizes for all components of SPSW and C-PSW were obtained from a mesh convergence study.

Yield strength for the columns, beams and LBE members around opening was selected as 370 MPa and for infill steel plate it was selected as 305 MPa. The concrete had a compressive strength of 28 MPa and tension and compression damages were also considered in the models. Bolts were modeled using beam connectors for C-PSWs. For SPSWs, an initial imperfection pattern corresponding to the first buckling mode of each infill plate was applied in the model

which helped initiate buckling in the infill plates and development of the tension fields. A value of h/1000 was selected for the peak magnitude of initial imperfections in the infill plates.

In order to conduct a seismic analysis, "gravity-leaning- column" was added to the model. This column was not part of the lateral force resisting system, but it was essential for obtaining the destabilizing effects from the gravity load assigned to the columns (P-Δ effects). The dummy column in the model had 2-node linear 3-D truss elements (ABAQUS T2D3) and was connected to the shear wall system at every floor level using ABAQUS connector (pin ended rigid links). This connection was selected so that it could restraint the horizontal displacement between the dummy column and the shear wall system. The base of this column was pin supported to ensure that the gravity column did not have any lateral stiffness.

Mass and gravity loads were also considered in seismic analysis. At each floor, the seismic weight as well as the corresponding mass were applied on the VBEs, while the dummy columns at each floor carried one fourth of the seismic weight applied on the whole building plan area minus the amount carried by the VBEs and the corresponding mass. The seismic masses and gravity loads were applied on top of the columns at each floor as point masses and concentrated loads, respectively. A Raleigh proportional damping of 5% was selected for all seismic analyses.

Frequency analysis was conducted prior to seismic analysis to find out the fundamental periods and the Rayleigh damping coefficients (alpha and beta). The FE models with dummy gravity column were used for this type of analysis. The results from frequency analysis showed that the fundamental periods for the 3-storey and 5-storey SPSWs without LBEs around door opening are 0.87 and 1 second. And for SPSWs owing LBEs around door opening are 0.42 and 0.75, for C-PSW with LBEs around the door opening are 0.32 and 0.66 and C-PSWs without LBEs around the opening are 0.27 and 0.56, respectively. These periods are longer than what was calculated based on NBC 2015.The expression presented by NBC 2015 for fundamental period of the structure is:

$$T_a = 0.05(h_n)^{3/4} \qquad 4.30$$

In the above equation h_n is the total building height in meters.

The obtained fundamental period of the structure from FE model was used for scaling ground motion time histories which is described later.

4.6 Ground motion time histories

In order to investigate the behavior of the structure under seismic time history records, ASCE 7-16 recommends minimum three ground motion records for response history analysis when peak maximum response are considered for component checking and minimum seven ground motion records when the average of maximum response are considered for component checking.

In this research, as the buildings were located in Vancouver, ground motion records were selected in a way to be compatible with the earthquake hazard spectrum of Vancouver region provided by NBC 2015. Eight ground motions were selected and scaled for the time history analysis. Four of these records were real ground motions records and four were artificial records. All records were compatible with Vancouver spectrum. Real ground motions were selected to have A/V close to 1.0, as recommended by Naumoski et al. (2004), to simulate the expected earthquakes in Vancouver, where A is the peak ground acceleration with unit of "g" and V is the peak ground velocity with unit of m/s^2 and "g" is the acceleration due to gravity with unit of m/s^2.

Based on Canadian earthquake database during the years 1600-2006, most of the earthquakes occurred in Vancouver and the offshore region of British Colombia have the magnitude between 6.0 and 7.0 in Richter scale (Lamontagne et al. 2008). Therefore, two earthquake records sets with the magnitude of 6.5 and 7.5 for soil class "C" and the A/V close to 1 were selected. The horizontal component of the ground motion records was selected as input for the time history analysis. The four simulated and four real ground motion records selected for analyses are shown in Table 4.2 and

Table **4.3**. Also, the acceleration time histories are presented in Figure 4.9 and Figure 4.10.

The selected ground motions were scaled based on ASCE/SEI (7.16) method. In this method, the mean spectrum taken from response spectra of a set of ground motions within the interval of $0.2T_1$ to $1.5T_1$ should fit or be above the uniform hazard spectrum for Vancouver, where T_1 is the fundamental period of the vibration obtained from frequency analysis. The response spectrum was considered for 5% of critically damped single degree of freedom system in soil class C.

The considered range of the period for scaling ($0.2T_1 - 1.5T_1$) encompasses the most probable range of the vibration during the earthquake event. Plastic deformations may increase the period of the building, so the scaling factor is increased up to 1.5 times of fundamental period ($1.5T_1$). Higher mode effect is taking into account by the lower limit of the range ($0.2T_1$) (Naumoski et al. 2004).

Table 4.2: Characteristics of selected real ground motion records

Event Name	Magnitude	Station	PGA(g)	PGV(m/s)	A/V
Imperial valley California, 1979	6.53	El Centro	0.466	0.478	0.974
Kobe, Japan,1995	6.9	HIK	0.149	0.147	1.02
San Fernando, California, 1972	6.61	LA-Hollywood Stor FF	0.163	0.169	0.96
Kern County, California, 1952	7.36	Taft Lincoln School	0.180	0.186	0.97

Table 4.3: Characteristics of simulated ground motion records

Event Name	Magnitude	Distance(Km)	PGA(g)
West6c2.2	6.5	19.7	0.27
west6c2.17	6.5	21.8	0.176
west7c1.23	7.5	20.3	0.325
west7c2.13	7.5	30.2	0.203

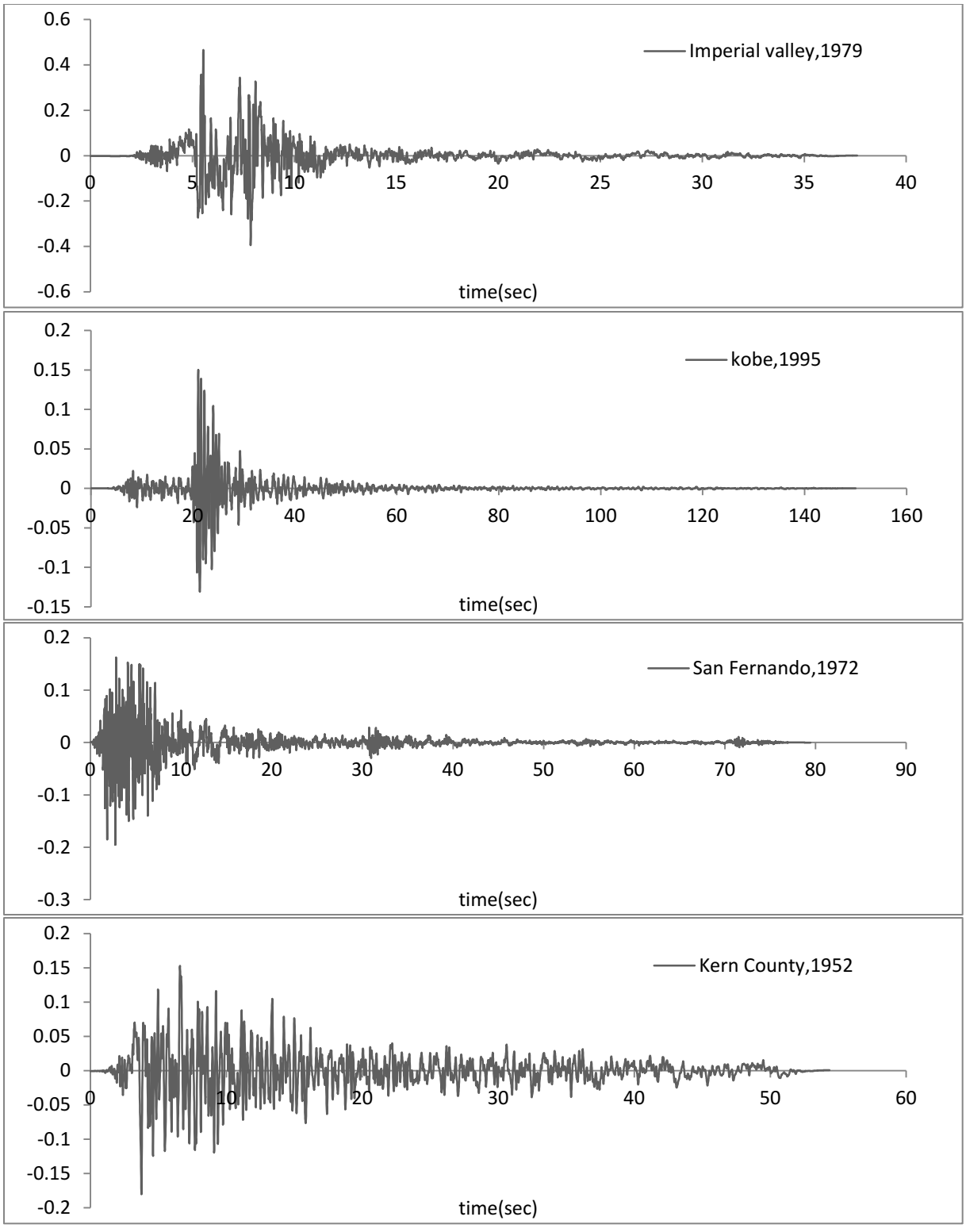

Figure 4.9: Selected real unscaled Ground Motions Records

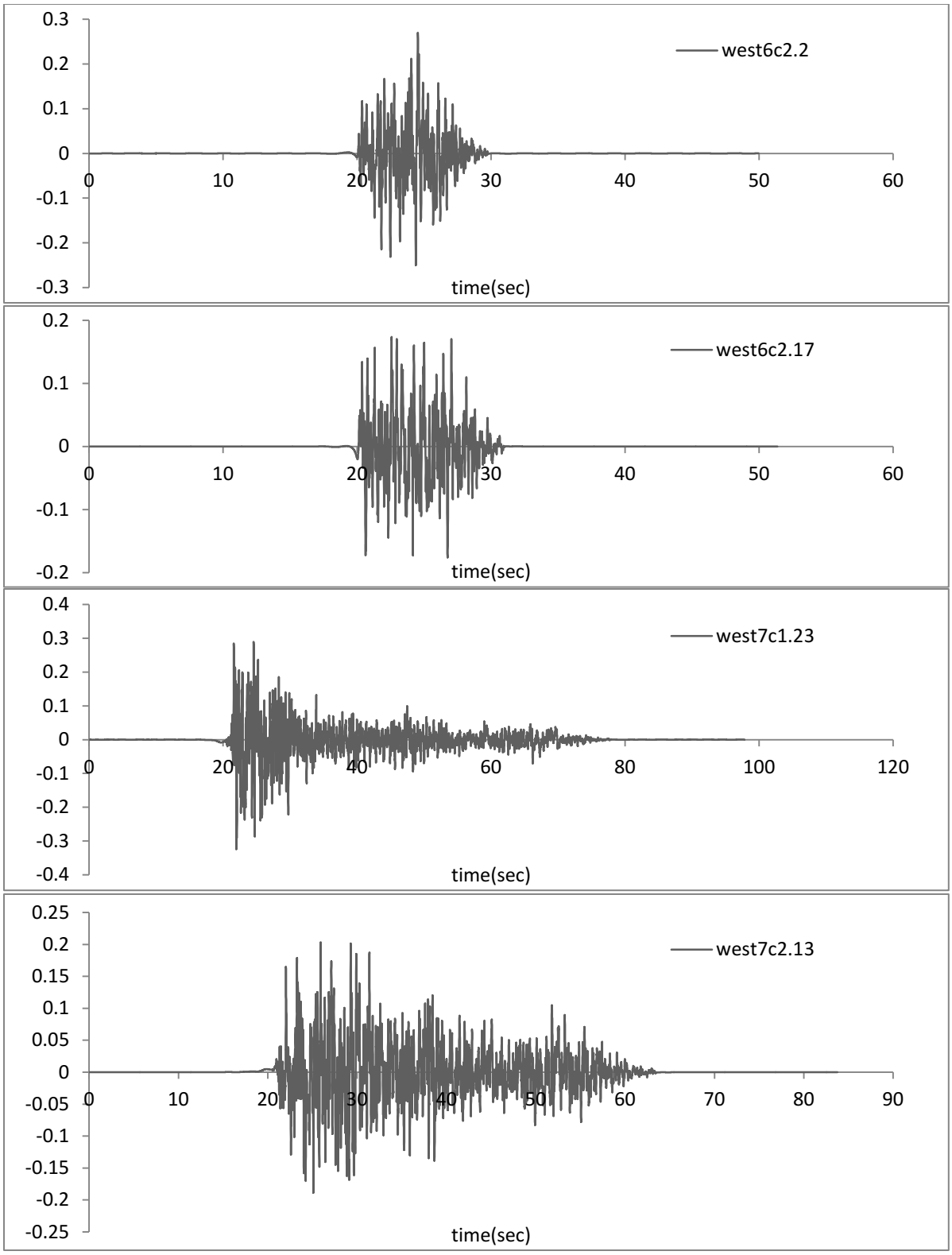

Figure 4.10: Selected simulated unscaled Ground Motions Records

Chapter Five

5. Performance of Steel Plate Shear Walls with Rectangular Openings

5.1 Introduction

In the previous chapters, the FE model was validated and a 3-storey and 5-storey SPSWs with openings were designed. In this chapter, seismic behavior of the selected SPSWs is carried out by conducting a series of time history analysis using a suite of 8 ground motions compatible with the design response spectrum of Vancouver, Canada. Maximum contribution of various structural components in resisting applied lateral loads is calculated from seismic analysis. The effectiveness of the designed stiffeners to limit both in-plane and out-of-plane deformations around the rectangular openings is examined from seismic analysis. Also, whether the use of the local boundary elements (stiffeners) around the rectangular openings alters the recommended yielding sequence of the SPSW system is investigated in this chapter.

5.2 Seismic response of SPSWs with door opening and LBEs around the opening:

Before conducting seismic analysis of SPSWs, the selected eight (8) earthquake records were scaled to response spectrum of Vancouver, BC.

Figure 5.1 to Figure 5.5 present the response spectra for the 8 selected ground motions together with design spectrum and mean spectrum for two different cases of unscaled and scaled, respectively, for the selected SPSWs. It is observed from Figure 5.2 to Figure 5.5 that the mean spectrum of scaled seismic records for 3-storey and 5-storey SPSWs with openings are higher than the NBC 2015 design spectrum.

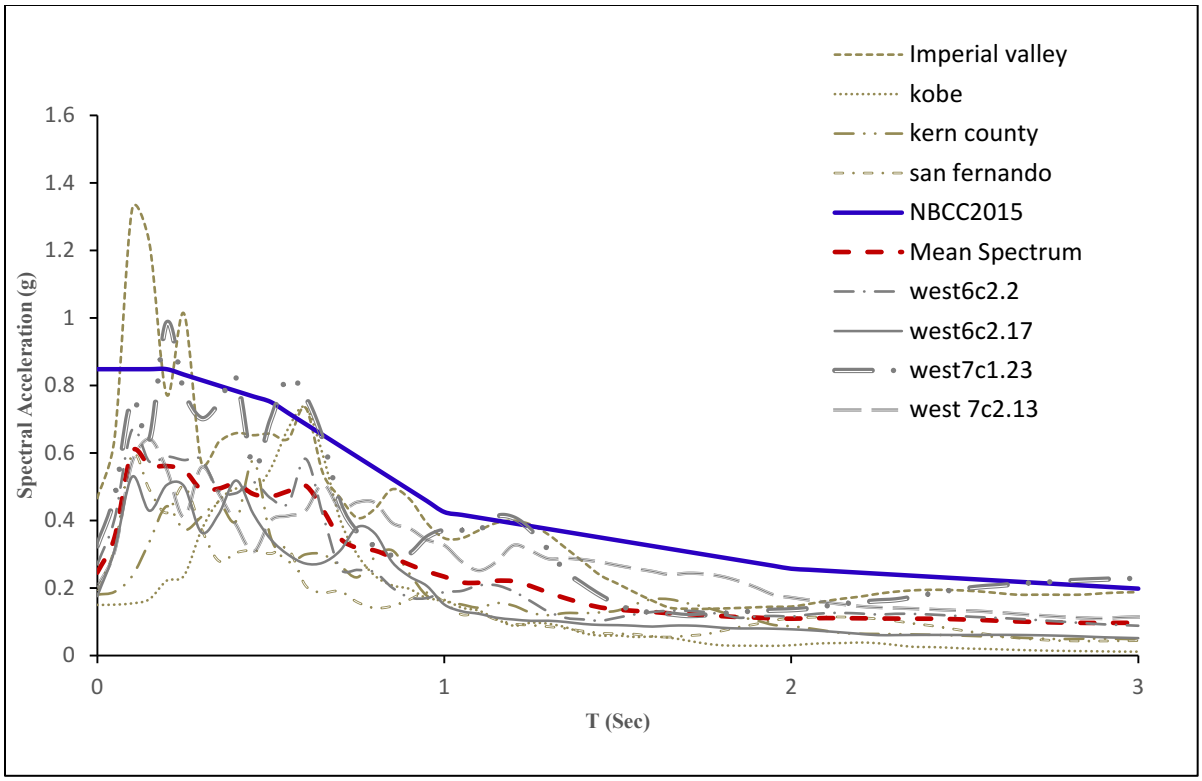

Figure 5.1: Response spectra of unscaled ground motions along with mean and design spectrum

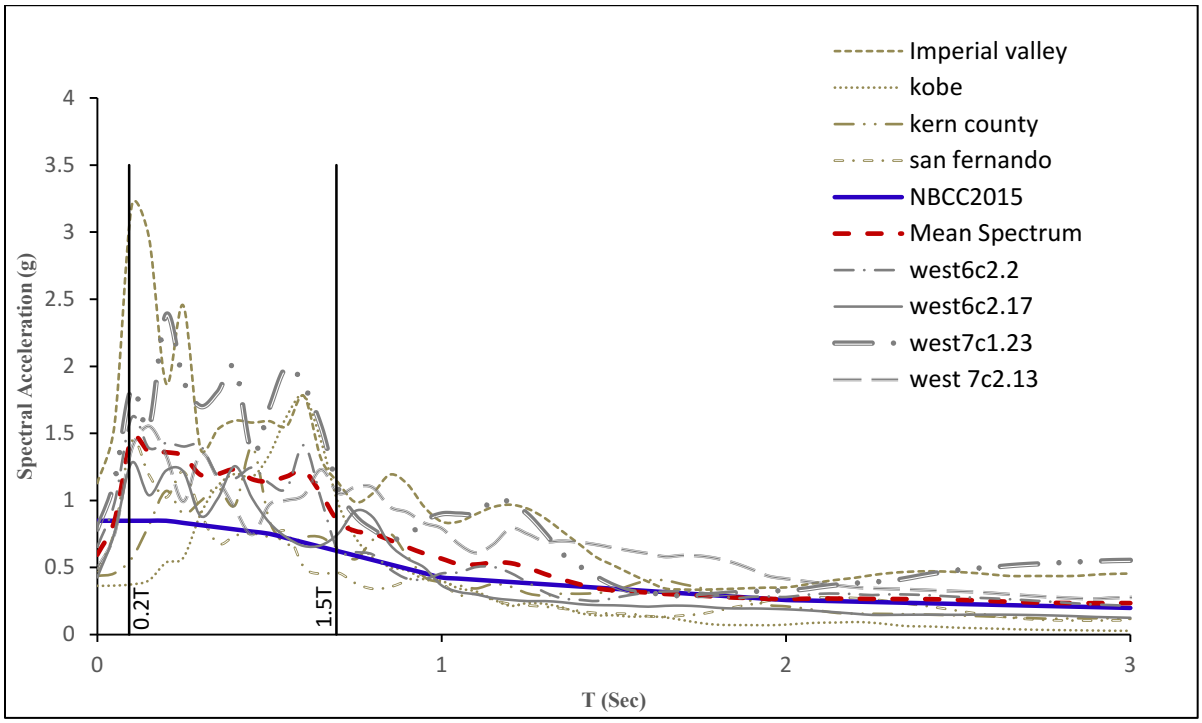

Figure 5.2: Response spectra of scaled ground motions for 3-storey SPSW with LBEs around the opening along with mean and design spectrum

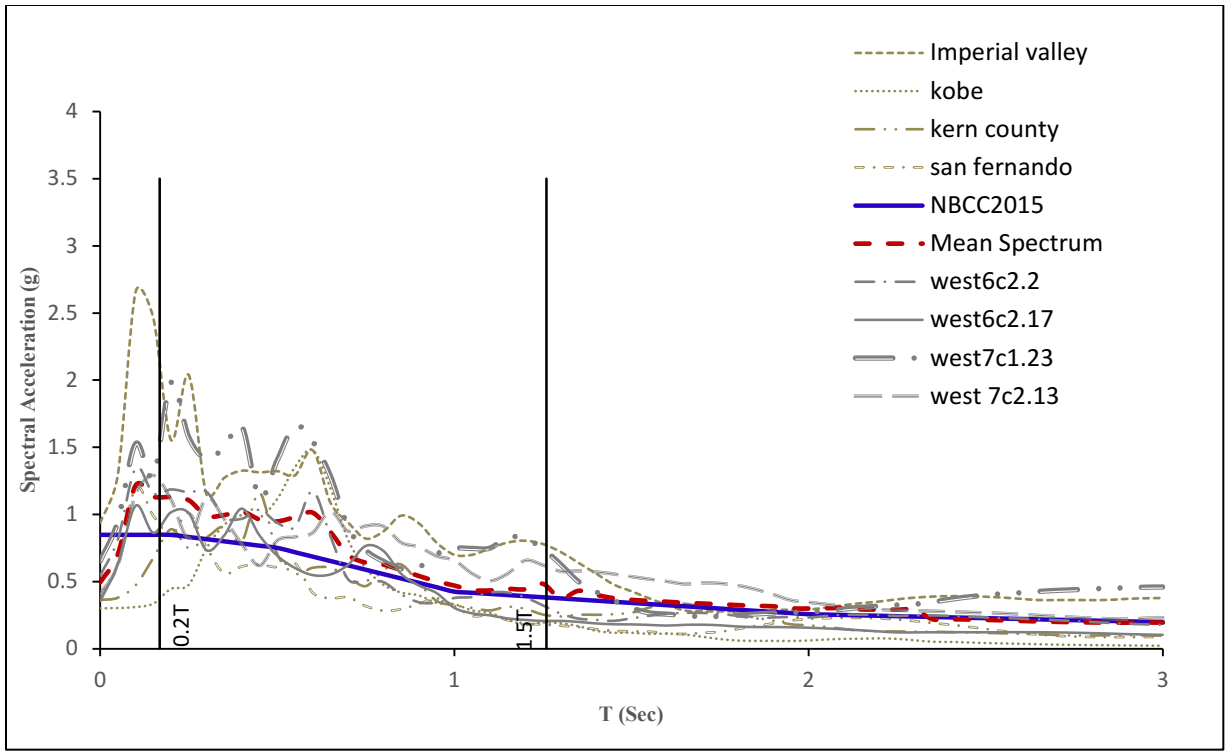

Figure 5.3: Response spectra of scaled ground motions for 5-storey SPSW with LBEs around the opening along with mean and design spectrum

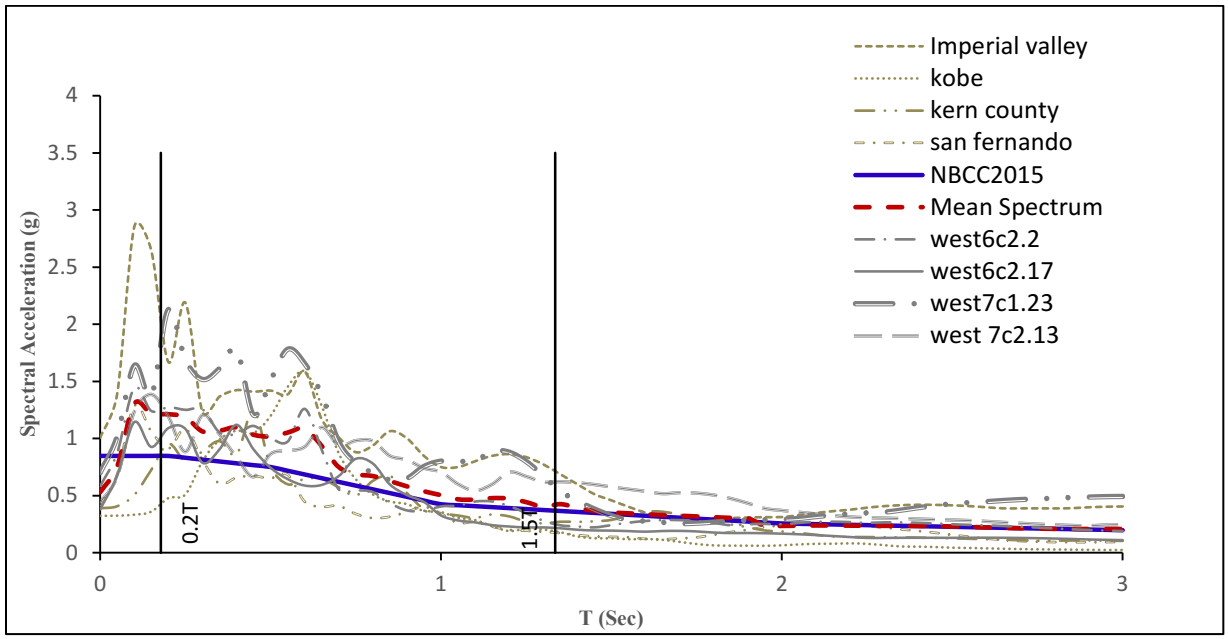

Figure 5.4: Response spectra of scaled ground motions for 3-storey SPSW without LBEs around the opening along with mean and design spectrum

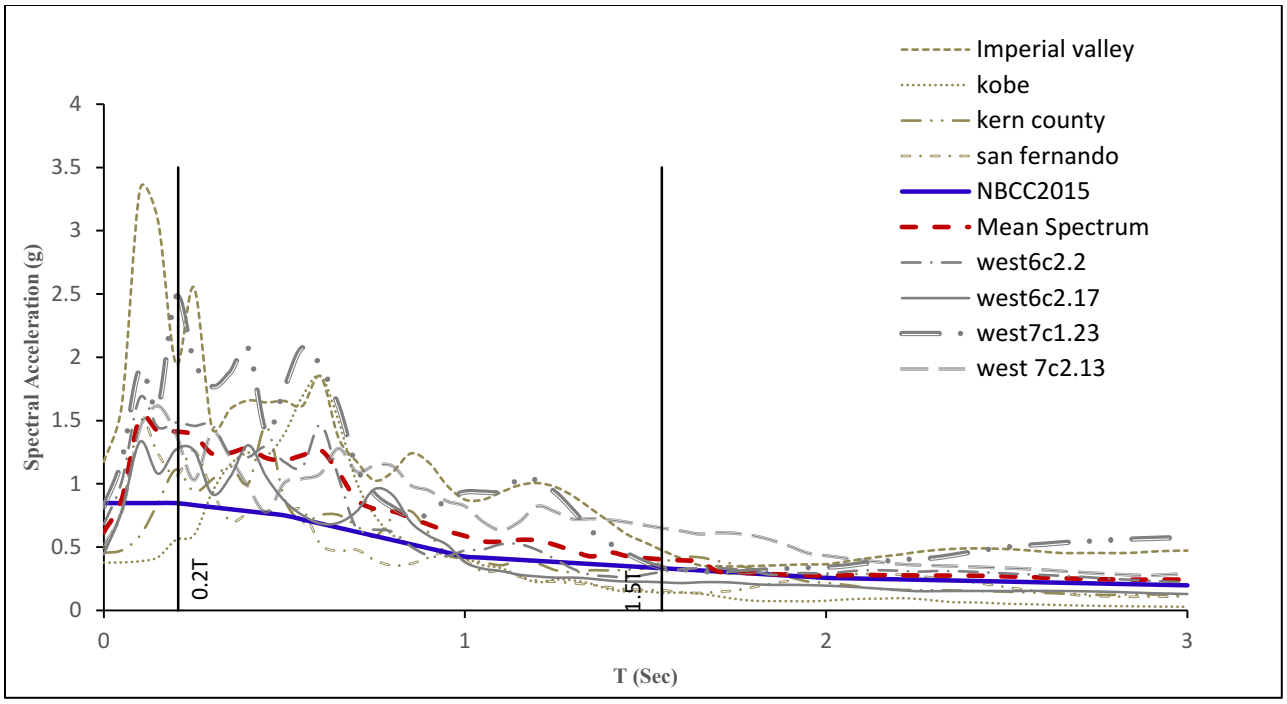

Figure 5.5: Response spectra of scaled ground motions for 5-storey SPSW without LBEs around the opening along with mean and design spectrum

Nonlinear seismic analysis was performed for 3- and 5-storey SPSWs for the selected ground motions. From the non-linear time history analysis, it was observed that the maximum base reaction for the 3-storey SPSW under artificial ground motions of West6c2.2, West 6c2.17, West7c1.23, West7c2.13 were 4435 kN, 3262 kN, 5160 kN and 4386 kN, respectively. The base reaction forces for the 3-storey SPSW under real records of Imperial Valley, Kobe, San Fernando and Kern County were 5040 kN, 4329 kN, 3041 kN and 4185 kN, respectively.

The maximum base reactions for 5-storey SPSW under artificial ground motions of West6c2.2, West 6c2.17, West7c1.23, West7c2.13 were 3826 kN, 2998 kN, 5004 kN and 4088 kN, respectively. Similarly, the base reaction forces for the 5-storey SPSW under real records of Imperial Valley, Kobe, San Fernando and Kern County were 4559 kN, 2366 kN, 2586 kN and 3148 kN, respectively. Figure 5.6 and Figure 5.7 show base reaction time histories of the 3-storey and 5-storey SPSWs under the selected ground motions.

The obtained dynamic storey shear forces from nonlinear analyses show that NBC 2015 calculated static base and storey shear forces much lower than the dynamic shear distributions occur under earthquake event. Figure 5.8 and Figure 5.9 show the maximum base and storey

shears under all earthquake events. Average maximum base reaction of selected ground motion records is 4230 kN for the 3-storey SPSW and 3572 kN for the 5-storey SPSW. The calculated nominal shear strength at the level of opening proposed by AISC guide 20 is 27% lower than the average peak dynamic shear for the 3-storey and 32% for the 5-storey SPSW. The reason behind was that the storey shear was not only resisted by the steel plate but also by the boundary steel columns and local beam elements around the opening The average peak storey shear contribution of various elements are shown in Figure 5.10 and Figure 5.11. On the other hand, in the design process, the thickness of steel infill plate was selected based on practical availability and constructability, so the plate was much thicker than the design requirement. Therefore, the SPSWs had higher strength.

As observed from Figure 5.10 and Figure 5.11 for the 3-storey SPSW, under all earthquake records the average of maximum shear contributions of the columns, infill steel plates and LBEs at the base are 53%, 29% and 18%, respectively. For the 5-storey SPSW these values are 51%, 31% and 18% for the columns, infill steel plates and LBEs, respectively.

The peak relative storey displacement and maximum interstorey drifts were obtained from seismic analyses and are illustrated in Figure 5.14 and Figure 5.15. Under all seismic events, the interstorey drifts were much lower that the NBC 2015 limit. The floor displacement patterns are presented in Figure 5.12 and Figure 5.13 for the instant of maximum roof displacement. As can be observed, the pattern is the same for all the earthquakes.

The extent of yielding in the 3-storey and 5-storey SPSWs under event “west7c1.23” is presented in Figure 5.16. Seismic analyses showed that in the 3-storey SPSW the steel infill plates of the 2 bottom floors and the panel right above the opening in the third floor were fully yielded under all earthquake records and panels at the side of opening in the third floor partially yielded under the earthquake records. Under event “west 7c1.23” and “Imperial Valley”, webs of 2nd and 3rd storey beams right below the opening reached the yield point and at the same time, very slight yielding was observed at the base of the columns.

In the 5-storey SPSW, all the steel infill plates of the 3 bottom floors and the panel above the opening in all the floors were fully yielded under all ground motion records and the infill steel plates of the 4th floor were partially yielded under the seismic records. Only in events “west7c1.23” and “Imperial Valley”, webs of 2nd, 3rd and 4th storey beams right below the opening reached the yield point and at the same time, column base showed very slight yielding.

Boundary columns were essentially elastic under most of the seismic events though satisfying the design objective of column. The undesired shear yielding of the storey beam observed above the opening was due to the additional shear imposed by LBEs on the beam, which is underestimated by AISC guide 20. This phenomenon was also reported by Hosseinzadeh and Tehranizadeh (2012).

The obtained axial forces and moments of columns for both the 3-storey and 5-storey SPSW were less than the calculated values from capacity design.

Finally, from the seismic analyses it was observed that if the LBEs around the opening and the thickness of infill plates are designed based on AISC Design guide 20, they will not alter the recommended yielding sequence of the SPSW system.

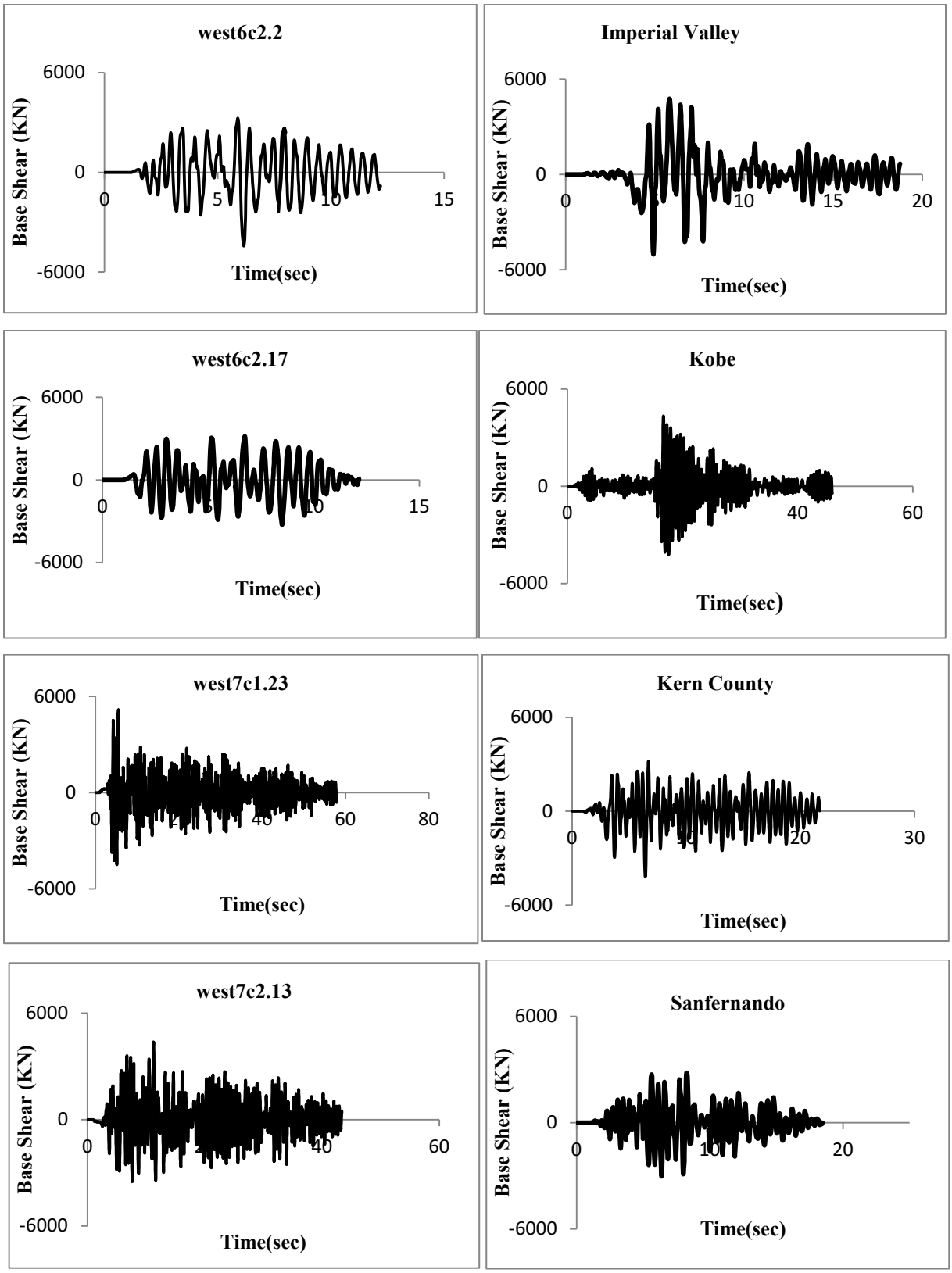

Figure 5.6: Base shear history of 3-storey SPSW

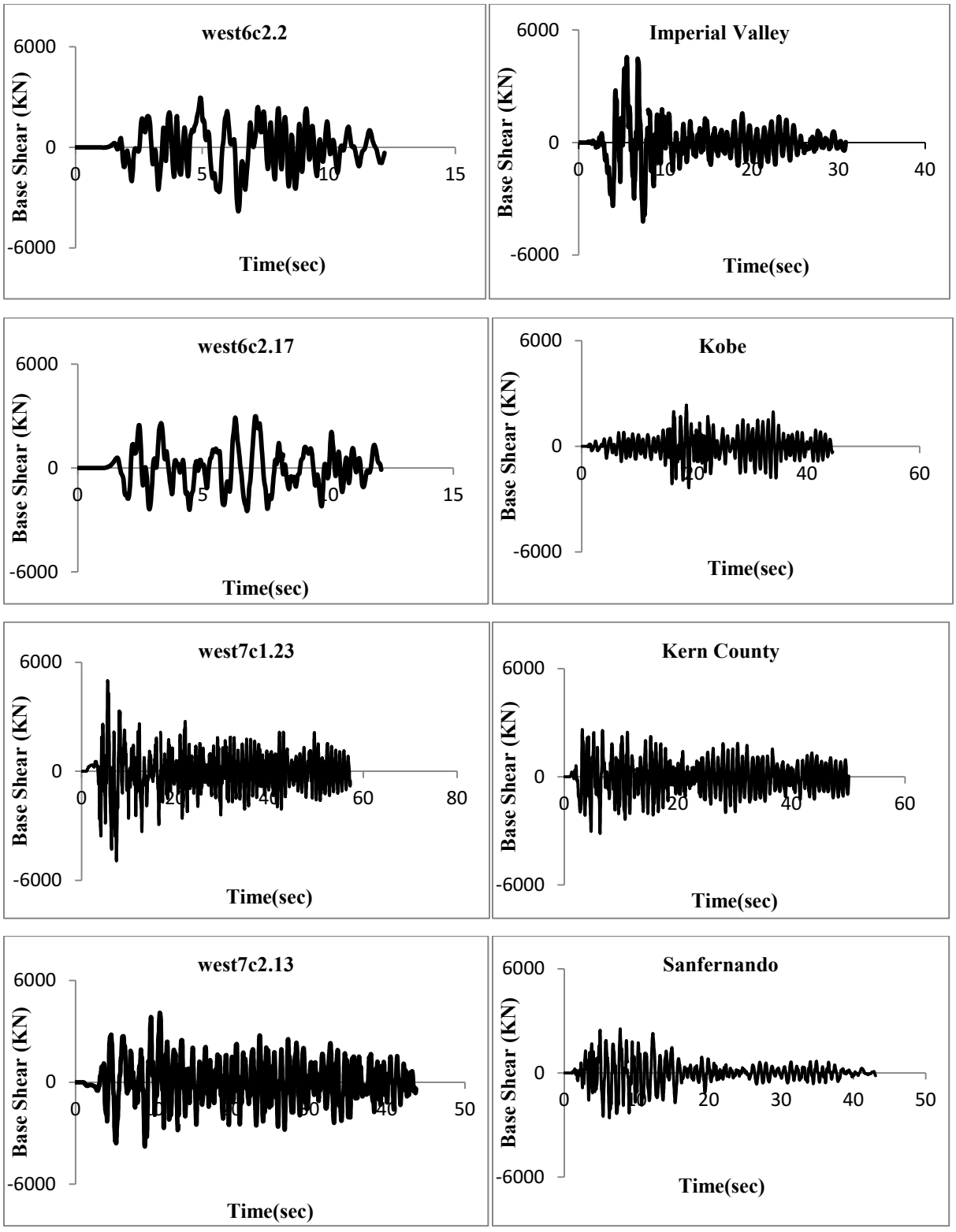

Figure 5.7: Base shear history of 5-storey SPSW

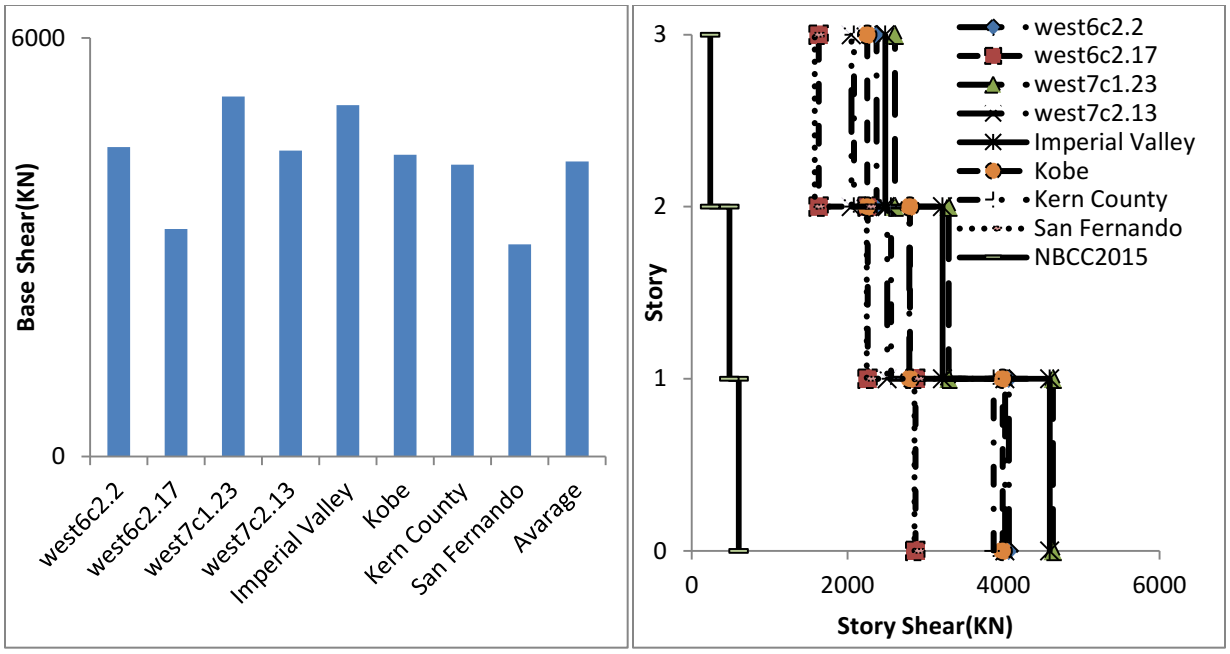

Figure 5.8: Maximum base shear (left) and storey shear distribution (right) of 3-storey SPSW under selected earthquake events

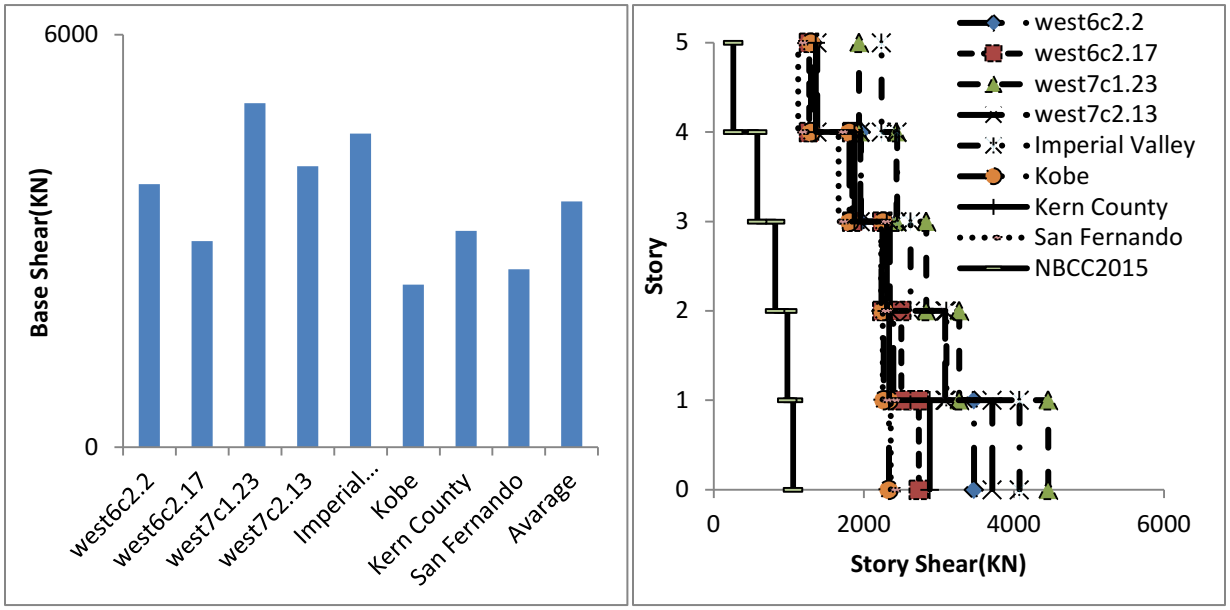

Figure 5.9: Maximum base shear (left) and storey shear distribution (right) of 5-storey SPSW under selected earthquake events

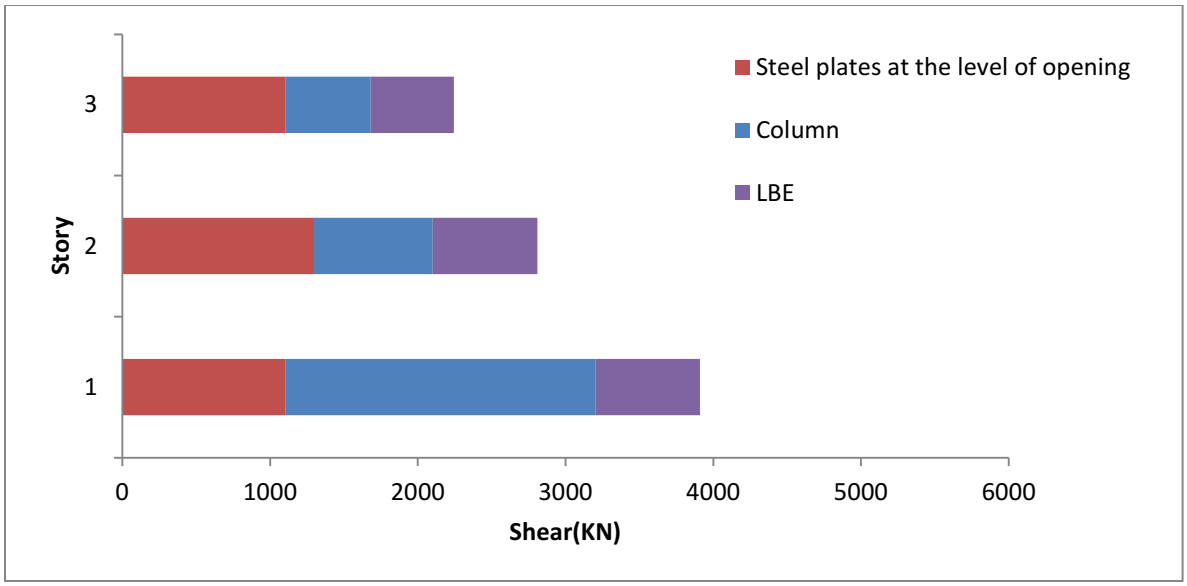

Figure 5.10: Average peak storey shear contributions of 3-storey SPSWs

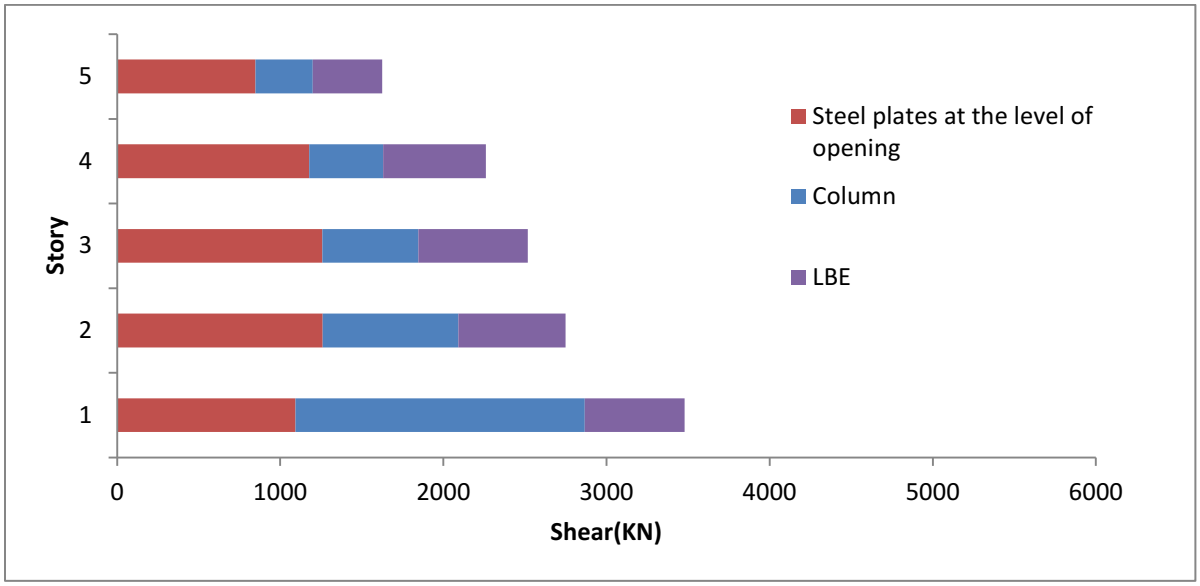

Figure 5.11: Average peak storey shear contributions of 5-storey SPSWs

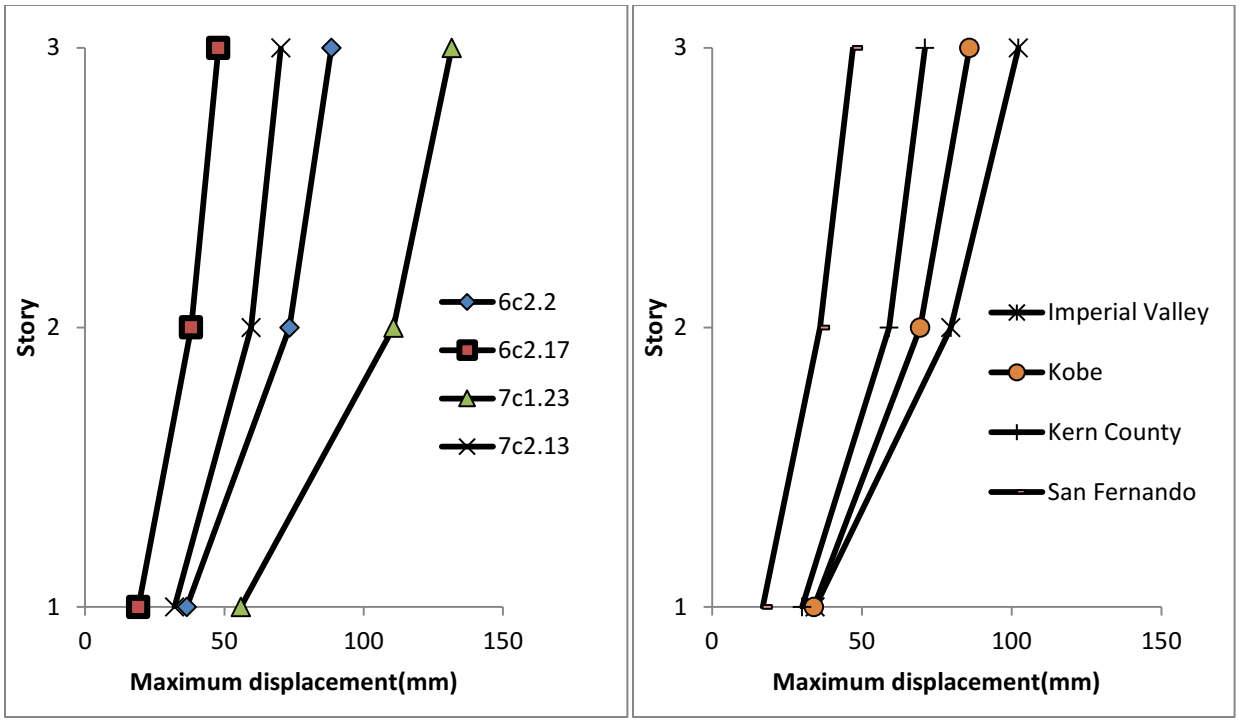

Figure 5.12: Maximum storey displacements at instant of peak top storey displacement for 3-storey SPSW under: simulated ground motions (left) real ground motions (right)

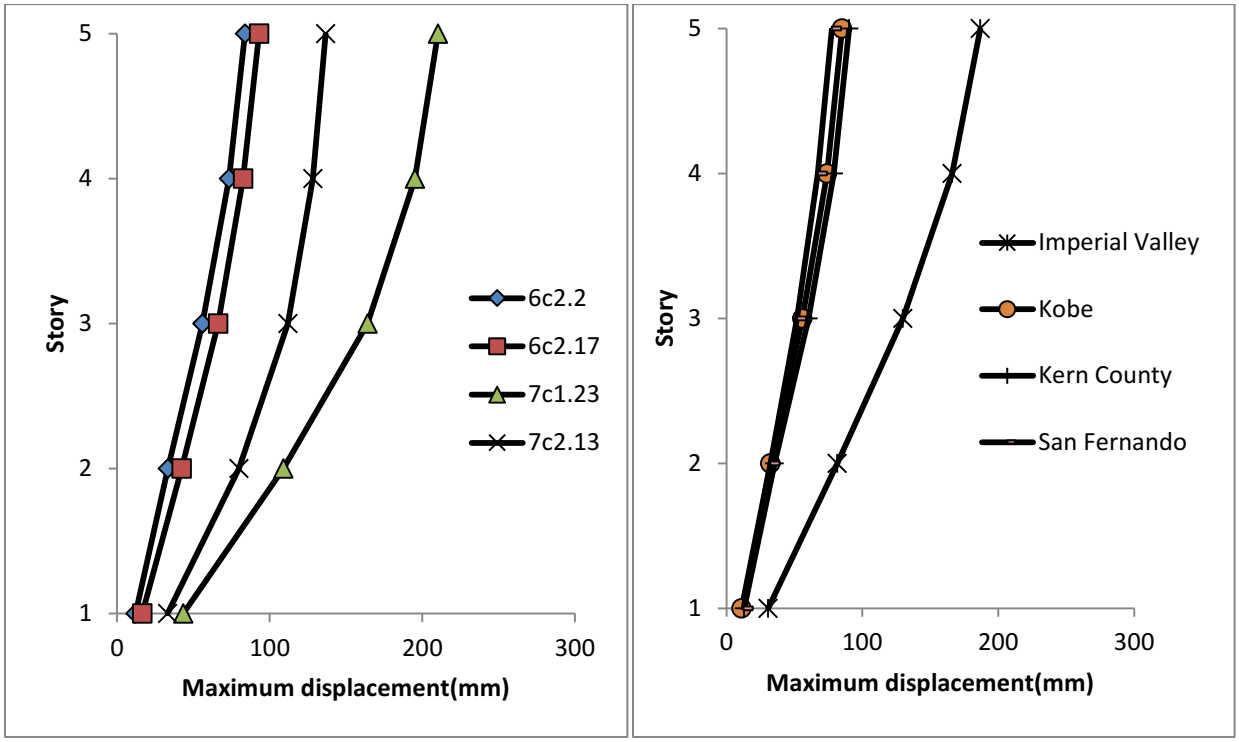

Figure 5.13: Maximum storey displacements at instant of peak top storey displacement for 5-storey SPSW under: simulated ground motions (left) real ground motions (right)

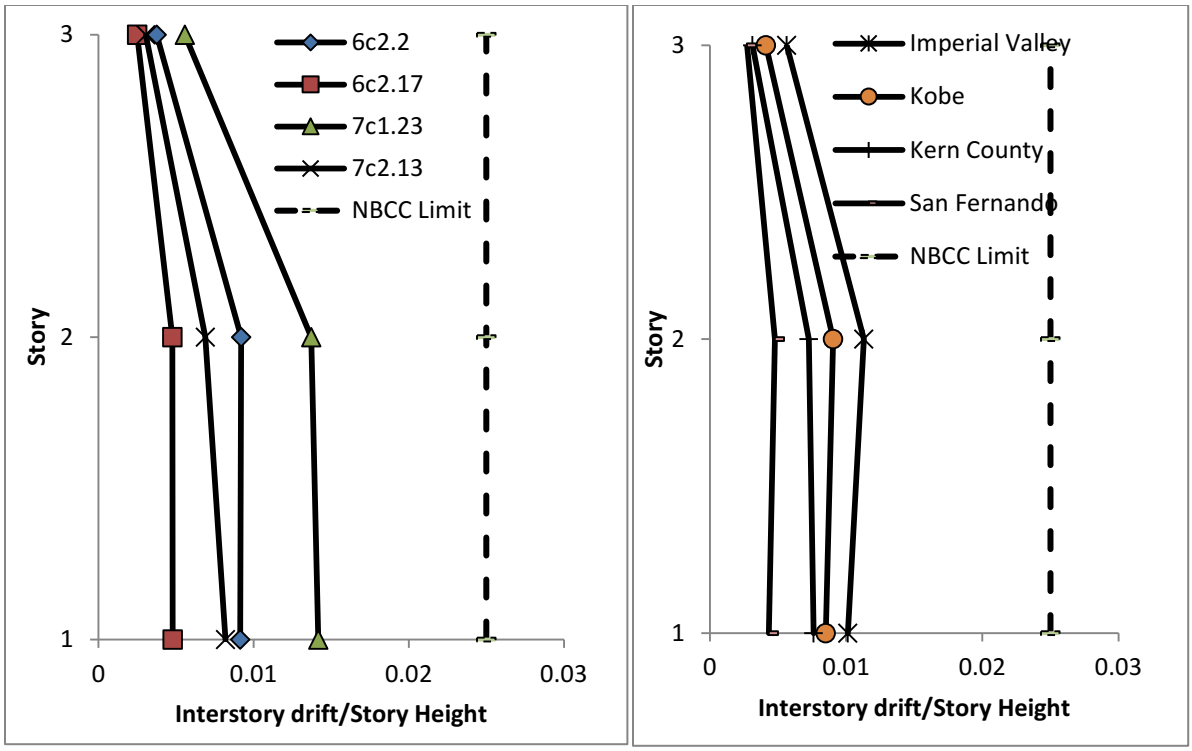

Figure 5.14: Maximum interstorey drifts for 3-storey SPSW system under: simulated ground motions (left) and real ground motions (right)

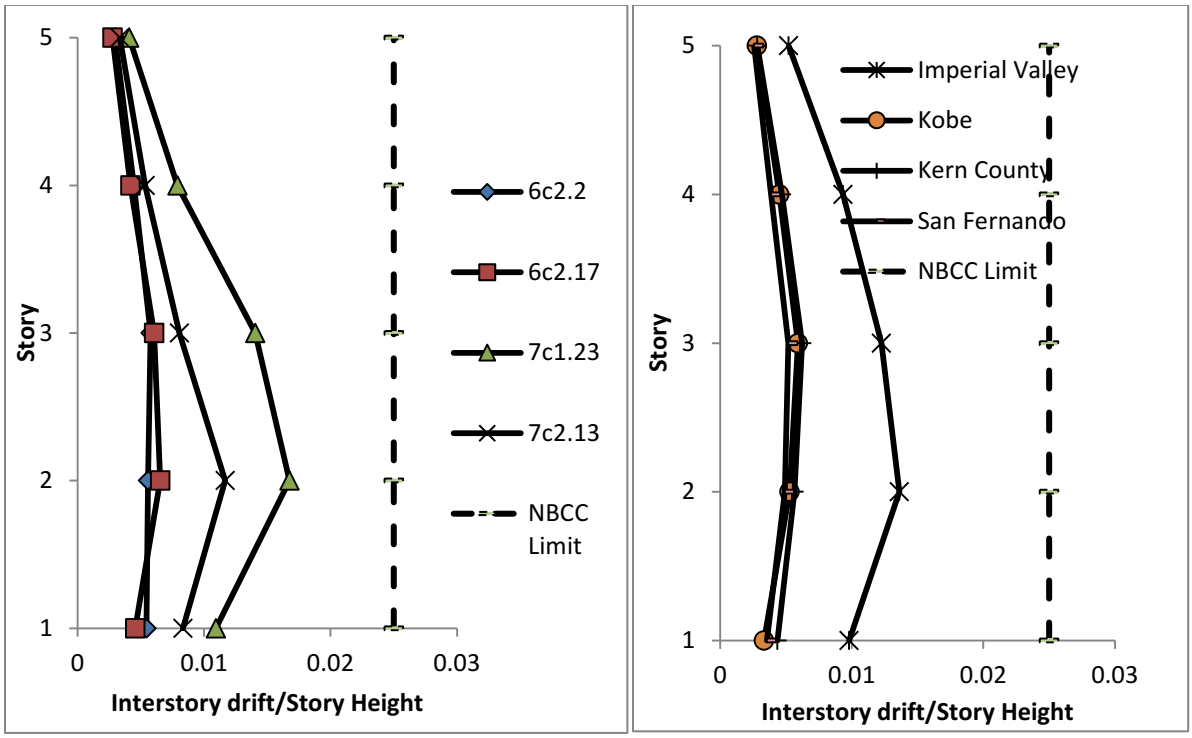

Figure 5.15: Maximum interstorey drifts for 5-storey SPSW system under: simulated ground motions (left) and real ground motions (right)

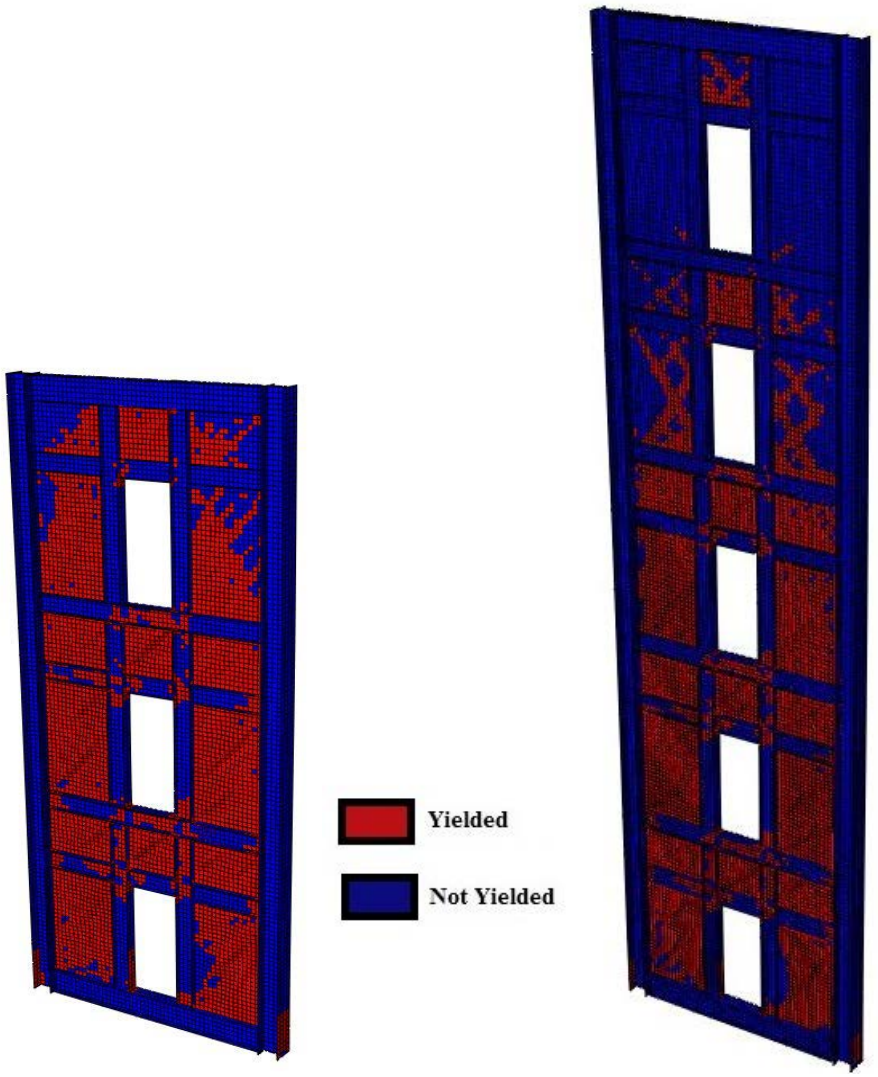

Figure 5.16: Yield pattern of 3-storey (left) and 5-storey (right) SPSW at peak base shear instant under event west7c1.23

5.3 Seismic performance of SPSW with and without LBEs around the opening

Current AISC design standard recommends use of horizontal and vertical local boundary elements (LBE), in the form of stiffeners, around openings in the SPSWs to anchor the tension field developed in the infill plate. In this section, the effects of utilizing LBEs around the opening are studied. Other than the presence of LBEs, all other properties were considered to be the same for the 3- and 5- storey SPSWs. The performance of the four models (3- and 5- storey SPSWs with and without LBEs) under the same ground motion is assessed.

The yield pattern of the 3-storey SPSWs with and without LBEs around the opening under the same records at the instant of peak shear is shown in Figure 5.17. It is observed that the LBEs provide enough stiffness for the steel plates to develop tension field action and become fully yielded.

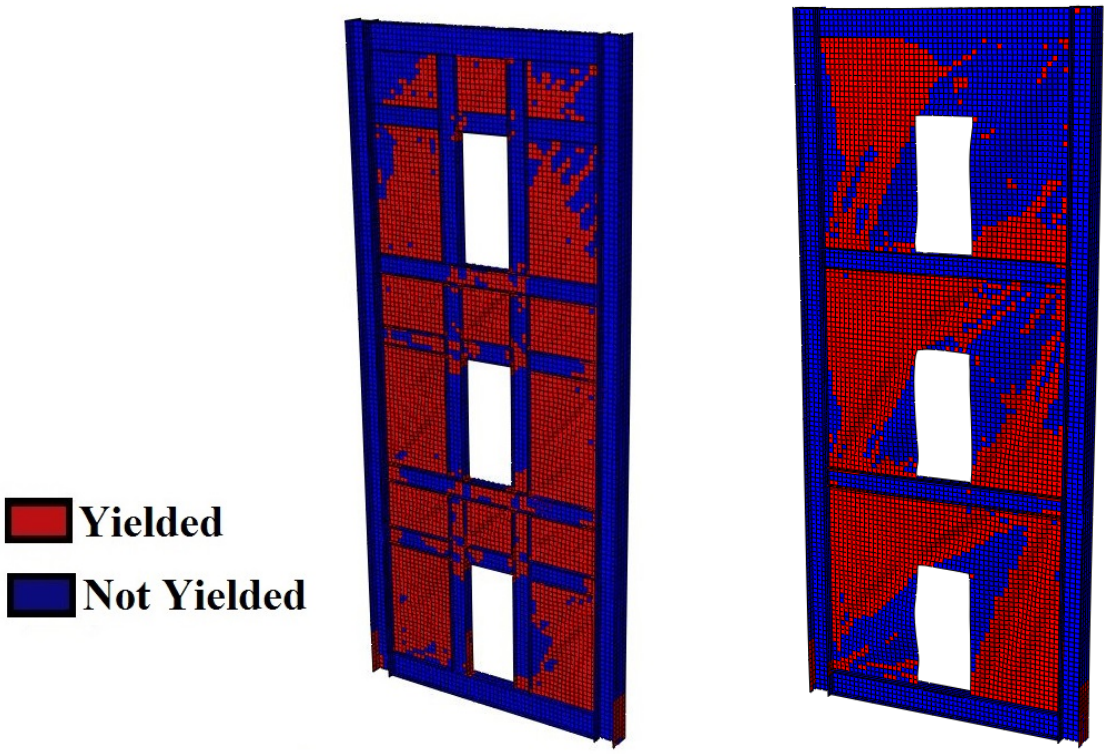

Figure 5.17: The yield pattern at the instant of peak shear for 3-storey specimens

5.4 Effectiveness of Stiffeners (LBEs) around the opening

Figure 5.18 shows the out of plane deformation around the opening for the SPSWs with and without LBEs. Under the same ground motion, the maximum out of plane displacement around the opening in the absence of LBEs was significantly higher for the 3-storey and 5- storey SPSWs, while in the presence of these elements, the out of plane deformation was almost prevented. The maximum out of plane deformation around the opening has the value of 164mm in 3-storey SPSW without LBEs while this value is 2mm for 3-storey SPSW with LBEs around the opening.

In the SPSWs without LBEs around the opening, as the plate is not anchored, the amount of out of plane deformation of the steel plate around the opening shows high sensitivity to the extent of initial imperfection of the steel plate.

The maximum in plane deformation around the opening was 72 mm for the SPSWs without LBE and 34mm with the presence of LBEs around the opening.

Therefore, the LBEs bring adequate stiffness to reduce the out of plane and in plane deformation around the opening.

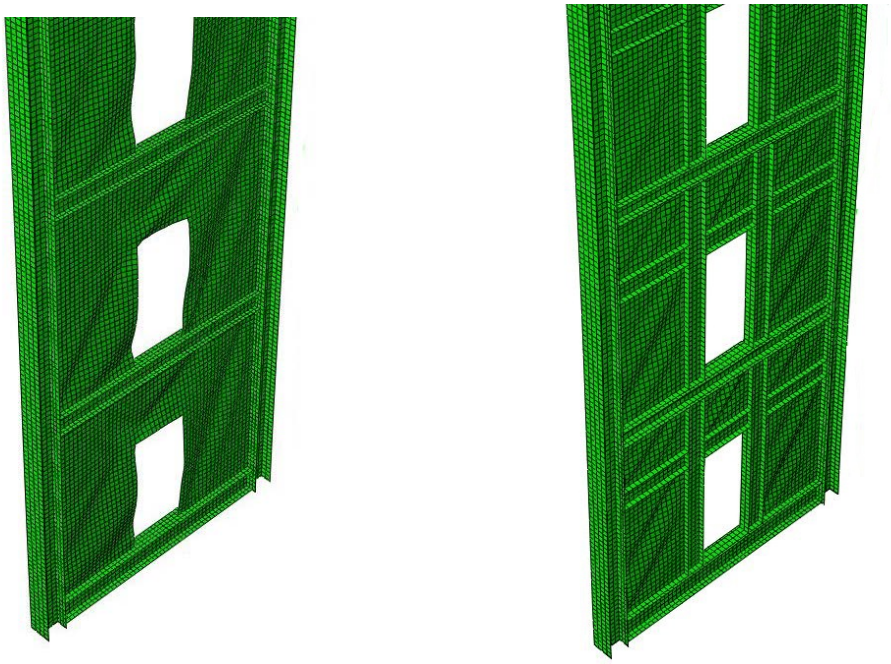

Figure 5.18: The deformation of steel plates around the opening: in the absence of LBEs (left) ; and with the presence of LBEs (right)

5.5 Alternative stiffener arrangement

As observed in the previous section, the presence of stiffeners around the opening is required to prevent in-plane and out-of-plane deformation of infill plate around the rectangular opening. Nevertheless, introduction of stiffeners around all sides of the opening is very expensive. Using less stiffeners offers a lighter structure, decreases foundation and steel material costs.

In order to determine whether fewer stiffeners are able to anchor tension field developed in the steel plate properly, a new stiffener arrangement was considered. The new stiffener

arrangement, as shown for the 3 storey SPSW, was identical to the previous SPSW, except the horizontal LBEs at the sides of opening were removed. The new SPSW model (model-1) and the previous SPSW with AICS suggested stiffener arrangement (model-2) are depicted in Figure 5.19. Deformation around the opening and the yield pattern of the two models are shown . inFigure 5.20 and Figure 5.21.

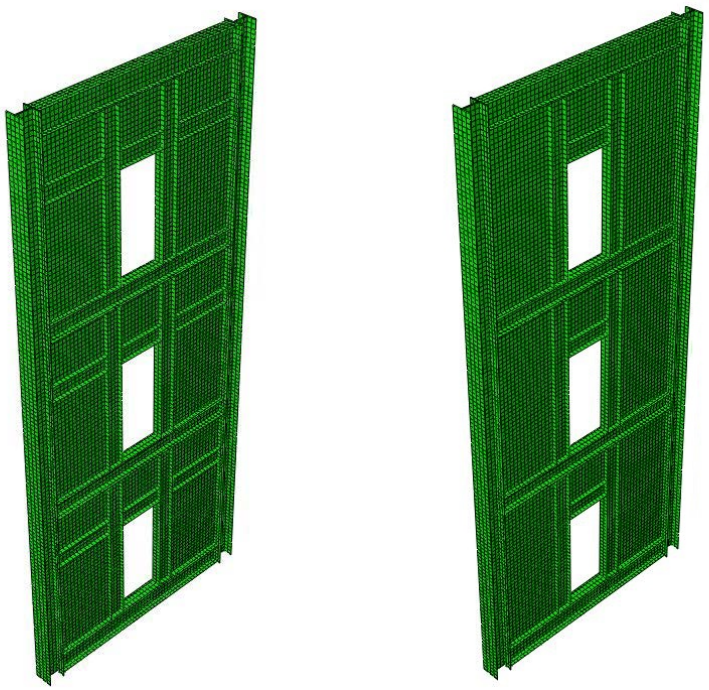

Figure 5.19: 3- storey SPSWs with: stiffeners arrangement according to AISC (model-2)(left); proposed stiffener arrangement (model-1)(right)

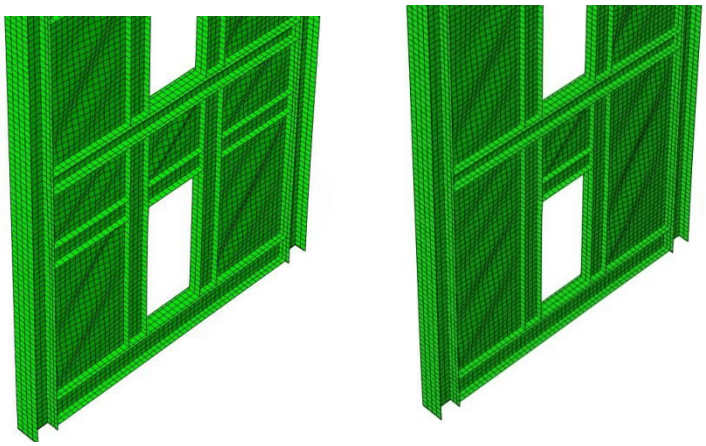

Figure 5.20: The deformation of steel plates around the opening for 3- storey SPSWs with: stiffeners arrangement according to AISC (model-2)(left); proposed stiffener arrangement (model-1) (right)

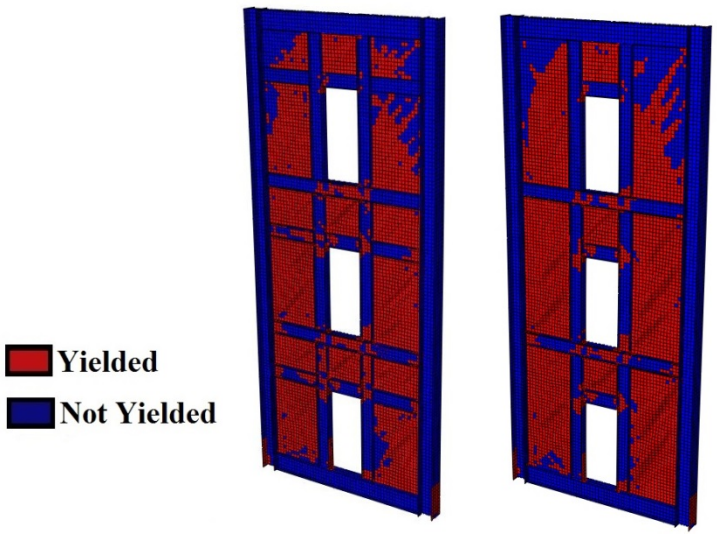

Figure 5.21: The yield pattern for 3- storey SPSWs with: stiffeners arrangement according to AISC (model-2)(left); proposed stiffener arrangement (model-1)(right)

Push-over analyses were conducted on both FE models and the results are compared in Figure 5.22. Both models were pushed up to the drift of 3.6%.

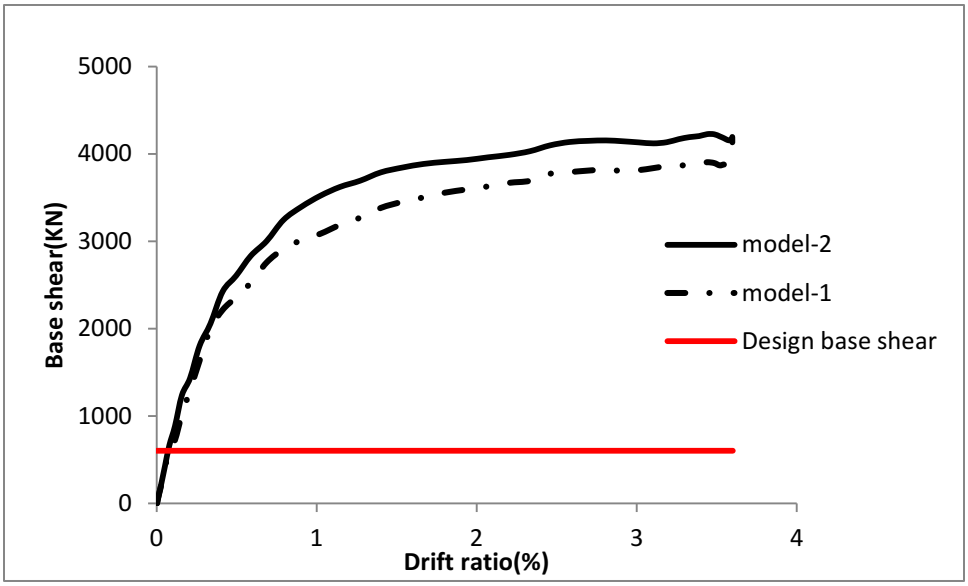

Figure 5.22: Push over curves for the 3-storey SPSW with two different boundary element arrangements

Non-linear time history analyses were performed on both SPSWs with different stiffener arrangements. Both models were subjected to selected scaled ground motions West6c2.2, West7c1.23 and Imperial Valley.

The maximum base reaction for SPSW with proposed stiffener arrangement (model-1) under artificial ground motions of West6c2.2 and West7c1.23 were 4119KN and 4874 kN, respectively. The maximum base reaction force under real record of Imperial Valley was 4748 kN. While the maximum base reactions for SPSW with stiffener arrangement according to AISC design guide 20 (model-2) are 4435 kN, 5160 kN and 5040 kN for West6c2.2, West7c1.23 and Imperial Valley, respectively. Figure 5.23 compares base shear history of SPSW with two different stiffener layouts around the door-sized openings.

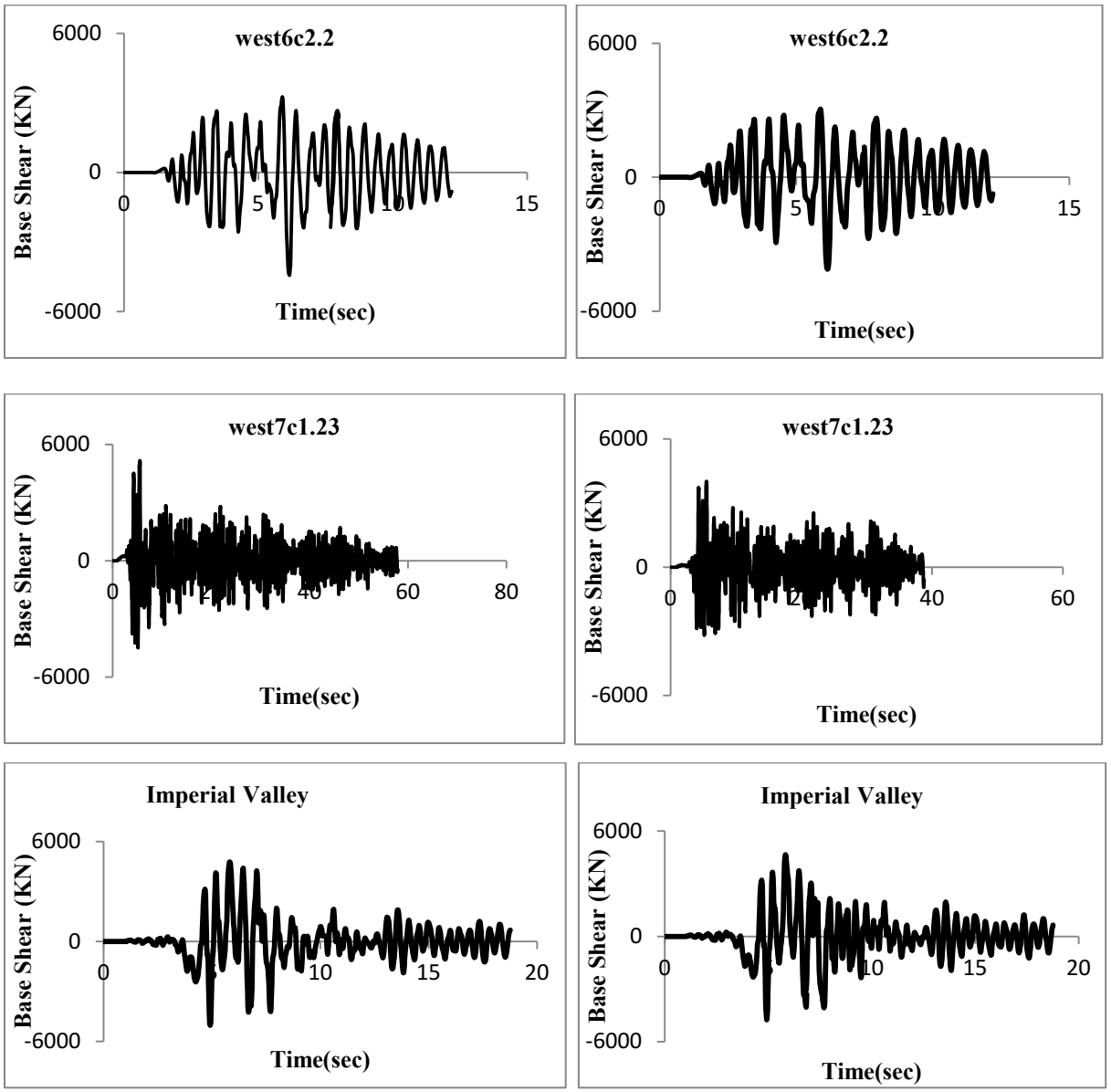

Figure 5.23: Base shear history of: SPSW with stiffener arrangement according to AISC design guide 20 (left); SPSW with proposed stiffener arrangement (right)

The peak relative storey displacement and maximum interstorey drifts were obtained from seismic analyses for both models and the comparison is illustrated in Figure 5.24 to Figure 5.26. As can be observed, under all seismic events the interstorey drifts were much lower that the NBC 2015 limit for the model with fewer stiffeners. The floor displacement patterns are presented for the instant of maximum roof displacement for both models.

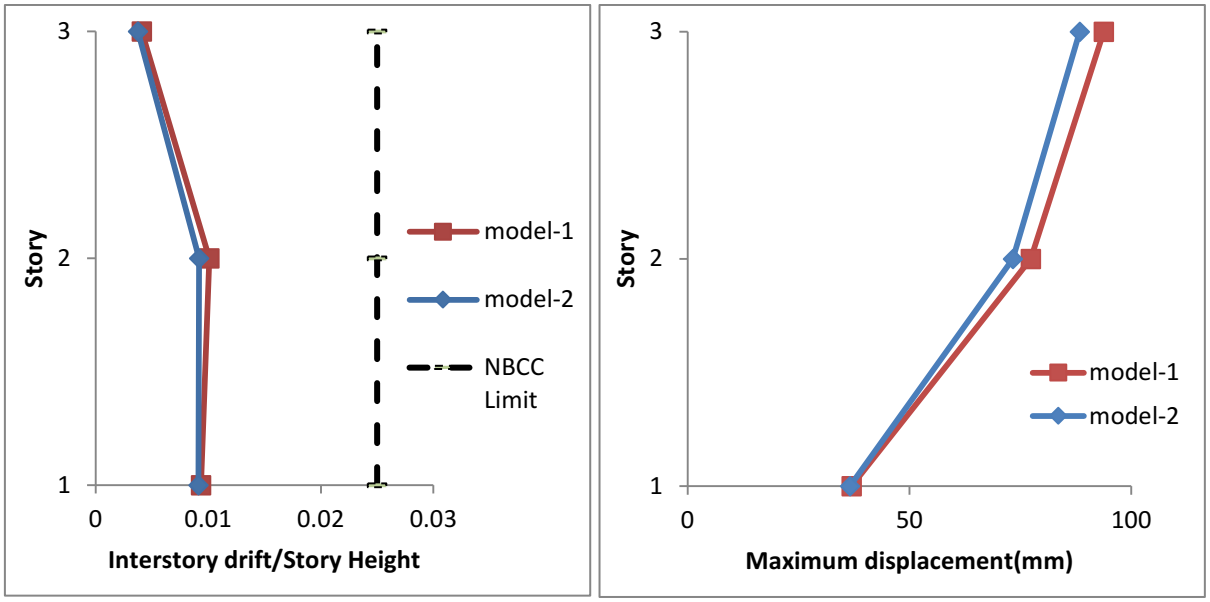

Figure 5.24: Interstorey drifts (left) and maximum displacements (right) of the two models under west6c2.2 ground motion

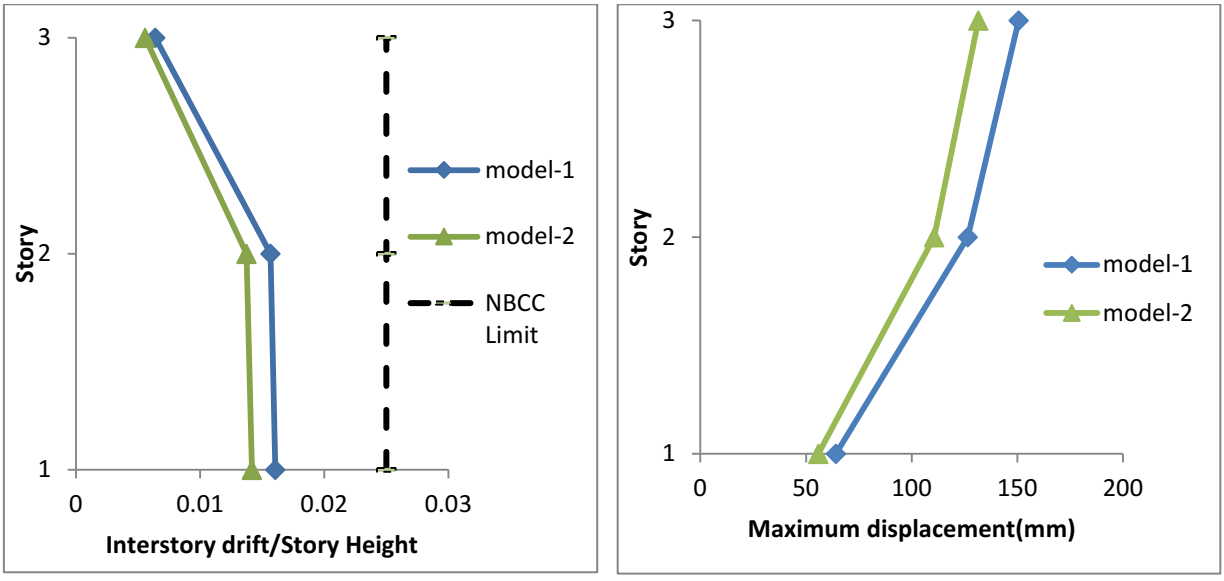

Figure 5.25: Interstorey drifts (left) and maximum displacements (right) of the two models under west7c1.23 ground motion

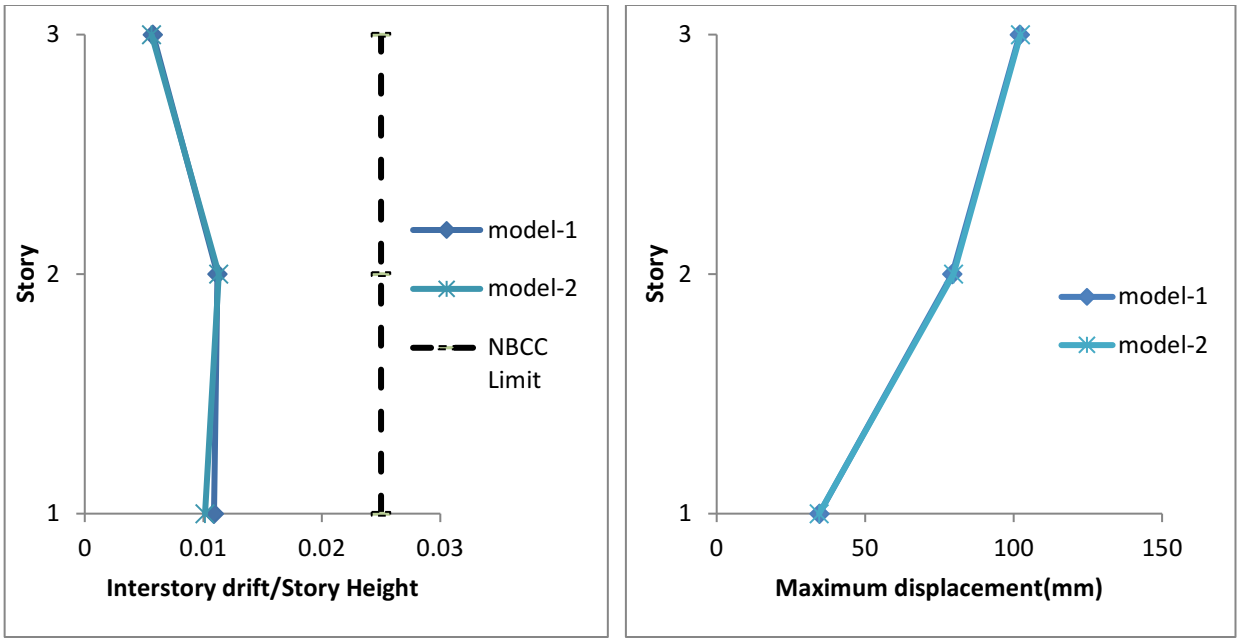

Figure 5.26: Interstorey drifts (left) and maximum displacements (right) of the two models under Imperial Valley ground motion

From seismic analyses it was observed that the stiffeners in model-1 can properly anchor the out of plane deformation around the opening. So, this stiffener arrangement can be used as alternative to the previous models to and cut the costs.

Also it is observed that using the proposed stiffener arrangement did not alter the recommended yielding sequence of the SPSW system.

5.6 SPSW with window size opening:

In order to investigate the behaviour of SPSW with window opening, a 3story SPSW with rectangular windows size opening was modeled and analyzed under 3 seismic records. The model is depicted in Figure 5.27. The SPSW was the same shear wall located in the proposed building.

For conducting seismic analysis, the West6c2.2, West7c1.23 and Imperial Valley ground motions were scaled and applied to the model.

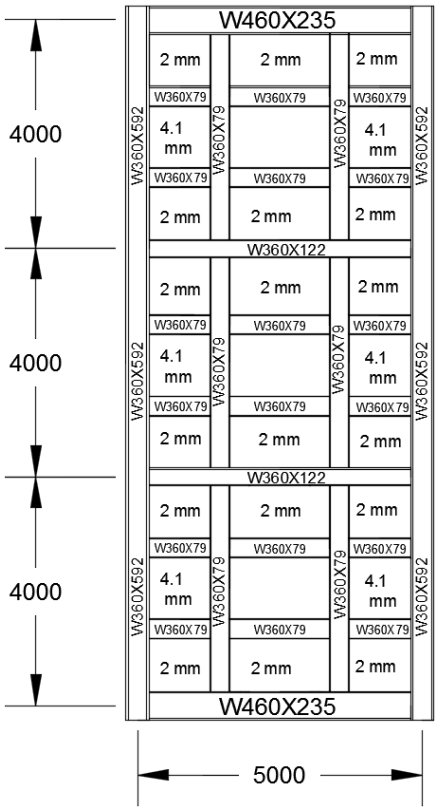

Figure 5.27: Elevation view of the selected shear wall with window size opening

The maximum base reaction for SPSW with window opening under artificial ground motions of West6c2.2 and West7c1.23 were 4773 KN and 5365 KN, respectively. The maximum base reaction force under real record of Imperial Valley was 5276 KN.

Similar to SPSW with door opening, the obtained base shear forces from nonlinear analyses were higher than the amounts calculated according to NBC 2015. The base shear for the 3-storey SPSW was calculated as 604 KN according to NBC 2015.

The peak relative story displacement and maximum interstorey drifts were obtained from seismic analyses and are illustrated in Figure 5.29 and Figure 5.30. Under all seismic events, the interstorey drifts were much lower that the NBC 2015 limit. The floor displacement patterns are presented in Figure 5.29 for the instant of maximum roof displacement. As can be observed, the pattern is same for all the earthquakes.

The extent of yielding in the 3-story SPSW under event “west7c1.23” is presented in Figure 5.31. Seismic analyses showed that in the 3-story SPSW the steel infill plates of the 2 bottom floors and the panel right above and below the opening in the third floor were fully

yielded under all earthquake records and other panels of the third floor were partially yielded under the earthquake records. Under the selected records, some parts of LBEs at the sides of the opening at the first floor reached the yield point and at the same time very slight yielding was observed at the base of the columns.

The shear yielding of the storey beam was not observed in the model with window size openings and the reason behind is that forces of the webs and LBEs above and below the storey beam mostly cancel each other.

Finally, from the seismic analyses it was observed that with the LBEs around the opening and infill plates designed based on AISC Design guide 20, the recommended yielding sequence of the SPSW system will not alter.

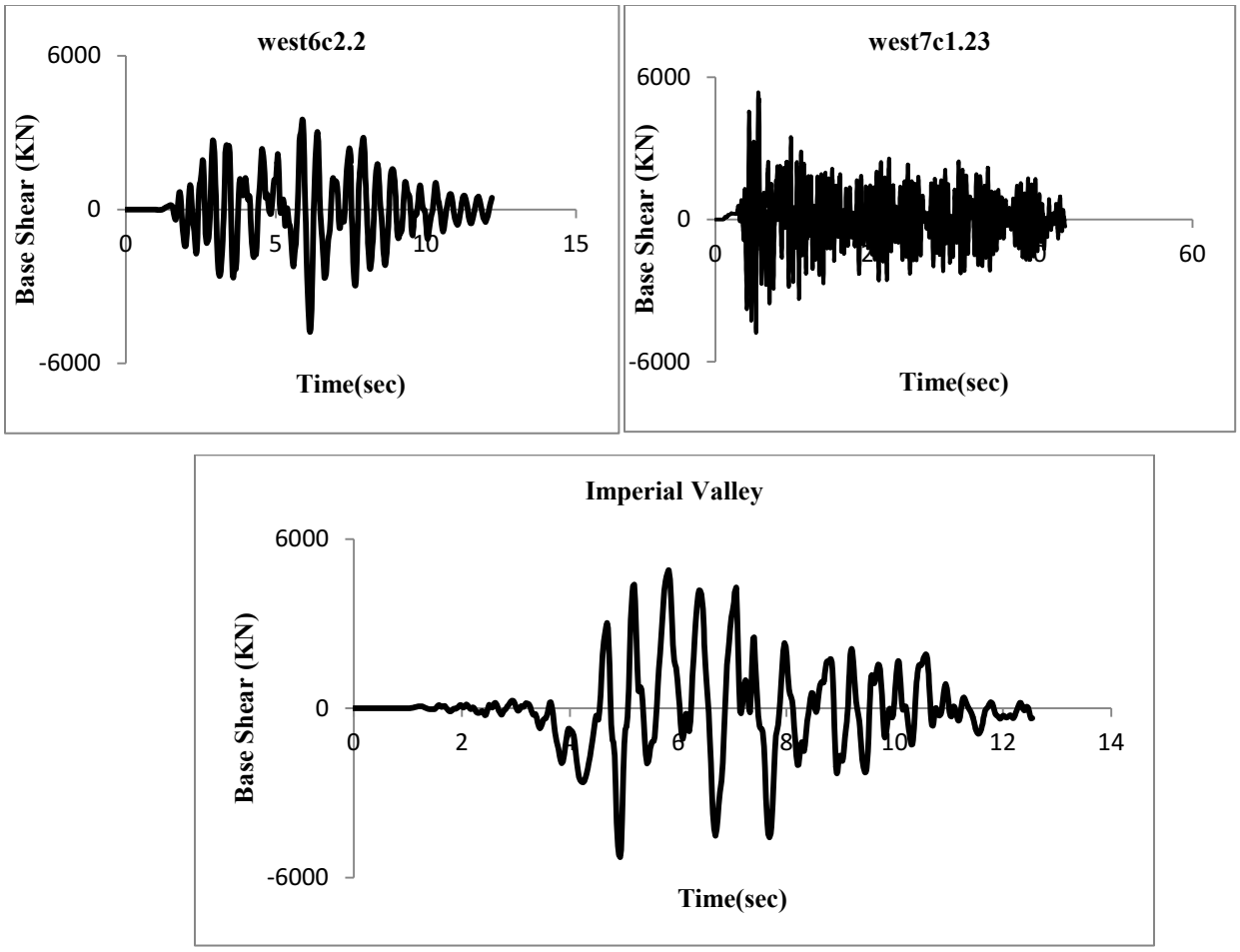

Figure 5.28: Base shear history of 3-storey SPSW with window openings

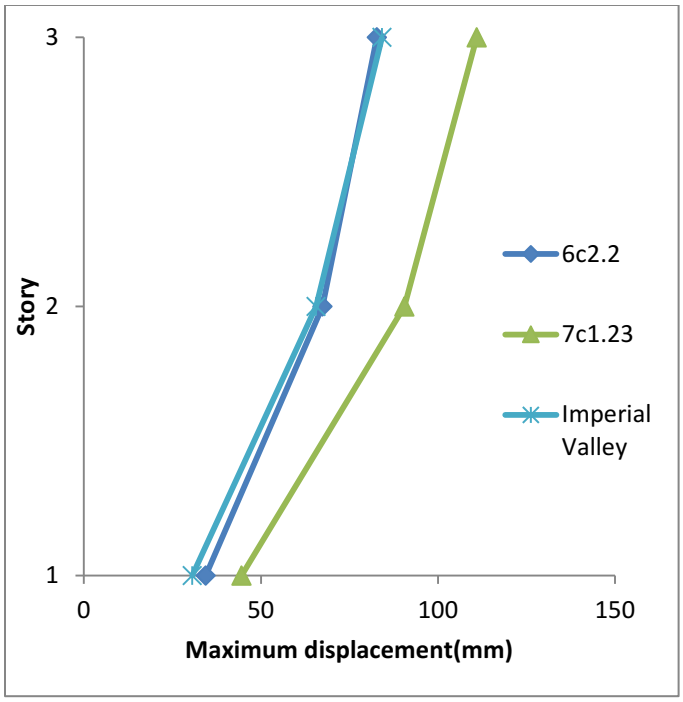

Figure 5.29: Maximum storey displacements at instant of peak top storey displacement for 3-storey SPSW with window openings

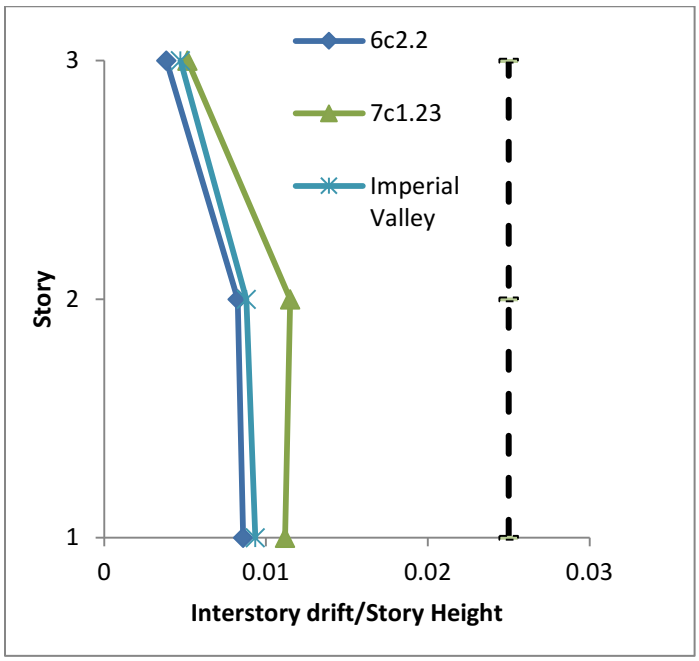

Figure 5.30: Maximum interstorey drifts for 3-storey SPSW with window openings

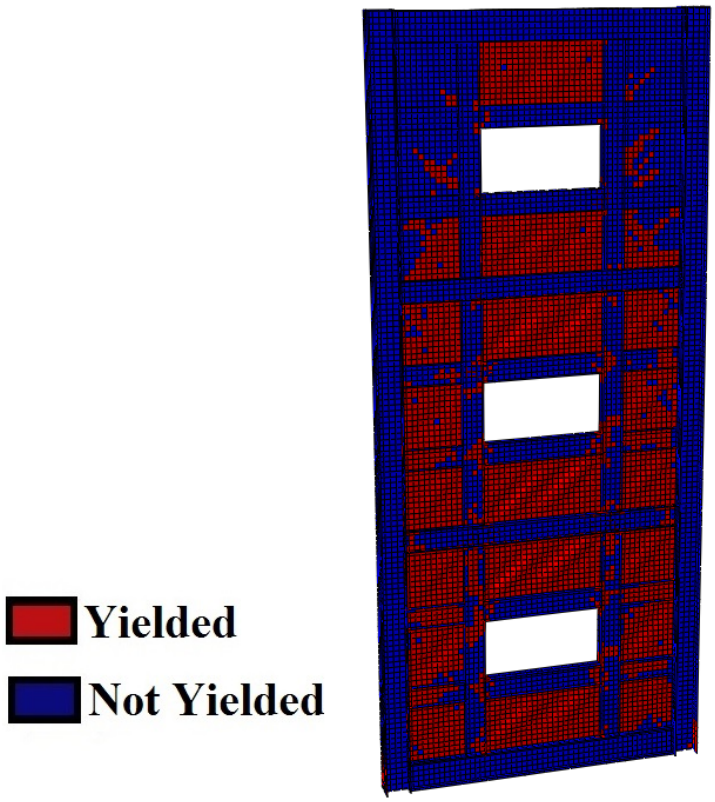

Figure 5.31: Yield pattern of 3-storey SPSW with window openings under event west7c1.23

5.7 Conclusion

Non-linear time history analyses were conducted to evaluate the seismic behavior of the SPSW with large opening in the web and assess the effectiveness of LBEs around the opening and the yielding sequence of the SPSW system. Two multi-storey (3- and 5-storey) SPSWs with standard door sized openings were selected and designed following the guidelines of current design codes and AISC design guide 20. The non-linear seismic analyses were carried out by conducting a series of time history analysis using a suite of 8 ground motions compatible with the design response spectrum of Vancouver, Canada. It was observed from analyses that SPSWs with large openings in the web showed excellent seismic performance in terms of high shear strength, ductility and stiffness. The shear strength of SPSW was more than what is presented in the current design code. The reasons are the constraint for steel plate thickness for handling issues and the contribution of other elements like columns and LBEs in resisting shear which are not considered in the code.

The boundary columns that were designed with capacity design concept serves well under seismic events. Under all seismic records the column axial forces and bending moments were lower than the designed forces. The steel plates were fully yielded while the boundary elements remained elastic under most of the earthquake events. However, undesired shear yielding was observed under two events for the beams under the door size openings which was due to additional shear imposed on beams, which is underestimated in the design procedure of AISC Design Guide 20.

It was observed that the presence of LBEs around the opening was necessary as it was recommended by AISC 341-16. The effectiveness of LBEs designed according AISC Design Guide 20 in eliminating the out of plane and in plane deformations around the opening were observed. The LBEs designed according AISC Design Guide 20 also showed adequate stiffness as they allowed the infill steel plates to reach their shear yield strength. Under all seismic events, the presence of the LBEs around the opening does not alter the recommended yielding sequence of the SPSW system.

Finally, an alternative LBE layout around opening with less number of elements was proposed. The proposed layout was found adequate in reducing the out of plane and in plane deformations around the opening.

Chapter Six

6. Performance of Composite Plate Shear Walls with Rectangular Openings

6.1 Introduction

In this chapter, performance of selected C-PSWs with door size openings is investigated through conducting a series of time history analysis using a suite of 8 ground motions that were developed for Western Canada and are compatible with Vancouver design response spectrum. C-PSWs with and without local boundary elements around the openings are considered. Maximum contributions of various structural components (i.e., infill plate and boundary members) in resisting applied lateral loads are calculated from seismic analysis. Since interstorey drift is an important indicator of performance in earthquake engineering analysis, the variation of maximum interstorey drift in all stories for both multi-story C-PSWs are obtained. In addition, requirements of stiffeners around the door sized openings of C-PSW system are evaluated from nonlinear seismic analysis.

6.2 Seismic response of C-PSW with opening and LBEs

Before conducting seismic analysis of C-PSWs, the selected ground motions were scaled to response spectrum of Vancouver, BC. Figure 6.1 to Figure 6.5 present the response spectra for of the 8 selected ground motions together with design spectrum and mean spectrum for two different cases of unscaled and scaled, respectively, for the selected C-PSWs. It is observed from Figure 6.2 to Figure 6.5 that within the period interval of 0.2T to 1.5T (where T is the fundamental period of selected C-PSW) the mean spectrum of selected seismic records for 3-storey and 5-storey C-PSWs with openings are higher than the NBC 2015 design spectrum.

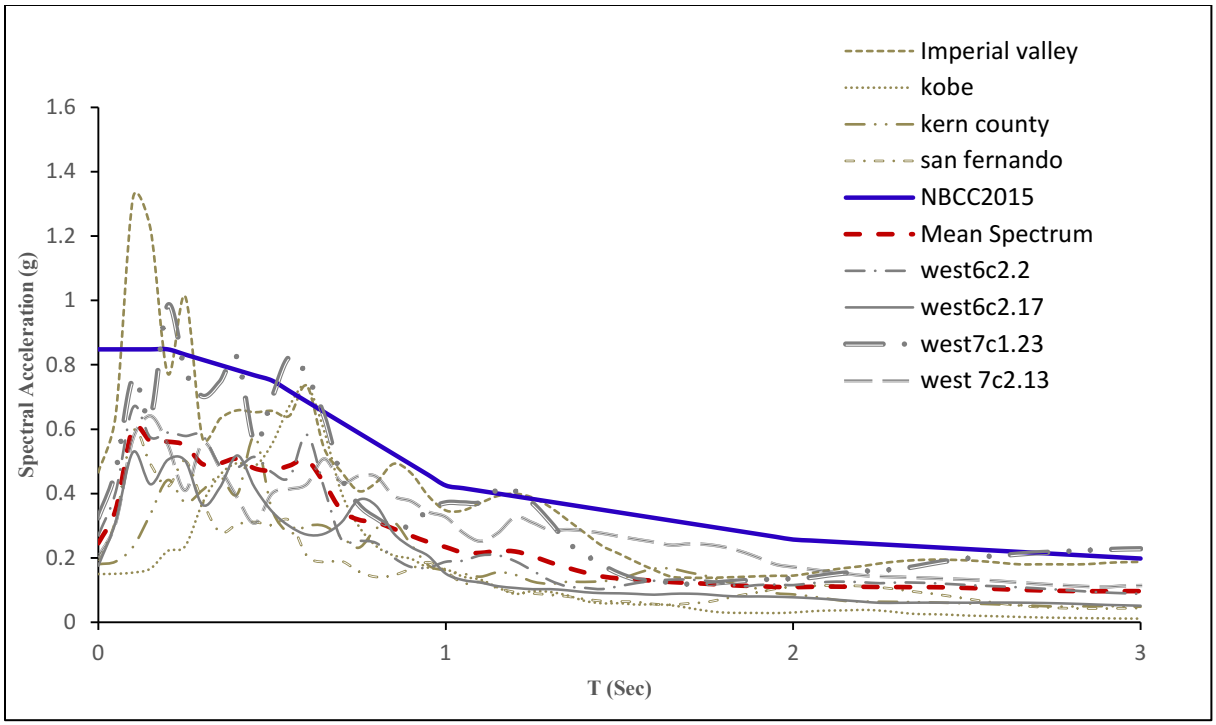

Figure 6.1: Response spectra of unscaled ground motions along with mean and design spectrum

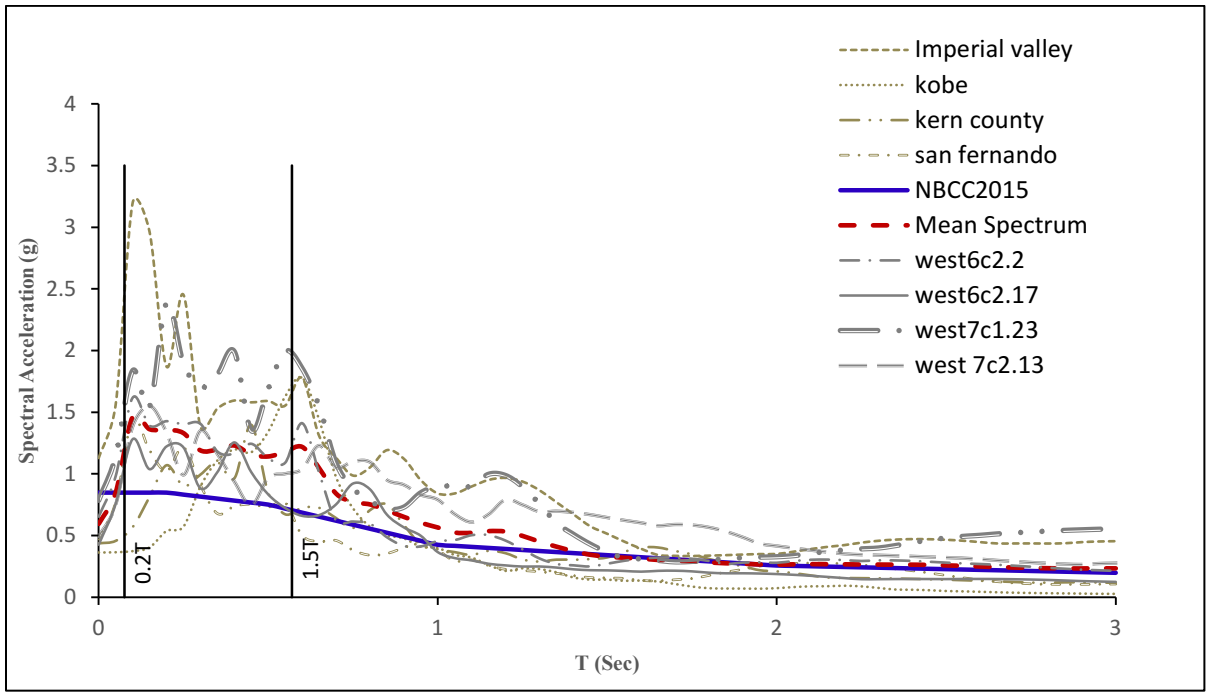

Figure 6.2: Response spectra of scaled ground motions for 3-storey C-PSW with LBEs around the opening along with mean and design spectrum

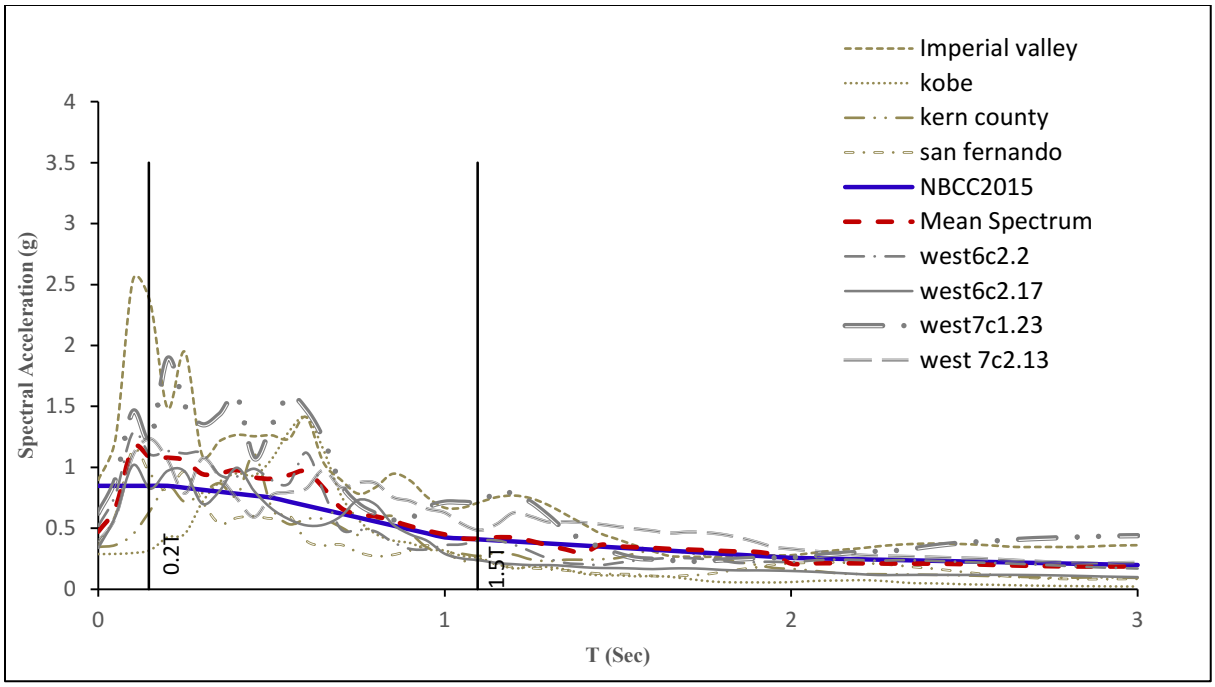

Figure 6.3: Response spectra of scaled ground motions for 5-storey C-PSW with LBEs around the opening along with mean and design spectrum

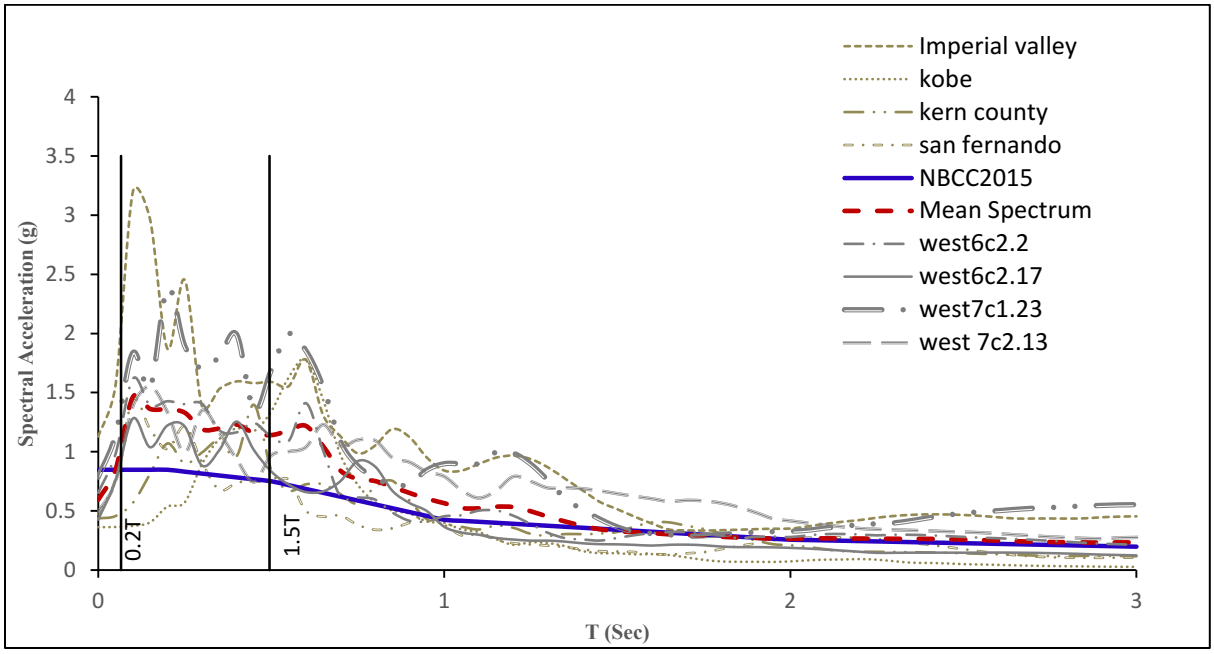

Figure 6.4: Response spectra of scaled ground motions for 3-storey C-PSW without LBEs around the opening along with mean and design spectrum

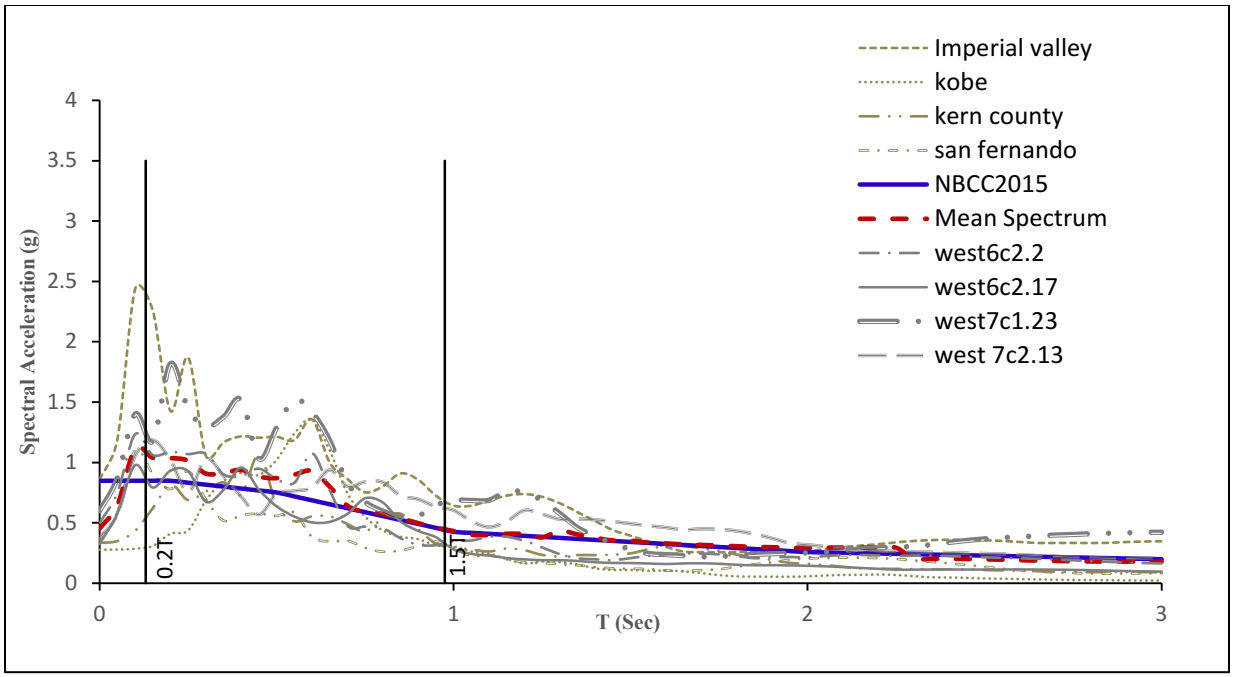

Figure 6.5: Response spectra of scaled ground motions for 5-storey C-PSW without LBEs around the opening along with mean and design

Nonlinear time history analyses were performed in ABAQUS. Under all earthquake records, it was observed that the selected 3-storey and 5- storey C-PSWs exhibited excellent seismic performance with high ductility and strength. .The maximum base reaction for the 3 story C-PSW under artificial ground motions of West6c2.2, West 6c2.17, West7c1.23, West7c2.13 were 4142 KN, 3706 KN, 4340 KN and 3515 KN, respectively. The base reaction forces under real earthquake records of Imperial Valley, Kobe, Kern County and San Fernando were 5386 KN, 4223 KN, 3579 KN and 2879 KN, respectively.

The maximum base reactions for 5-storey C-PSW under artificial ground motions of West6c2.2, West 6c2.17, West7c1.23, West7c2.13 were 3381 KN, 3511 KN ,4993 KN and 4461 KN, respectively. Similarly, the base reaction forces under real records of Imperial Valley, Kobe, Kern County and San Fernando were 5168 KN, 2981 KN, 3186 KN and 3150 KN, respectively.

From the seismic analysis, as shown in Figure 6.6, it is observed that the calculated storey and base shears according to NBC 2015 are much lower than the shears that the C-PSWs experienced under earthquakes. This was because of selected thicker infill steel plate than required by design to meet the practical and handling requirements. This caused over strength in

C-PSW. Moreover, a significant portion of shear was resisted by boundary columns, LBEs and reinforced concrete panel which are not considered in the current shear strength calculation of C-PSW and the total shear is assumed to be carried only by the infill steel plate.

Figure 6.6 presents the maximum and average peak story shears occurred under these ground motions for the 3-storey and 5-storey C-PSWs. The maximum contribution of various structural components of the C-PSW, namely, the steel infill, boundary columns, vertical LBEs and the RC panel in resisting applied lateral loads are calculated for each ground motion and the average under all ground motions are depicted in Figure 6.7 for the 3-story and 5-story C-PSWs.

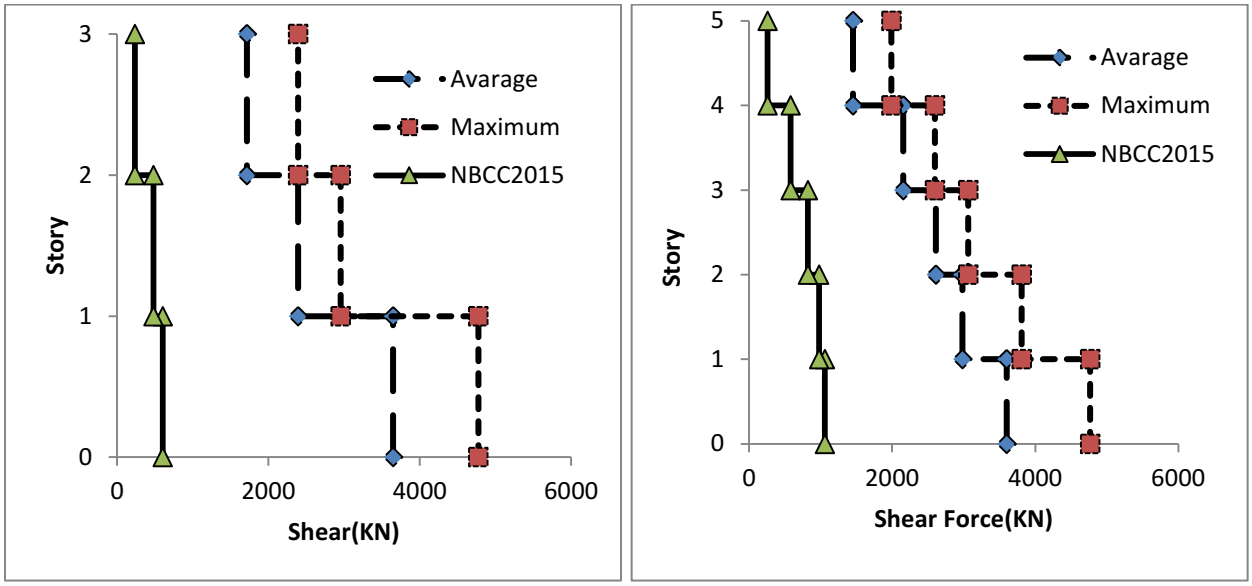

Figure 6.6: Maximum peak story and the average peak story shear occurred under all seismic records for the 3-storey C-PSW (left) and 5-storey C-PSW (right)

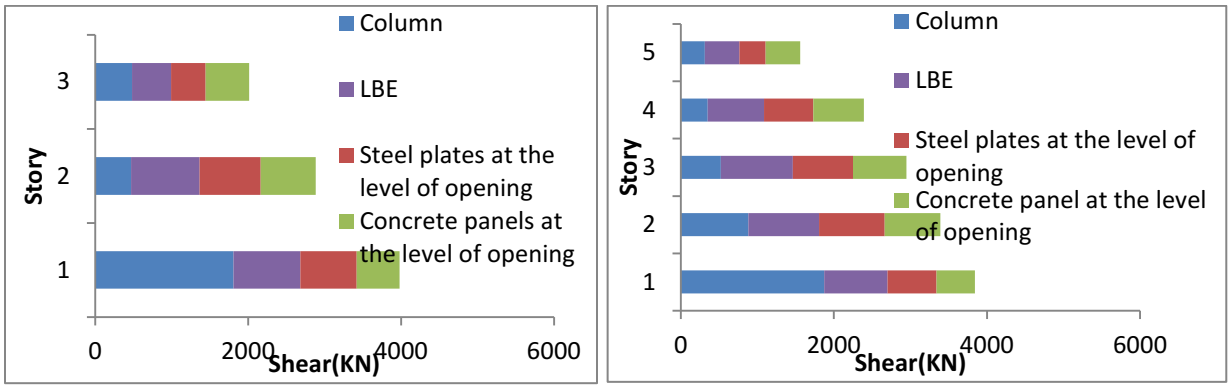

Figure 6.7: Average peak storey shear contributions of 3-storey (left) and 5-storey (right) C-PSWs

For the 3-storey C-PSW, the average base shear under all ground motions was obtained as 3971.5 KN and the maximum base shear occurred under event “Imperial Valley” with the value of 5386 KN. Under this event, the peak storey shear contributions at the base for the boundary columns is 51%, the LBEs is 20%, infill steel plates at the level of opening is 17% and RC panel is 12% . As illustrated in Figure 6.7, for 3-storey C-PSW under earthquake records the average of maximum shear contributions by the columns, LBEs, infill steel plates and RC panels are 47%, 21%, 18% and 14%, respectively.

For the 5-storey C-PSW the average base shear under all ground motions was obtained 3854 KN and the maximum base shear occurred under event “Imperial Valley” which was equal to 5168 KN. For the 5-storey C-PSW under this event, the peak storey shear contributions at the base for the boundary columns is 51%, the vertical LBEs is 22%, infill steel plates at the level of opening is 15% and RC panel is 12%.

As observed from Figure 6.7, for the 5-storey C-PSW under earthquake records, the average of maximum shear contributions of the columns, LBEs, infill steel plates and RC panels are 49%, 21.5%, 16.5% and 13%, respectively.

Yielding of infill plates happen when the dynamic shears reach or exceed the nominal shear strength of the web plate. For 3-storey C-PSW, the calculated shear strengths of the web plate according to equations 4.11 and 4.12 are 1493 KN and 1484 KN for above and at the level of opening, respectively. For 3-storey C-PSW, the steel infill plates of the first and second storey were partially yielded under all ground motions and the steel plates right above the openings in all the stories were partially yielded under all ground motions. Also, it was observed that the dynamic shear of steel plates at the yielded locations reached the calculated nominal shear strength of the plate web.

In 5- storey C-PSW, yielding in the infill plates occurred in the bottom three floors under all ground motions and in the plates right above the opening in all stories. The amount of shear at the yielded location reached the calculated shear strength for the above and at the level of the opening which were 1482 KN and 1473 KN, respectively.

Figure 6.8 (a) and Figure 6.8 (b) present the extend of yielding for the 3-storey and 5-storey C-PSWs at the instance of maximum base shear under event “Imperial Valley”.

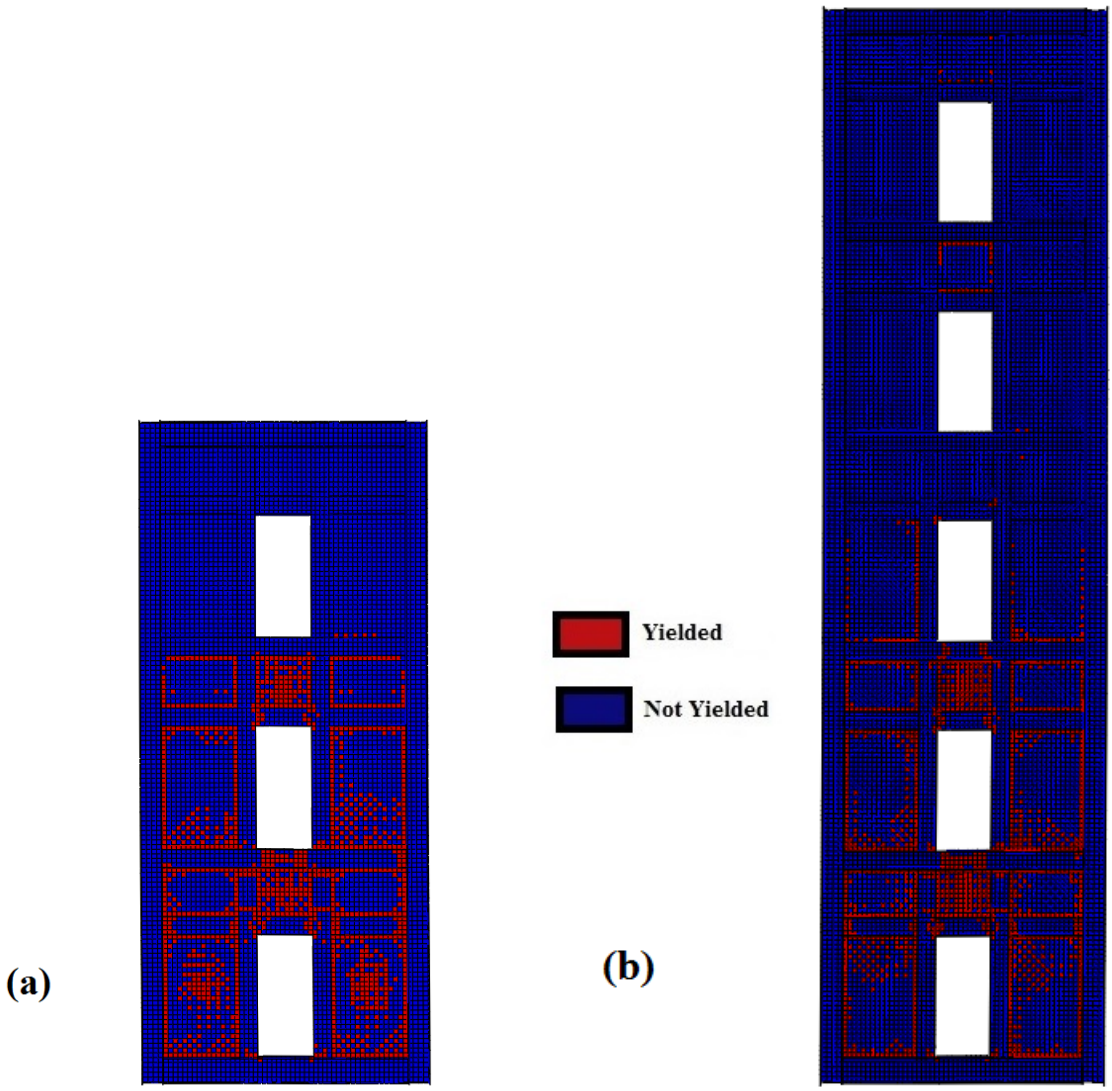

Figure 6.8: Yield pattern of the infill steel plate for: (a) 3-storey and (b) 5-storey C-PSW

The frequency analyses showed that the current code formula predicts the fundamental periods shorter than what was obtained from FE analysis. The current code estimates the period 0.33 and 0.48 second for 3-storey and 5-storey C-PSWs, respectively, while the frequency analysis gave the values of 0.32 and 0.66 seconds for 3- and 5- storey C-PSWs.

Boundary columns were essentially elastic under most of the seismic events and the design objective of columns to remain elastic while sustain the full yield force from the steel infill was achieved.

Undesired yielding was observed in the beam webs right below the opening. The undesired shear yielding in the beam webs below the opening was due to reaction forces of vertical LBEs imposed on the beams. In fact, beams should resist more shear in reality under seismic events and the amount of shear that AISC Design Guide 20 consider for the design of beams were less than the shear applied due to selected earthquake.

Seismic analysis showed that for all ground motions, the obtained columns axial forces and moments in all floors were lower than the design axial forces and moments obtained from the capacity design method. Figure 6.11 and Figure 6.12 show the displacements in every storey obtained from the seismic analyses for the set of ground motions chosen at the instant of peak top storey displacement.

Interstorey drift is an important indicator of performance in earthquake engineering analysis. The variation of maximum interstorey drift in all stories were obtained from seismic analysis and are presented in Figure 6.9 and Figure 6.10. It is observed that the interstorey drifts for the 3-storey and 5-storey C-PSWs are within the code limit.

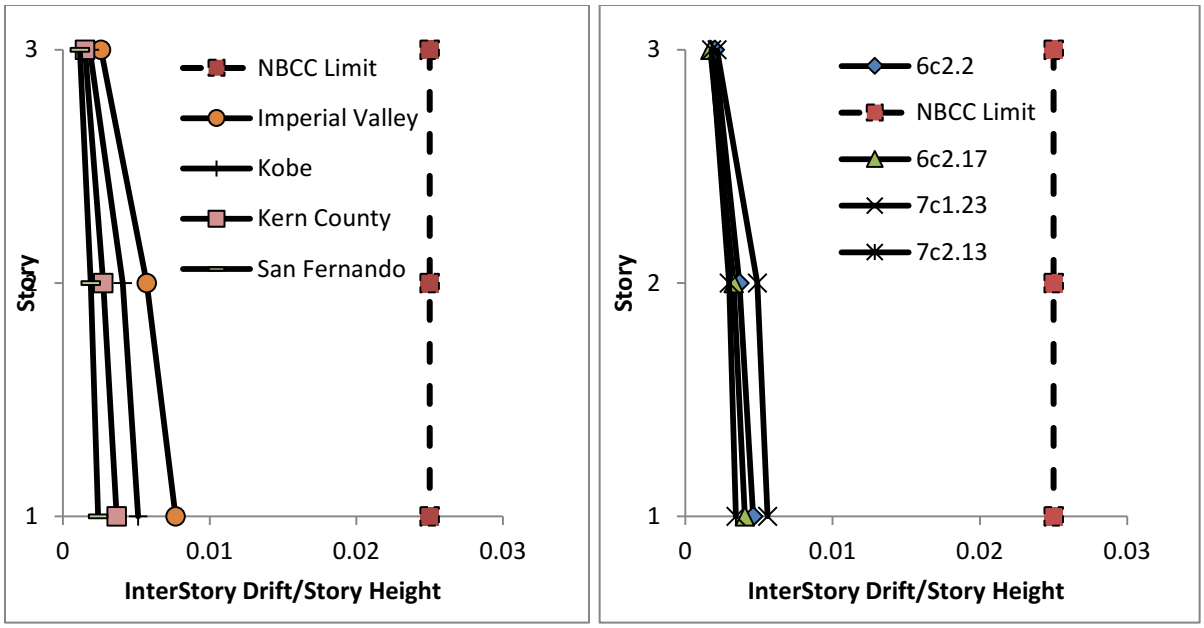

Figure 6.9: Interstorey Drift of the 3-storey C-PSW under: real ground motion records (left); simulated ground motion records (right)

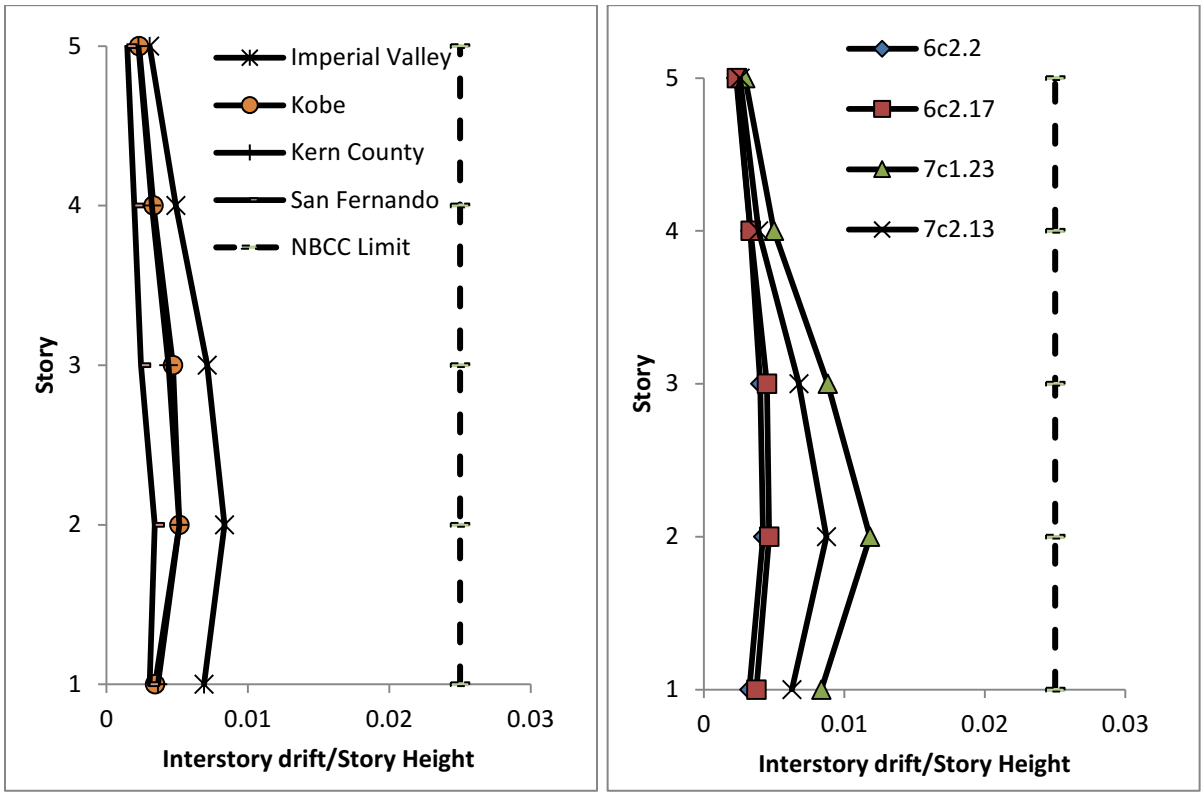

Figure 6.10: Interstorey Drift of the 5-storey C-PSW under: real ground motion records (left); simulated ground motion records (right)

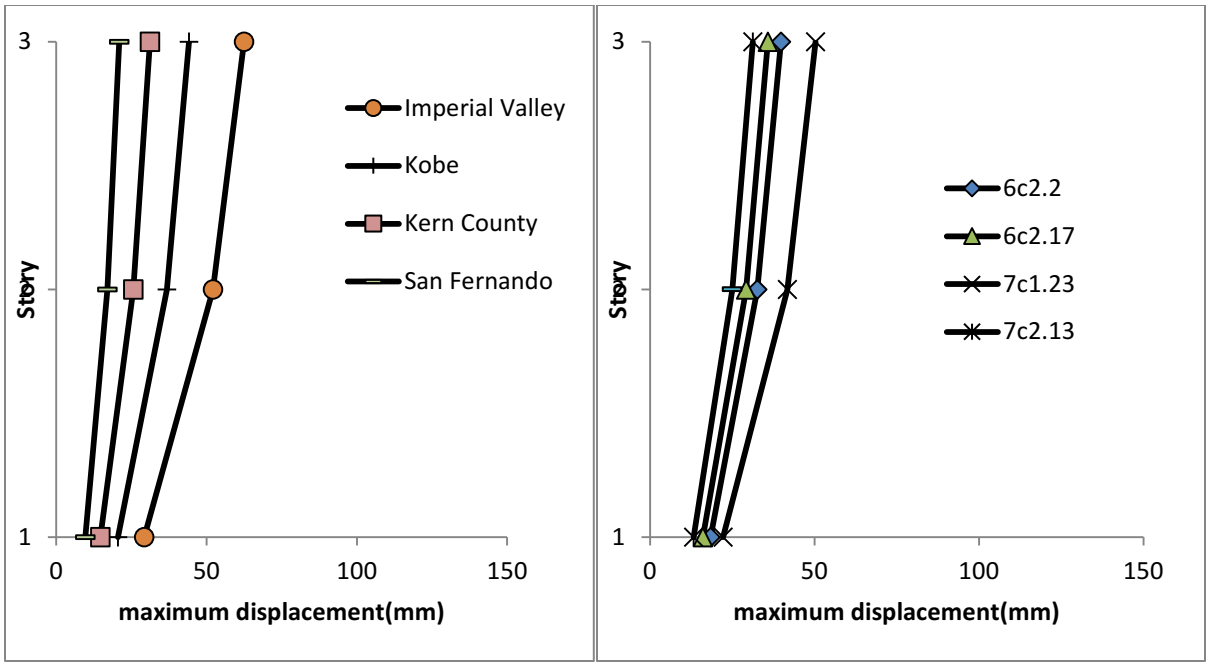

Figure 6.11: Storey displacements at instant of peak top storey displacement for 3-storey C-PSW under: real ground motion records (left); simulated ground motion records (right)

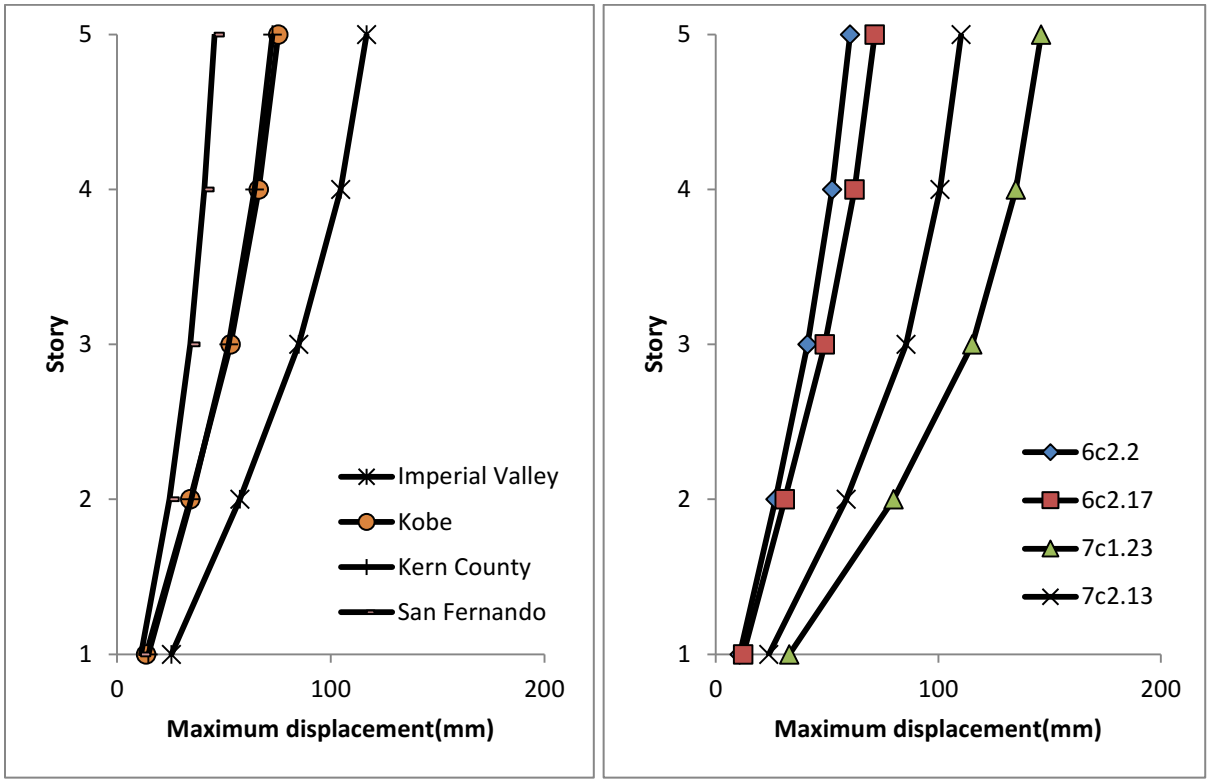

Figure 6.12: Storey displacements at instant of peak top storey displacement for 5-storey C-PSW under: real ground motion records (left); simulated ground motion records (right)

6.3 Comparison of Seismic response of C-PSWs with and without LBEs around the opening

In this section, the effects of utilizing LBEs around the opening are studied. Other than the LBEs, all other properties were considered to be the same as for the 3- and 5- storey C-PSWs previously studied. The performance of the four models (3- and 5- storey C-PSWs with and without LBEs) under the same ground motion was assessed.

Under event 6c2.2, the maximum base shear for 3-storey C-PSW with LBEs was obtained as 4142 KN and for its counterpart without LBEs the maximum base shear was 3337 KN. The 5-storey C-PSW with LBEs had maximum base shear of 3381 KN and the one without LBEs had a maximum base shear of 2648 KN.

The von Mises stress distribution of the 3- and 5- storey C-PSWs with and without LBEs around the opening is shown in Figure 6.13 and Figure 6.14. Figure 6.15 compares the inter storey drifts of the 3- and 5- storey C-PSW with and without LBEs around the opening. The C-PSWs with LBEs around the opening have higher interstorey drift, but for both systems the value are within the code limit.

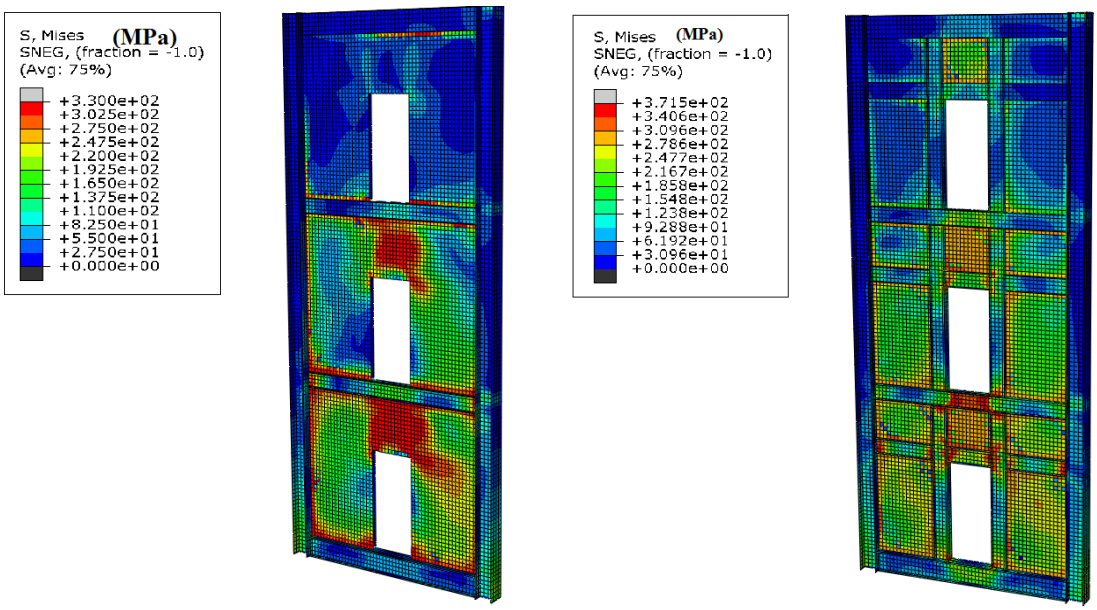

Figure 6.13: von Mises stress distributions at the instant of peak shear for 3-storey C-PSWs: without LBEs (left) and with LBEs (right)

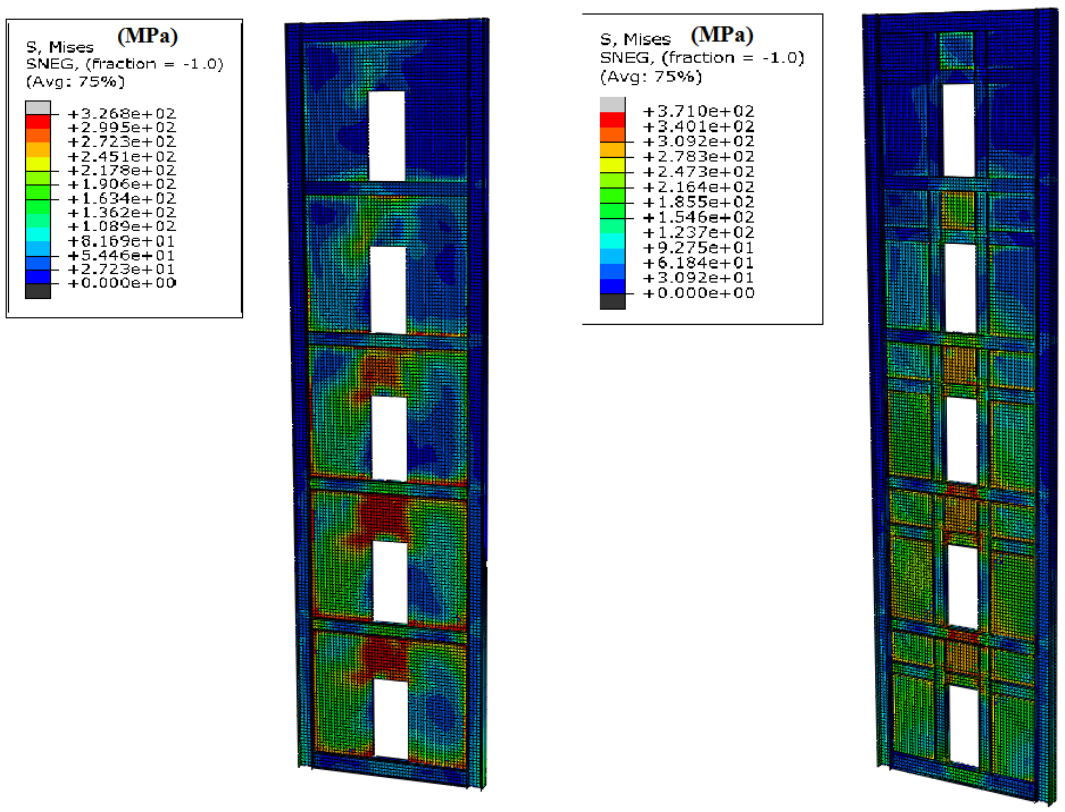

Figure 6.14: von Mises stress distributions at the instant of peak shear for 5-storey C-PSW without LBEs (left) and with LBEs (right)

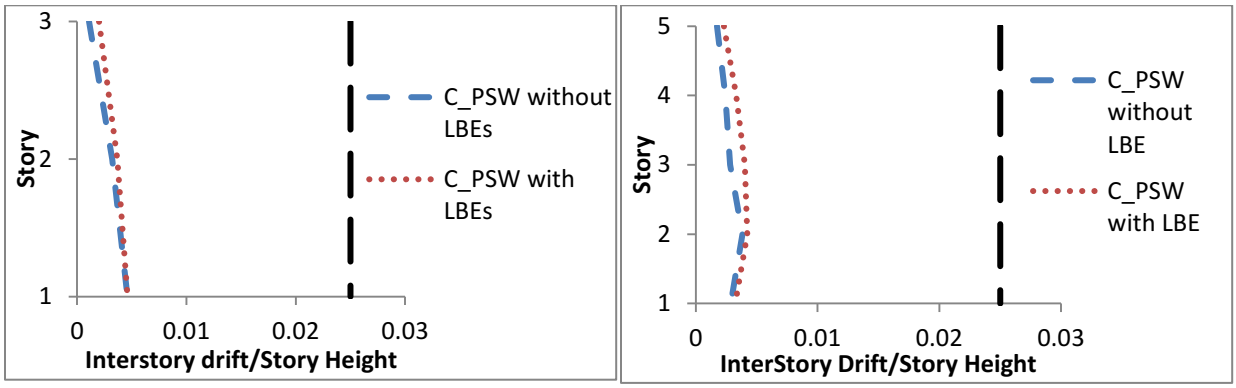

Figure 6.15: Effect of introducing LBEs around the opening on the interstorey drift

Figure 6.16 and Figure 6.17 show the out of plane deformations around the opening for the C-PSWs with and without LBEs around the opening. Under the same ground motion, the maximum out of plane displacement around the opening in the absence of LBEs are 36 mm for the 3-storey and 20 mm for 5 storey C-PSWs, respectively, while in the presence of these

elements these values are equal to 5 mm and 5 mm, respectively. Therefore, the LBEs bring adequate stiffness to reduce the out of plane deformation around the opening.

In C-PSW, the RC panels act as stiffener for the steel plate. The analysis showed that not only the concrete panels prevented buckling of the steel plate but also they prevented occurrence of large out of plane deformations around the openings. As observed, the maximum out of plane deformation around the opening was not large when there was no LBE around the openings of C-PSWs. If this amount of deformation could be handled during construction not to make huge damage in the building during the earthquake, the LBEs can be ignored for C-PSWs.

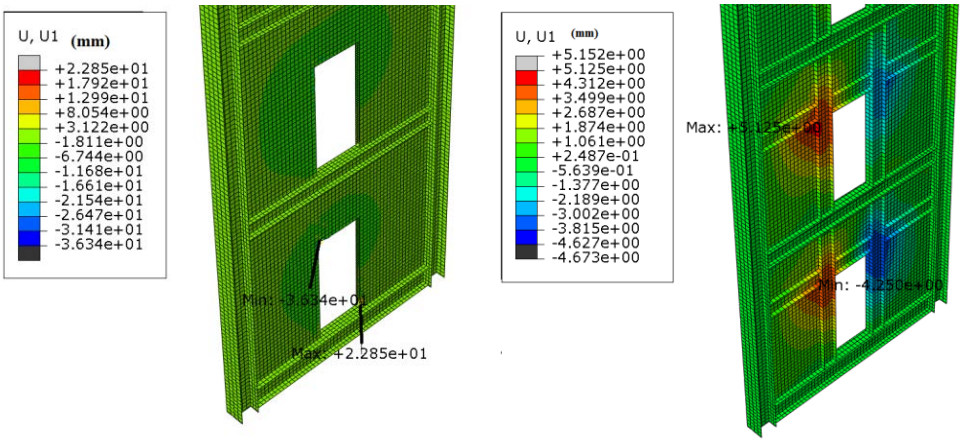

Figure 6.16: Maximum out-of-plane displacement around the opening in the 3-storey C-PSWs with LBEs (right) and without LBEs (left)

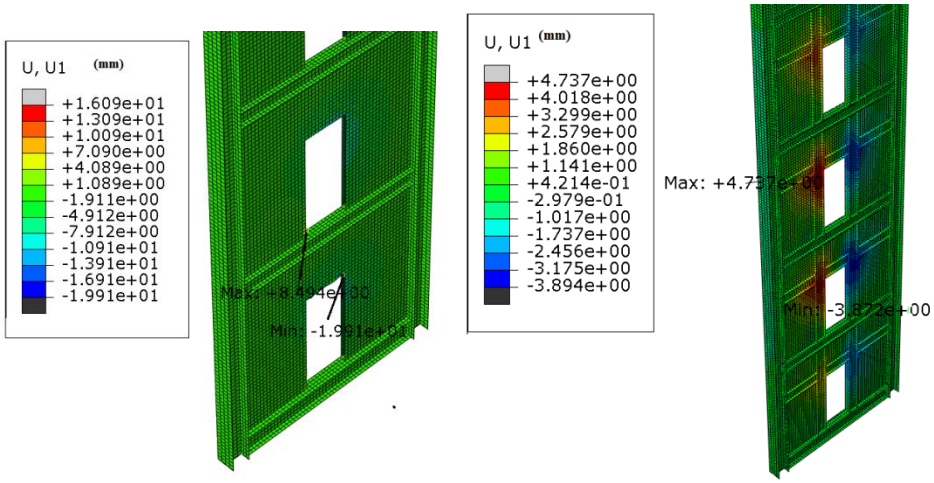

Figure 6.17: Maximum out-of-plane displacement around the opening in the 5-storey C-PSWs with LBEs (right) and without LBEs (left)

6.4 Conclusion

Nonlinear seismic analyses were conducted on C-PSWs with door openings under ground motion records compatible with Western Canada. The performance of selected 3-storey and 5-storey C-PSWs with openings was evaluated. Also, the effect of presence of LBEs around the opening is assessed. The followings can be concluded from this chapter:

- The 3-storey and 5-storey C-PSWs with opening under selected ground motion records showed ductile behaviour and provided excellent structural performance in terms of stiffness and strength.
- The obtained fundamental periods of the systems from frequency analysis were higher than the values calculated according to the NBC 2015 code formula.
- As shown in seismic analysis, the moment resisting frame and LBEs have significant contributions in resisting shear which is not considered in the current AISC 341-16.
- The FE analyses showed that the columns remain essentially elastic and the columns axial forces and bending moments are calculated conservatively in the current capacity design procedures.
- The 3-storey and 5-storey C-PSWs under all selected ground motion records have the interstorey drift less than NBC 2015 limit which is 2.5% of the storey height.
- The LBEs designed based on AISC Design Guide 20 provide enough stiffness and allow the infill steel plates to reach shear yield strength.
- The presence of LBEs around the opening is effective for reducing the out of plane and in plane deformation around the openings.
- From FE results it can be understood that addition of concrete panel to the infill steel plate in C-PSWs not only prevents the buckling of steel plate, but also in case of opening it stiffens the steel plate and prevent it from large out of plane deformations.
- The procedure presented by AISC Design Guide 20 for designing HBEs is not perfect and undesired yielding was observed in the beam webs below the opening. This is because reaction forces from LBEs impose additional shear forces and moment on the beams which are not considered in the current design procedure.

Chapter Seven

7. Summary, Conclusion and Recommendations

7.1 Summary

A finite element model has been developed to study the behavior of unstiffened steel plate shear walls and composite steel plate shear walls with large rectangular openings, like door and window sized openings. Both types of shear walls had rigid beam-to-column connections. The finite element model was validated using the existing experimental studies. The validated FE model was used to conduct seismic analyses on 3-storey and 5-storey SPSWs and C-PSWs with openings. Two multi-storey (3- and 5-storey) buildings located in Vancouver and having SPSWs and C-PSWs with standard door sized openings are designed following the capacity design approach and guidelines of current AISC design guide 20. Seismic behavior of the selected SPSWs and C-PSWs is investigated by conducting a series of time history analysis using a suite of 8 ground motions compatible with the design response spectrum of Vancouver, Canada. Also, key seismic parameters such as storey displacements, interstorey drifts, and base shears were obtained. Maximum contribution of various structural components in resisting applied lateral loads were calculated from seismic analysis.

Additionally, the stiffness requirements for the local boundary elements around the opening recommended by AISC 341.16 were evaluated from nonlinear seismic analysis. It was investigated if the presence of local boundary elements alters the yielding sequence of the shear wall system. In addition, effectiveness of proposed stiffener arrangement around rectangular opening was investigated.

7.2 Conclusions

The main findings of this research are described below:

- The finite element model developed was found to be successful in capturing the behavior of the SPSW and C-PSW system. For the C-PSW tested by Zhao et al. (2004), initial stiffness was predicted well and the ultimate capacity was overestimated by only 2%. Also, for the Arabzadeh et al. (2017) specimen the FE model showed an excellent prediction of the initial stiffness and the peak capacity was overestimated by about 6.5%.

- The 3-storey and 5- storey SPSWs and C-PSWs with openings and LBEs around the openings have good seismic performance in terms of stiffness, ductility, and high shear strength.
- Seismic analyses showed that the shear strength of SPSW and C-PSW are more than what is presented in the current design code. A considerable amount of the shear is resisted by boundary columns, LBEs and reinforced concrete (for C-PSW), which are not considered in the current design approach.
- The boundary columns that were designed with capacity design concept showed excellent seismic performance and under all seismic records the column axial forces and bending moments were lower than the designed forces.
- The interstorey drift which is an important indicator of performance in earthquake engineering were below the NBC 2015 drift limit of 2.5% of storey height under all seismic records for both C-PSWs and SPSWs.
- The obtained fundamental periods of the systems from frequency analysis showed that fundamental periods of the systems were higher than the values calculated according to the NBC 2015 code formula.
- In SPSW the presence of LBEs around the opening were found out to be essential to eliminate the out of plane and in plane deformations around the opening
- The LBEs designed according AISC Design Guide 20 also showed adequate stiffness as they allowed the infill steel plates to reach their shear yield strength and anchored the out of plane and in plane deformations around the openings.
- In the C-PSW, the RC panel also acted as stiffener to restrain the deformation around the opening. It was observed that the out of plane deformation of C-PSW with opening and without LBEs was much less than the identical SPSW.
- Undesired shear yielding was observed in the beams below the openings which was due to additional shear imposed on beams that was not considered in the design procedure of AISC Design Guide 20.
- Under all seismic events, the presence of the LBEs around the opening did not alter the recommended yielding sequence of the SPSW and C-PSW system.

7.3 Recommendations for Future Study

Limited numbers of SPSWs and C-PSWs with openings were analyzed. More C-PSW and SPSW systems with various geometry and height needed to be analyzed. Also SPSW or C-PSW with different opening dimensions, shapes and location needed to be analyzed to see the overall performance of these structures in a wider scale.

Experimental studies should be carried out on C-PSWs with LBEs, which is not performed to date. Also, the effects of concrete with and without gap with boundary elements can be examined on this system.

Additionally, the C-PSW with large opening and without LBEs can be investigated more experimentally to capture the deformations around the opening and evaluate the recommendations of the current code for utilizing LBEs around the opening.

The impact of the concrete reinforcement ratio, type and numbers of bolts used for connecting the steel infill and the RC panels on the shear contribution of the RC panels is needed to be studied in a detailed manner.

To obtain more realistic behavior of these systems three dimensional dynamic analysis can be conducted. The effect of torsion and transverse loading also can be captured in buildings with unsymmetrical plans.

More SPSW and C-PSWs should be analyzed to develop an empirical formula to estimate the fundamental periods of these systems closer to reality.

More studies are also needed to modify the design of HBEs above and below the door opening level due to additional shear forces imposed on the beams.

Various LBE arrangements should be studied to find the most efficient arrangement in terms of cost and practicality.

References

ABAQUS User's Manual: Version 6.11. Hibbitt, Karlsson, Sorensen, Inc., (HKS); 2011.

AISC. 341–16. American Institute of Steel Construction, Chicago, IL: Seismic provisions for structural steel buildings; 2016.

AISC. Steel design guide 20, steel plate shear walls. Chicago, IL. American Institute of Steel Construction; 2007.

Allen, H.G. and Bulson, P.S. Background to Buckling. McGraw Hill Book Company, U.K; 1980.

Alavi E., Nateghi F. Experimental study on diagonally stiffened steel plate shear walls with central perforation. J Constr Steel Res 2013; 89:9–20.

Alinia M.M., Sarraf Shirazi R., On the design of stiffeners in steel plate shear walls, Journal of Constructional Steel Research 2009; 65:2069_2077.

Arabzadeh A, Soltani M, Ayazi A. Experimental investigation of composite shear walls under shear loadings. Thin-Walled Struct (7) 2011; 49:842–54.

Arabzadeh A., and Kazemi Nia Korrani H. Numerical and Experimental Investigation of Composite Steel Shear Wall with Opening. International Journal of Steel Structures 2017; 17(4):1379-1389.

ASCE. Minimum design loads for buildings and other structures. ASCE/SEI 7-16. Reston, VA.

Astaneh-Asl A. Seismic studies of innovative and traditional composite shear walls. Research project in-progress, Dept of Civil and Env Engineering: Univ. of California, Berkeley. 1998-2000.

Astaneh-Asl A. Cyclic tests of steel shear walls. Research project, Berkeley: Dept of Civil and Env Engineering, Univ of California. 2000-2001.

Astaneh-Asl A. Seismic Behaviour and Design of Composite Steel Plate Shear Walls. Structural Steel Educational Council. 2002.

Ayazi A, Farahbod F, Rassouli B, Shafaei S. Experimental research on concrete stiffened steel plate shear wall. 2015.

Barkhordari M.A., Asghar Hosseinzadeh S.A, Seddighi M., Behavior of steel plate shear walls with stiffened full-height rectangular openings, Asian Journal of Civil Engineering (BHRC), 2014; 15 (5):741-759.

Behbahanifard, M., Gilbert, R., Grondin, Y., and Elwi, A.E. Experimental and Numerical Investigation of Steel Plate Shear Walls. Department of Civil and Environmental Engineering, University of Alberta, Edmonton. 2003.

Belarbi, H., and T. C. C. Hsu. Constitutive laws of concrete in tension and reinforcing bars stiffened by concrete. ACI Structural Journal 1994; 91(4):465–474.

Berman, J., and Bruneau, M. Plastic analysis and design of steel plate shear walls. Journal of Structural Engineering, 2003; 129(11):1448-1456.

Berman JW, Bruneau M. Experimental investigation of light-gauge steel plate shear walls. J Struct Eng, ASCE 2005; 131(2):259–67.

Berman, J.W., and Bruneau, M. Capacity design of vertical boundary elements in steel plate shear walls. ASCE, Engineering Journal, 2008; first quarter 57-71.

Bhowmick, A.K., Driver, R.G. and Grondin, G.Y. Seismic Analysis of Steel Plate Shear Walls Considering Strain Rate and P–Delta Effects. Journal of Constructional Steel Research, 2009; 65 (5): 1149-1159.

Bhowmick, A.K., Grondin, G.Y., and Driver, R.G. Performance of Type D and Type LD steel plate walls. Canadian Journal of Civil Engineering, 2010; 37: 88-98.

Bhowmick, A. Seismic Behavior of Steel Plate Shear Walls with Centrally Placed Circular Perforations. Thin-Walled Structures, 2014; 75: 30-42.

Caccese V, Elgaaly M, Chen R. Experimental study of thin steel-plate shear walls under cyclic load. J Struct Eng-ASCE 1993; 119(2):573–87.

Canadian Standards Association. CAN/CSA-S16-14. Limit states design of steel structures. Toronto, Ontario, Canada; 2014.

Chang, G.A., and Mander, J.B. Seismic Energy Based Fatigue Damage Ananlyses of Bridge Columns. Part 1 – Evaluation of Seismic Capacity. NCEER Technical Report No. NCEER-94-0006, State University of New York, Buffalo, N.Y. 1994.

Chen, R. Behavior of unstiffened thin steel plate shear walls, Ph.D. Thesis, University of Maine. 1991.

Dey S., Bhowmick A.K., Seismic performance of composite plate shear walls, Structures 2016; 6:59–72.

Deylami A, Daftari H. Non-linear behavior of steel shear wall with large rectangular opening. Proceeding on CD-Rom. 12th World Conference on Earthquake Eng, NewZealand; 2000. [Paper No.408].

Driver, R. G., Kulak, G. L., Elwi, A. E., and Kennedy, D. L. FE and simplified models of steel plate shear wall. Journal of Structural Engineering, 1998a; 124(2):121-130.

Driver RG, Kulak GL, Kennedy DJL, Elwi AE. Cyclic test of four-story steel plate shear wall. J Struct Eng-ASCE 1998; 124(2):112–30.

Elgaaly M, Lui Y. Analysis of thin-steel-plate shear walls. J Struct Eng-ASCE 1997; 123(11):1487–96.

Elgaaly, M. Thin steel plate shear walls behavior and analysis. Thin-Walled Structures, 1998; 32(1–3):151-180.

Farzampour A., Laman J. A. Behavior prediction of corrugated steel plate shear walls with openings. J Constr Steel Res 2015; 114:258–68.

Genikomsou, A.S., and Polak, M.A. Finite element analysis of punching shear of concrete slabs using damaged plasticity model in ABAQUS. Engineering Structures 2015; 98:38-48.

Ghosh S., Kharmale S.B., Research on steel plate shear wall: past, present and future, Structural Steel and Castings: Shapes and Standards, Properties and Applications, Nova Science Publishers Inc, Hauppauge, USA, 2010.

Guo L., Rong Q., Ma X., Zhang S., Behavior of steel plate shear wall connected to frame beams only, Int. J. Steel Struct. 2011; 11(4):467–479.

Hogenstad. E., A study of combined bending and axial load in reinforced concrete members, Bulletin No 399, Engineering Experiment Station, University of Illinios.Urbana,1951.

Hosseinzadeh A.A., Tehranizadeh M., Introduction of stiffened large rectangular openings in steel plate shear walls" Journal of Constructional Steel Research 2012; 77:180–192

Hsu, L.S. and Hsu C.T.T. Complete stress-strain behaviour of high-strength concrete under compression. Magazine of Concrete Research, 1994; 46(169): 301-312.

Hsu. T. T. C., and Zhang, Tension stiffening in reinforced concrete membrane elements. ACI Structural Journal 1996; 93(1):108–115.

Hsu, T. T. C., and Zhu, R. R. H. Softened membrane model for reinforced concrete elements in shear. ACI Structural Journal 2002; 99(4): 460–469.

Jankowiak I., Kąkol W., Madaj A.: Identification of a continuous composite beam numerical model, based on experimental tests, 7th Conference on Composite Structures, Zielona Góra, 2005, pp. 163–178.

Kharrazi, M. H., Ventura, C. E., and Prion, H. G. Analysis and design of steel plate walls: analytical model. Canadian Journal of Civil Engineering, 2010a; 38(1): 49-59.

Kharrazi, M. H., Ventura, C. E., and Prion, H. G. "Analysis and design of steel plate walls: experimental evaluation." Canadian Journal of Civil Engineering, 2010b; 38(1): 60-70.

Kmiecik, P. and Kaminski, M.; "Modelling of Reinforced Concrete Structures and Composite Structures with Concrete Strength Degradation Taken into Consideration"; Archives of Civil and Mechanical Engineering XI, No. 3 ,2011.

Kulak G.L. Unstiffened steel plate shears walls. In: Narayanan R, Roberts TM, editors. Structures subjected to repeated loading-stability and strength. London: Elsevier Applied Science Publications; 1991: 237-276.

Lamontagne, M.S., Halchuk, J.F., Cassidy, and Rogers, G.C. Significant Canadian Earthquakes of the Period 1600–2006. Seismological Research Letters 2008; 79(2):211-224.

Lee, J., and Fenves, G. L. Plastic-Damage Model for Cyclic Loading of Concrete Structure. Journal of Engineering Mechanics, ASCE, 1998; 124(8):892-900.

Lubell, A. S. Performance of unstiffened steel plate shear walls under cyclic quasi-static loading. University of British Columbia. 1997.

Lubell AS, Prion HGL, Ventura CE, Rezai M. Unstiffened steel plate shear wall performance under cyclic loading. J Struct Eng-ASCE 2000; 126(4):453–60.

Lubliner, J., Oliver, J., Oller, S. and Onate, E. A Plastic-Damage Model for Concrete. International Journal of Solids and Structures, 1989; 25(3):299-326.

Mansour, M., Lee, J. and Hsu, T. T. C. Cyclic stress-strain curves of concrete and steel bars in membrane elements. ASCE Journal of Structural Engineering 2001; 127(12):1402–1411.

Meghdadaian M., Ghalehnovi M., Improving seismic performance of composite steel plate shear walls containing openings. Journal of Building Engineering 2019; 21:336–342.

NBCC. National Building Code of Canada. National Research Council of Canada (NRCC), Ottawa, ON, Canada, 2015.

Naumoski, N., Saatcioglu, M., and Amiri-Hormozaki, K. Effects of Scaling of earthquake excitations on the dynamic response of reinforced concrete frame buildings. 13th World Conference on Earthquake Engineering. 2004; 2917:2922.

Pang, X.D., and Hsu, T. T. C. Behaviour of reinforced concrete membrane elements in shear. ACI Structural Journal 1995; 92(6):665–679.

PEER. NGA strong motion database. Pacific earthquake engineering research center; 2010.

Popovics, S., A Numerical Approch To The Complete Stress-Strain Curve Of Concrete, Cement and Concrete Research ,1973; 3 (5): 583-599.

Purba RH, Bruneau M. Finite element investigation and design recommendations for perforated steel plate shear walls. J Struct Eng ASCE 2009; 135(11):1367–76.

Qu B, Bruneau M, Lin CH, Tsai KC. Testing of full-scale two-story steel plate shear wall with reduced beam section connections and composite floors. J Struct Eng, ASCE 2008; 134(3):364–72.

Qu, B., Bruneau, M. Capacity Design of Intermediate Horizontal Boundary Elements in Steel Plate Shear Walls. ASCE Journal of Structural Engineering 2010; 136 (6): 665-675.

Rabotnov Y.N., Creep problems in structural members, North-Holland, Amsterdam 1969.

Rahai A. and Hatami F. Evaluation of composite shear wall behavior under cyclic loadings.” J. Constr. Steel Res. 2009; 65:1528-1537.

Rezai M. Seismic behaviour of steel plate shear walls by shake table testing. PhD Dissertation, Dep of Civil Eng, University of British Columbia, Vancouver, BC; 1999.

R.G. and Kulak G.L. and Kennedy D.J.L. and Elwi A.E. Cyclic tests of four-story steel plate shear wall. Journal of Structural Engineering, ASCE, 1998; 124(2):112-120

Roberts TM, Sabouri-Ghomi S. Hysteretic characteristics of unstiffened perforated steel plate shear panels. Thin-Walled Struct 1992; 14:139–51.

Sabouri-Ghomi, S., Ventura, C. E., and Kharrazi, M. H. Shear analysis and design of ductile steel plate walls. Journal of Structural Engineering, 2005; 131(6):878-889.

Sabouri-Ghomi S, Ahouri E, Sajadi R, Alavi M, Roufegarinejad A, Bradford MA. Stiffness and strength degradation of steel plate shear walls having an arbitrarily located opening. J Constr Steel Res 2012; 79:91–100.

Saenz.L.P., "Equation for the sress-strain curve of concrete in uniaxial and biaxial compression of concrete", Journal of ACI. 1955; 61(9): pp 349-359,

Seydel, E. Über das Ausbeulen von rechteckigen isotropen oder orthogonalanisotropen Platten bei Schubbeanspruchung. Ing. Arch., 1933; Vol. 4: p. 169.

Shafaei S., Ayazi A., Farahbod F. The effect of concrete panel thickness upon composite steel plate shear walls” Journal of Constructional Steel Research, 2016; 117:81–90

Shi, Y., and Astaneh-Asl, A. Lateral Stiffness of Steel Shear Wall Systems. Structures Congress, ASCE, April 24-26. Vancouver, Canada, 2008: pp.10.

Soheil Shafaeia, Farhang Farahbodb, Amir Ayazic, Concrete Stiffened Steel Plate Shear Walls with an Unstiffened Opening. Structures 2017; 12: 40–53

Smith.G.M, Young.L.E. Ultimate Theory in Flexture by Exponetial Function, Journal of ACI 1955; 52(3):349-359.

Syed S.Q. Seismic Probabilistic Fragility Assessment of Reinforced Concrete Shear Wall Structures in Nuclear Power Plants. North Carolina State University. 2012.

Thorburn L.J., Kulak G.L. and Montgomery C.J. Analysis of Steel Plate Shear Walls. Department of Civil Engineering, University of Alberta, Edmonton, Alberta: Structural Engineering, 1983; Report No. 107.

Timler P.A., and Kulak G.L. Experimental Study on Steel Plate Shear Walls. Structural Engineering Report 114, Department of Civil Engineering, University of Alberta, Edmonton, Canada. 1983.

Tromposch, E., and Kulak, G. L. Cyclic and static behaviour of thin panel steel plate shear walls, Department of Civil Engineering, University of Alberta, Edmonton, Canada.1987.

Vian D. and Bruneau M. Testing of special LYS steel plate shear wall. 13th World Conference on Earthquake Eng, 2004: Paper No.978.

Yip.W.K. Generic Form of Stress-Strain Equations for Concrete. Cemente and Concrete Research, 1998; 28(4):499-508,

Zhao Q., Astaneh-Asl A., "Cyclic behavior of traditional and innovative composite shear walls", J. Struct. Eng. 2004; 130 (2):271–284.

Zhao, Q. H., and Astaneh-Asl, A. Experimental and Analytical Studies of a Steel Plate Shear Wall System. Structures Congress, ASCE, April 24-26. Vancouver, Canada, 2008: pp.10.

Zhen G. and Yingshu Y. Experimental study of steel plate composite shear wall units under cyclic load. International Journal of Steel Structures, 2015; 15:515-525.